

Raman Spectroscopic Investigation of Kitaev Quantum Spin Liquids

Vivek Kumar^{*,1} and Pradeep Kumar^{*,2}

^{}School of Physical Sciences, Indian Institute of Technology Mandi, Mandi-175005, India*

Abstract

Quantum spin liquids, a highly topologically entangled, dynamically correlated state where quantum fluctuations preclude any long-range ordering down to absolute zero. In the search for a topologically robust qubit, the scientific community has been in continuous hunt for real quantum spin liquid systems. Alexei Kitaev in his exactly solvable model for a spin-1/2 two-dimensional honeycomb lattice, presented a system that hosts a topologically protected state (Majorana zero-modes). Under an applied external field, the Kitaev spin liquids turn into a topologically non-trivial chiral spin-liquid state with non-abelian anionic excitations, which is crucial for quantum computing. Earlier theoretical predictions advocated that Kitaev physics can be realized in spin-orbit-coupled Mott insulators such as honeycomb irradiates and ruthenates. However, the experimental findings continuously challenge the theoretical aspects, indicating the presence of non-Kitaev interactions in real materials, where the dimensionality, disorder (vacancy), chemical composition, generalized spin-S, and external perturbations (pressure, magnetic field, temperature) can actively tune the Kitaev interactions and the ground state excitations. In this review article, a comprehensive discussion is included with an updated literature survey in the context of the potential of Raman spectroscopy as a probe for Kitaev quantum spin liquids.

¹vivekvke@gmail.com

²pkumar@iitmandi.ac.in

Keywords: Kitaev Spin Liquids, Raman Spectroscopy, Topological order, Majorana fermions

Table of Contents

Abstract	1
1. Introduction	3
2. Fundamental components of Quantum Spin Liquid	13
2.1 Topology	13
2.2 Quantum entanglement and Anyons	15
2.3 Gauge field theory	17
3. Kitaev Spin Liquids (KSL)	21
3.2 Proximate and Beyond-ideal Kitaev Materials	25
3.3. Effect of Dimensionality	27
3.4. Effect of High-Spin and Disorder	29
4. Experimental Probes for Quantum Spin Liquids	35
5 Inelastic Light Scattering Investigation (Raman)	39
5.1 Magnetic Excitations	41
5.2. Evidence for Kitaev Quantum Spin Liquids	44
5.2.1. Quasi-elastic Scattering	55
5.2.2. Phonon Anomaly	61
5.2.3. Fano Asymmetry	64
5.2.4. Effect of Polarization	67
5.2.5 Effect of Magnetic Field	74
5.2.6. Effect of Pressure	79
6. Outlook	82
Data availability statement	83
Author contribution statement	83
Declaration of competing interest	83
Acknowledgment	83
References	84

1. Introduction

Magnetism in solids has always been a fascinating phenomenon that has provided significant technological advances over time, having applications in broad fields from data storage, energy generation, magnetic levitation, sensors, medical applications, and electromagnetic devices to next-generation technologies such as quantum computation, quantum communication, energy harvesting, and magnetic refrigeration. The physics in two-dimensional (2D) regime of these quantum magnetic materials is provides a big boost to the development of nanoscale engineering [1].

In conventional magnetic materials interaction between quantum spins gives rise to a phase transition from a disordered spin state at high temperature to an ordered spin state or a spin-solid state at low temperature. Signatures of such a transition are reflected in thermodynamic observables, for example, spin entropy reduces to zero as the system attains a unique ground state. The symmetry breaking plays an important role in the emergent states, often it is accompanied by a phase transition, which lowers the overall energy of the system. For instance, inversion symmetry is broken in Ferroelectric materials below the Curie point and in the case of superconductors, $U(1)$ gauge symmetry is compromised below a critical temperature. An interesting scenario appears when the spin entropy is released without breaking any symmetry down to absolute zero, and no local order parameter exists, which goes beyond the classical understanding of the phase transitions [2,3]. This novel state forms a highly non-local entangled phase where electron spins behave like a fluid and is known as a Quantum Spin Liquid (QSL).

The ground state of a QSL is an exotic state of matter where quantum spin fluctuations preclude spin ordering even down to absolute zero kelvin. It is an electronically insulating state containing an odd number of electrons per unit cell (Mott-insulator) and that preserves spin-rotation symmetry [4]. The Lev Landau's [5] framework of symmetry breaking and

phase transition fails to describe the underlying physics of QSLs, and the subject was further enriched by the insights of Philip Anderson [6] to classify novel phases of condensed matter. Some key features applicable to broken-symmetry states noted by Anderson [6] are (i) in a magnetically ordered state (broken spin-rotation symmetry), there is an inherent inertia which costs energy to deform the spin structure, (ii) new emergent excitation, such as magnons, which is a particle-like excitation formed from a single smeared-out spin. For a system of $S = 1/2$ spins, a flip represents an $S = 1$ excitation. The nature of excitation is subjected to the kind of order and symmetry the system Hamiltonian possesses.

Fractional quantum hall liquid (FQHL), a state of matter realised in a 2D electron system when subjected to high magnetic fields. These highly correlated systems may exhibit excitations obeying fractional quantum numbers, which are neither bosons nor fermions, but have their own unique quantum statistics and are known as anyons [7]. The anyonic statistics can be altered by varying the magnitude of the external magnetic field, but these cannot be distinguished on the grounds of symmetry breaking. That is where the concept of topology, the study of shapes of mathematical objects and spaces, comes into the picture, and FQHL adheres to a topological quantum order. Unlike conventionally ordered states, a topologically ordered state is highly entangled and has a high ground-state degeneracy that is robust against perturbations depending on the topology and symmetry of the given system.

The underlying physics of typical ferromagnets and antiferromagnets, where the neighboring spins align parallel and antiparallel, respectively, was described by Heisenberg back in 1928 [8]. The origin of exchange interactions can be well understood in the Heisenberg model. In the case of classical spins, the spin quantum number $S \rightarrow \infty$, but we are interested in how a system of quantum mechanical spins behaves. The nearest neighbor Heisenberg interaction Hamiltonian for a magnetic solid of an N -spin lattice site where generally $N \rightarrow \infty$ can be written as:

$$H = \frac{1}{2} \sum_{\langle ij \rangle} J_{ij} \vec{S}_i \cdot \vec{S}_j \quad - 1$$

Here J_{ij} is the exchange integral and its origins have quantum mechanical roots which is related to the anti-symmetric nature of the overall wavefunction of the electrons (fermion). The sign of J_{ij} determines the preferred spin orientation in order to minimize the energy, i.e.

$J_{ij} < 0$ corresponds to Ferromagnetism and $J_{ij} > 0$ corresponds to Anti-ferromagnetism.

The spins in this case \vec{S}_i are 3-D vectors with dimensionality $D = 3$, unlike the Ising model where $D = 1$. The summation can be taken over a lattice of dimension D ($D = 1, 2, \text{ or } 3$)

The spin components on the same site follow a commutation relation given as

$$[S_j^\alpha, S_j^\beta] = i \sum_\gamma \epsilon_{\alpha\beta\gamma} S_j^\gamma. \text{ Here } \alpha, \beta, \gamma = x, y, z, \text{ whereas the spin components on different}$$

sites commute with each other and the spin operator S_i^2 has an eigenvalue of $S(S+1)$.

Equation 1 can also be written as:

$$H = \frac{1}{2} \sum_{\langle ij \rangle} J_{ij} \left(\frac{S_i^+ S_j^- + S_i^- S_j^+}{2} + S_i^z S_j^z \right) \quad - 2$$

Where the spin raising and lowering operators are defined as: $S_j^+ = S_j^x + iS_j^y$, $S_j^- = S_j^x - iS_j^y$.

The limitation here is that the exchange integral J_{ij} is non-zero only for nearest-neighbor lattice sites. For interaction between two spins, the Heisenberg Hamiltonian takes the following form:

$$\begin{aligned} H &= J \vec{S}_1 \cdot \vec{S}_2 = J \left[\frac{1}{2} (S^{tot})^2 - \frac{3}{4} \right] \\ &= \frac{1}{4} J; S^{tot} = 1 \text{ (Triplet) and} \\ &= -\frac{3}{4} J; S^{tot} = 0 \text{ (Singlet)} \end{aligned} \quad - 3$$

For $J > 0$, the anti-parallel alignment can take advantage of hybridization and reduce the kinetic energy ($\kappa.E. \propto 1/L^2$, where L is the length scale) by hopping to the other site where another electron is already present. This hopping is restricted for a parallel spin by the Pauli principle, which makes the singlet state favourable than the triplet state.

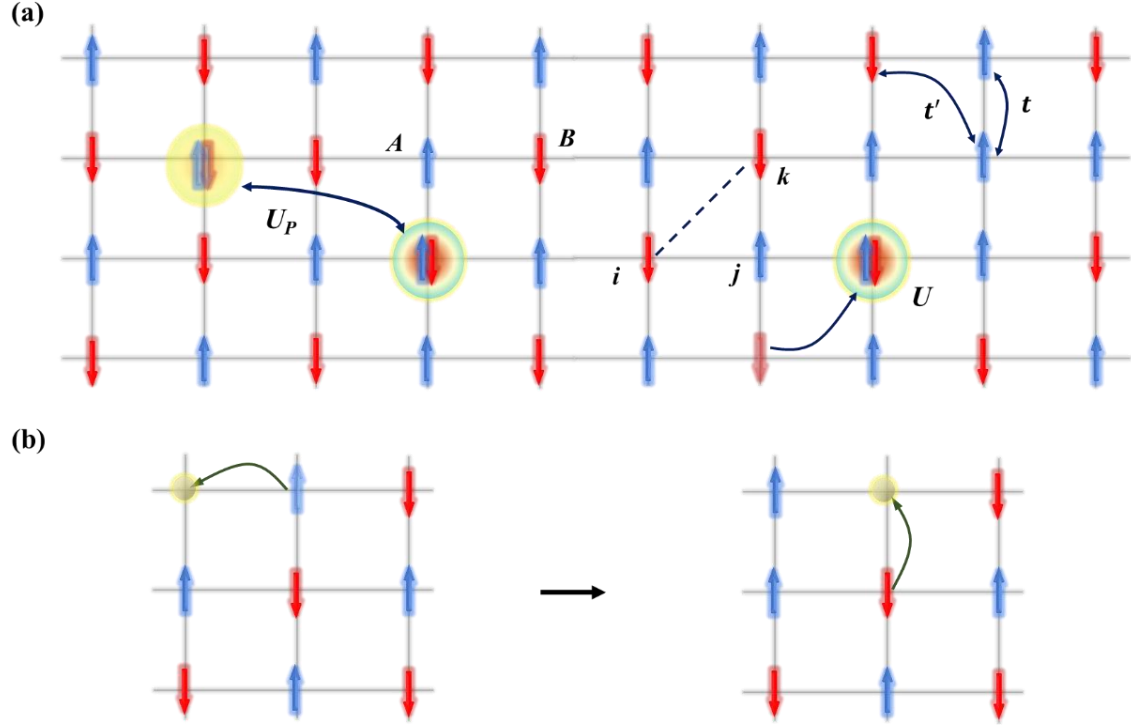


Figure 1: Key aspects of the Hubbard model: (a) Fermions represented by their position in the lattice and magnetic moment (up/blue or down/red arrow). The hopping integral for the nearest neighbour t and second-nearest neighbour t' is shown by a curved two-sided arrow. U and U_P are the onsite interaction and energy cost for pair hopping. (b) Presence of vacancy (yellow sphere), where the average density is less than one spin per site.

A more realistic approach in order to describe the behaviour of interacting fermions in quantum materials having a strong electronic correlation effect was proposed by John Hubbard in 1963 [9]. This model considers onsite Columb repulsion into the picture and is a modified version of the tight-binding model where non-interacting electron hopping occurs.

Figure 1 (a) shows an arrangement of fermions on a lattice, which is determined by its position in the lattice and magnetic moment, which can be either up or down (blue and red

arrows). In this model, the fermions can hop around in the lattice. This model has been successfully employed in order to study a wide variety of complex phenomena that are realized via the Hubbard model, such as Ferro/Anti-ferromagnetism, unconventional superconductivity, charge-density waves (CDWs), quantum spin liquids, etc. The Hubbard Hamiltonian is written as follows [10]:

$$H = -t \sum_{\langle i,j \rangle \sigma} (c_{i\sigma}^\dagger c_{j\sigma} + c_{i\sigma}^\dagger c_{j\sigma}) + U \sum_i n_{i\uparrow} n_{j\downarrow} - \mu \sum_i (n_{i\uparrow} + n_{j\downarrow}) \quad -4$$

Here $n_{i\sigma} = c_{i\sigma}^\dagger c_{i\sigma}$ is the number operator which counts the number of electrons with spin ‘ σ ’ on the i^{th} site. ‘ t ’ is the hopping interaction integral within the nearest neighboring sites ($\langle i, j \rangle$), which is also the kinetic energy term and is responsible for the creation of a fermion on the i^{th} site ($c_{i\sigma}^\dagger$) and the annihilation ($c_{j\sigma}$) at the j^{th} site. The second term ‘ U ’ represents the onsite screened Coulomb repulsion interaction between electrons and comes into the picture only if the site is doubly occupied. The third term is the chemical potential, which dictates the filling of electrons per lattice site. An interesting scenario occurs in the case of half-filling, where there is one electron per site. In this case, the relative strength of U and t i.e., U/t , determines the behaviour of the material. If the onsite coulomb repulsion $U/t \gg 1$, then it is difficult for the electrons to hop to a neighbouring site and hence are localized on a particular site, and the material is an Insulator. Such non-conducting materials, which contain an odd number of electrons per site, are known as Mott-insulators, which are predicted to be conductors in accordance with the band theory. If $U/t \ll 1$, then electrons can hop around and we have a conductor-like behaviour. If $U/t \gg 1$, the Hubbard model reduces to the Heisenberg Hamiltonian with $J \sim t^2/U$ and $\vec{S}_i = \frac{\hbar}{2} c_{i\sigma}^\dagger P_{\sigma\sigma'} c_{\sigma'i}$, here $P_{\sigma\sigma'}$ represents the three Pauli matrices [11]. If we consider higher-order terms, one has to introduce the ring-exchange process, second-nearest neighbour interactions. For example, up to the third order

in a strongly coupled Hubbard model, we get the three-spin ring-exchange term, which is

$$H_3 = -J_3 \sin(\phi_3) \sum_{\Delta_{i,j,k}} S_i \cdot (S_j \times S_k) \quad \text{here } J_3 = -24t^2 t' / U^2 \text{ is the corresponding three-spin}$$

exchange coupling constant described around an elementary triangle $\Delta_{i,j,k}$ on the square lattice as shown in **Figure 1 (b)**, where t and t' are the nearest and second-nearest hopping integrals. A magnetic flux Φ_3 is associated with $\Delta_{i,j,k}$ (i, j , and k are ordered anti-clockwise) having a scalar spin chirality $X_{i,j,k} = S_i \cdot (S_j \times S_k)$ and giving rise to non-trivial topological effects [12,13].

An interesting case arises if the average density of filling is less than one electron per site. Here, holes play a crucial role as they disturb the magnetic order in the lattice, as shown in **Figure 1 (c)**. Such an exotic nature has been studied by Mazurenko et al., [14] in a hole-doped antiferromagnet, where they demonstrated that microscopy of cold atoms in optical lattices can be instrumental to comprehend the low-temperature Fermi-Hubbard model. Another study showed that doping in the antiferromagnet may give rise to a pseudo gap and high-temperature superconductivity [15].

Heisenberg model for Ferromagnets at a temperature above T_c , the thermal fluctuations of order $K_B T$ affect the magnetic ordering, which is dictated by the spin-spin exchange interaction constant J (< 0). Here, the parallel alignment of spins minimizes the total energy to about $-|JS^2|$ per spin, and the ground state is an eigenstate of the Heisenberg Hamiltonian. Anti-ferromagnets can be thought of as consisting of two disjoint sub-lattices (bipartite) A and B, such that the interactions are allowed between sites of different lattices. Having opposite spins, the ground state of anti-ferromagnets is more complicated as compared to that of ferromagnets. Louis Néel proposed that due to positive exchange interaction, the spins at low temperatures will align anti-parallelly [16]. But the crucial point

is that the Néel state is not an eigenstate of the Heisenberg exchange Hamiltonian, and the quantum fluctuations flip the spins, which reduces the sublattice order and will eventually disturb the long-range anti-parallel ordering of the spins. However, the Néel state is found to be stable, as one can construct a stable Néel-like wave packet from an arbitrarily close eigenstate in macroscopic condensed matter systems [17]. According to Marshall's theorem [18], the absolute ground state for equal-size sublattices A and B is a singlet, i.e., as shown in **Figure 2 (b)**. However, this singlet ground state is not uniquely determined and would lead to fluctuations that randomize the spin order.

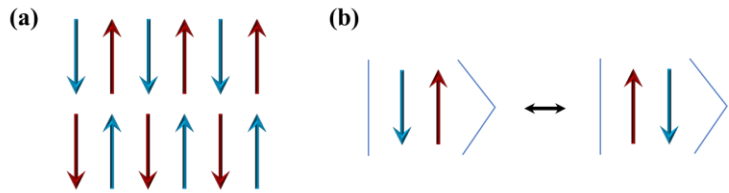


Figure 2: (a) Anti-ferromagnetic ordering as proposed by Néel, (b) Mutual spin flip due to quantum fluctuations, which would lead to RVB state or entangled singlet pairs.

In 1973, Philip W. Anderson advocated that the ground state may consist of a superposition of singlet pairs all over the lattice and named it a resonating valence bond (RVB) state, which will consume the Néel state [19]. In search of high-temperature superconductors, Anderson proposed that upon doping the parent compound La_2CuO_4 , which is a Mott-insulator, the singlet pairs are in the RVB state and can be visualized as Cooper pairs [20]. Theoretical investigation of high-temperature superconductors remains elusive, while there has been a surge in the study of quantum-disordered spin state systems [21]. Such states have been proposed for geometrically frustrated magnetic systems having corner-sharing triangles or tetrahedra [22].

This RVB state does not break spin rotational symmetry, as each bond represents an effective $S = 0$ spin state. The presence of frustration increases the ground state energy as compared to

the non-frustrated case. It is also reflected in the increased entropy of the ground state, owing to high degeneracy, which becomes macroscopic in the thermodynamic limit and destabilises the symmetry-breaking order. Generally, any physical system is considered frustrated if all the components of potential energy are not minimized simultaneously. In the case of magnetic materials having frustrated geometry, where interaction of magnetic moments induces an incompatibility in minimizing the system's energies. For example, in the case of an Ising spin on a triangular lattice as shown in **Figure 3 (a)**, where all bonds favour antiferromagnetic interaction ($J_{ij} > 0$) is frustrated and there are eight possible configurations out of which six are the lowest-energy configuration ($E = -J$), whereas rest two are excited states ($E = 3J$). However, a non-frustrated ferromagnetic alignment of spin is two-fold degenerate (up or down spin alignment) with energy $-3J$. Another example is for a 1D spin chain, the energy per bond of singlet dimers turns out to be $-3/4J$ whereas for the Néel state, it is $-1/4J$. Hence, the frustrated lattices will stabilize in an RVB state rather than Néel state. This lower energy of the singlet dimer state reflects the stronger quantum mechanical stabilization owing to entanglement, which is in contrast to the classical alignment in the Néel state. The problem of geometric frustration for a triangular lattice was resolved when each spin points to 120° (two-fold) with respect to each other and may lead to long-range magnetic ordering [23,24]. Other instances of geometrically frustrated lattices are Kagome and Honeycomb structures, as shown in **Figure 3 (c, d)**, where the geometrical frustration cannot be overcome by 120° spin orientation as in the case of the triangular lattice [23]. However, whether the ground state of a Kagome lattice is a QSL or not is still under debate, but there are theoretical studies that favor a QSL state [25-28].

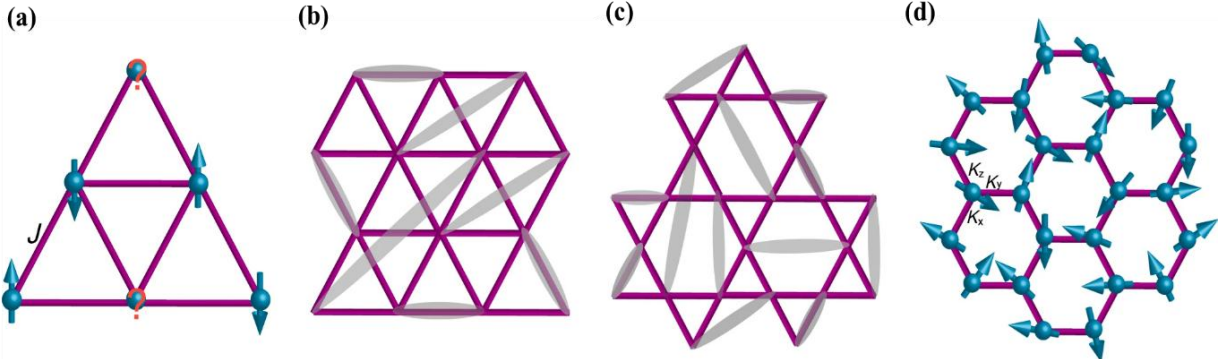


Figure 3: Instances of geometrically frustrated lattices (a, b) Triangular, (c) Kagome, and (d) Honeycomb. Blue arrows and grey ovals indicate quantum spins and spin-singlet, respectively. From Wen et al., 2019 [29].

In general, the fluctuation in a spin liquid can be classical or quantum. In the classical limit ($S \rightarrow \infty$ or $S \gg 1/2$) and the non-trivial commutation relation vanishes. Classical fluctuations are dominated by thermal fluctuations and geometric constraints, where the system undergoes a transition among different microstates. The fluctuations tend to decrease or cease totally as $k_B T \rightarrow 0$ and the system tends to attain an ordered state. In the case of quantum spins, where S is comparable to $1/2$, the quantum fluctuations are present even down to zero kelvin, known as zero-point energy, owing to the uncertainty principle. In contrast to classical spin liquids, quantum fluctuations in QSL are phase coherent and highly entangled and are in a superposition state of non-localized (long-range) spin configurations, as shown in **Figure 3 (b, c)**, where light shaded ovals are singlet pairs. This phase exhibits exotic features such as fractionalized excitations, which arise from its underlying gauge factor and topological character. These emergent quasiparticles are created in multiple pairs only. Such spin systems with high macroscopic ground state degeneracy induce strong thermal and quantum fluctuations, preventing any long-range ordering.

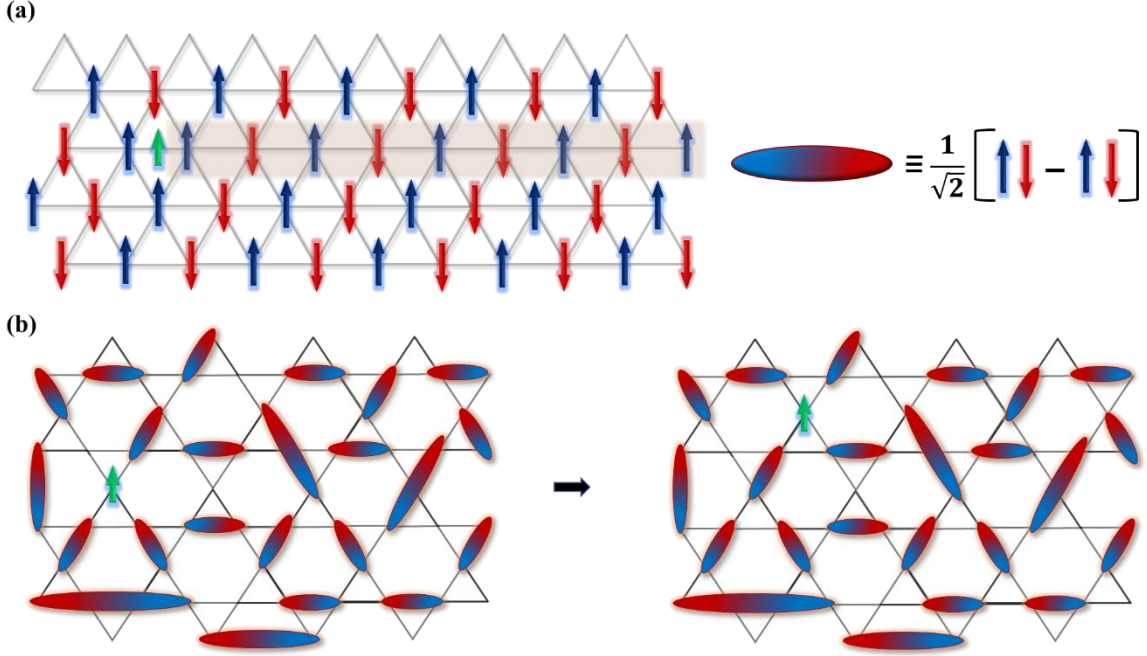


Figure 4: (a) Formation of Spinons (green arrow) by flipping the chain of spins (shaded region) on a quasi-1D lattice, (b) spinons (Kagome lattice) an unpaired spins (green arrow) which can move around via rearranging the valence bonds. The oval-shaped figure symbolizes a singlet pair.

QSL states are highly probable to be found in Magnetic insulators or Mott Insulators [30-32]. Theory predicts the presence of exotic quasiparticles that emerge from the collective excitation of the interacting spin system called spinons as shown in **Figure 4**. Unlike electrons (fermions) with spin $S = 1/2$ and charge $\pm e$ and phonons (or magnons) having integer spin ($S = 1$ for magnon and $S = 0$ for phonons), spinons are chargeless entities; however, they carry spin. Hence, it can support a chargeless conduction of heat, as electrons do in the case of metals. Spinons in 2D are much more mobile as compared to 1D, where they form the domain-wall like objects separating two antiferromagnetic ground states, which requires a coherent flip of an infinite number of spins. In the case of finite 1D chain, the energy cost is reduced due to the presence of a boundary, as also shown in **Figure 4 (a)**, where creating a spinon (yellow arrow) requires flipping of the chain of spins (shaded region). However, the spinon cannot hop between the chains as that would require coherent

flipping of an infinite number of spins in different counterpart chains. In 2D, they can be treated as an “empty place”, which in fact is an unpaired spin in a valence bond. Such an orphan spin can move around at a low energy cost by rearranging the nearby valence bonds, as also shown in **Figure 4 (b)** [22,33].

The characteristics of the high-dimensional (2D and 3D) QSL states may vary. Spinon may follow bosonic [34] or fermionic [35] or even anionic statistic and the associated excitations may be gapped, gapless, or the other kind (such as algebraic) [36] depending on the strength of interactions. The crucial aspect is how Spinons are also coupled to an underlying gauge field, which can be $U(1)$, Z_2 , or other in nature. The spin liquid state can be thought of as a deconfined phase where it is related to the lattice gauge coupled to the matter field. However, a complete analytical theory is still lacking to comprehend the possibilities these materials may hide.

2. Fundamental components of Quantum Spin Liquid

Landau’s classification of phases based on symmetry-based order in condensed matter is not applicable in case of quantum spin liquids [5]. In fact, a topological order [11,37-39] is associated with such an exotic phase which possess non-trivial long-range quantum entanglement [33,37]. Some of the key concepts that are crucial for the classification of a QSL state are topology, quantum entanglement, and gauge field theory. Next, these aspects will be discussed in brief detail in this section.

2.1 Topology

Topology is a branch of mathematics that introduces the mathematical structures that remain unaltered under continuous deformation. It is also known as “rubber-sheet geometry” as objects can be stretched, twisted, and contracted like a rubber without tearing them. For instance, in Euclidean geometry, a square (\square) is topologically equivalent to a circle (\circ) but

not to a symbol of infinity (∞). Such topological properties are also found in quantum systems in nature, where they appear due to boundary conditions imposed on the wave function. The boundary conditions can transform a flat surface into a space with twists or holes, and are responsible for inducing the topological nature. For instance, in the case of periodic boundary conditions, a line can be transformed into a circle, a hollow cylinder into a torus [40].

The interlinks of topology, geometry, and properties of quantum systems are well known. For instance, the topological phase, which is based on the geometry of single-electron wavefunctions, is the Integer Quantum Hall Effect (IQHE), where electron motion is constrained in a plane exposed to a strong magnetic field, leading to quantized transport properties [41]. Topological theories such as Chern-Simons theory, which was framed to explain FQH fluid, along with some QSL states. The crux of such a theory is that it lacks a notion of geometry (space-time intervals). This implies $\hat{H} = 0$, and all states are degenerate with zero energy. The extent of this degeneracy depends on the topology of the underlying space. The effect of the topology of the manifold can be seen in the case of a periodic 2D lattice, where the corresponding topological space is a torus. The consequence of such a topological feature is that it leads to a robust degeneracy [42].

The Hall conductivity in IQHE was found to be an integer multiple of $e^2/2\hbar$. The phenomenon was explained well in terms of Landau levels, which are the eigenstates of the electron moving in the presence of a magnetic field in a free space. However, another deeper perspective was proposed by Thouless, Kohmoto, Nightingale, and den Nijs in 1982 in order to comprehend the physics of electrons in a periodic potential. Their approach considers the topological aspects (TKNN integers or Chern numbers) to explain the robustness and quantization observed in IQHE [43]. This proposal was further complemented by Haldane a

few years later, where he showed how IQHE could arise even in the absence of an external magnetic field using a simple crystal model [44].

2.2 Quantum entanglement and Anyons

Quantum entanglement is a crucial aspect in describing QSLs. It is the phenomenon when certain properties of two or more particles are linked in such a way that they share the same quantum state (spin, polarization), defying the classical notion of space-time [45]. The measurement of one observable spontaneously affects the other. Such a state cannot be written as a product state even under a local change of basis. A spin singlet of two spins is one example, which gets more complex in the context of many-particle strongly correlated systems in the thermodynamic limit. An example of a highly entangled state can be found where a non-zero gap is consistently maintained above the ground state while the ground state wavefunction goes under a continuous deformation in response to the variation of local Hamiltonian parameters [46,47].

In systems like QSLs, the highly entangled ground state cannot be continuously deformed into a product state while staying within the phase. Classification of QSLs can be done depending on a variety of quasiparticle excitations (gapped or gapless). It can be a local particle-like excitation (fermionic, bosonic, or anyonic) that can have fractional quantum numbers. For instance, some support gapless, chargeless $S = 1/2$ fermionic excitations, i.e., spinons [48], whereas some excitations behave like a topological object (vortex). Further, even a bosonic quantum spin liquid for integer spin-S has also been proposed [49].

In quantum mechanics, exchange of two identical particles does not change the probability $|\psi(r_1, r_2)|^2 = |\psi(r_2, r_1)|^2$. It consequently imposes symmetry constraint on the allowed wavefunctions i.e., $\psi(r_1, r_2) = \pm \psi(r_2, r_1)$, where +/- implies bosons/fermions, having distinct statistics which is also reflected in the thermodynamic observables. Interestingly, in

2D, quantum mechanics allows distinct ways of exchange phenomenon described as $\psi(r_1, r_2) = e^{i\phi}\psi(r_2, r_1)$, here ϕ is an arbitrary constant ($\phi = n\pi$; $n \in \mathbb{Z}$ and is odd (even) for fermions (bosons)) [50,51]. To get an idea the exchange process is also schematically represented in **figure 5**. In the process of exchange, the individual particles end up at the same place where they started, where they may even move around each other. It can occur in variety of ways one is shown in Figure 5 (a) $r_1 \rightarrow r_1$ and $r_2 \rightarrow r_2$. In the process to exchange the particle in a counterclockwise path from $r_1 \rightarrow r_2$ a phase factor, $e^{i\phi}$, is acquired ($e^{-i\phi}$, for clockwise). This is equivalent to a half loop in the reference frame of one particle as shown in **figure 5 (b)**. However, a complete loop or double exchange, $e^{i2\phi}$, phase is acquired as shown in **figure 5 (c)**, and is also known as winding or braiding. In the case of anyons the phase (ϕ) $n \notin \mathbb{Z}$, and each n is related to distinct topological process which is independent of the size and shape of the exchange path or closed loop. One can smoothly distort the path but the number of times particles braid around each other may remain unchanged [52,53].

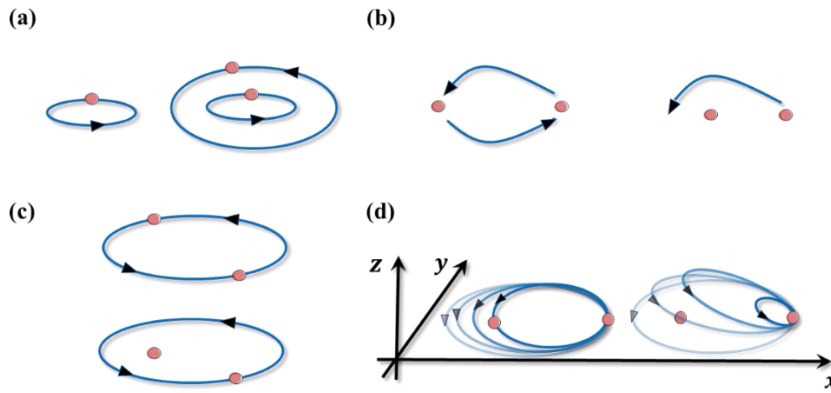


Figure 5: Schematic representation of various ways of exchanging quantum particles. (a) the particles end up back to the same positions. (b) exchange is equivalent to half a loop of one around another (in its rest frame of reference) and introduces a phase factor $e^{i\phi}$. (c) indicates complete loop or two- exchange and induces phase factor of $e^{i2\phi}$. (d) Effect of dimensionality on topological distinctness of various paths.

Unlike 2D, in 3D, the exchange processes are topologically equivalent, owing to the extra dimension which allows to move past the paths, shrinking all loops to zero as also shown in figure 5 (d). That means, in 3D, the swapping of places twice produces the same result as if the particles has not been exchanged at all. Also, a counterclockwise path can be smoothly transformed to clockwise implying $e^{i\phi} = e^{-i\phi}$ or $e^{2i\phi} = 1$ (bosons or fermions). However in 2D case one is not restricted to just bosons and fermions, but can have any exchange statistics and are known as (Abelian) anyons. [1,54].

Interestingly unlike Abelian anyons, non-abelian anyons exchange do not follow commutation relation and the state depends on the order of braiding [55]. Such a characteristic is crucial to store robust (topologically protected) information non-locally in topological qubits and naturally provides a fault tolerant quantum computation and has been proposed for, Majorana particles, theoretically proposed to exists in the fractional quantum hall state where such composite fermions together form a superconductor [52,53,56-59] and in Kitaev quantum spin liquids [60,61].

2.3 Gauge field theory

There are varieties of QSLs which can be classified by different patterns of long-range quantum entanglement which is crucial in dictating whether the excitation spectrum is gapped or gapless. There are certain mathematical groups used to name or classify the excitations in QSLs, such as Z_2 and $U(1)$. Most promising theoretical framework to classify, has been put forward is by involving emergent gauge fields, which are analogous to the vector potential quantity in electrodynamics [62]. Gauge theory encodes the consequences of non-local entanglement very well. The low-energy excitation in QSLs, where no spinon bound state exist (free spinon propagation), has been captured by deconfined gauge theory [4,11,15].

Different methods have been developed to describe the QSL state, such as, resonant-valence-bond (RVB) and slave-particle approach [11,19,37,39,63]. The slave-particle approach decomposes electron operator into fractionalized degree of freedom i.e., fermionic spinon for spin and a bosonic particle for charge. Such a representation enforces inherent constraints and results in an emergent lattice gauge field, which is instrumental to understand the interaction between fractionalized quasi-particles [64]. The mapping between the spin operator and the particle operator introduces the redundancy. For instance, for a lattice where spin resides on the bond between lattice points, the Abrikosov fermion representation of spin operator at i^{th} lattice site is, $\vec{S}_i = \frac{1}{2} f_{i\alpha}^\dagger \sigma_{\alpha\beta} f_{i\beta}$, here $f_{i\alpha} / f_{i\beta}$ is the annihilation/creation operator of the fermionic spinon at i^{th} site with spin α / β and $\sigma_{\alpha\beta}$ is the Pauli matrix [11]. Further the constraint of single spinon on each spin site requires $\sum_\alpha f_{i\alpha}^\dagger f_{i\alpha} = 1$. Interestingly, if the fermionic spinon acquire a phase, the spin operator remains unchanged under the transformation $f_i \rightarrow f_i e^{i\varphi}$. Such a symmetry is local, such that the phases of the spinon operator on each site can be independently chosen and the physical spin operator remain invariant. This is known as $U(1)$ local gauge symmetry, which arises from slave-particle approach of spin system [65,66]. In 3D pyrochlore lattice, where system enters a $U(1)$ QSL state, the emergent magnetic monopole-like excitations is linked to the emergent photons [67,68].

Another significant result of slave-particle approach is found in the exactly solvable spin-1/2 Kitaev honeycomb model, where Ising-like nearest-neighbour exchange interactions are present. Here, the exact solution was obtained by slave-particle representation of spins using four Majorana fermions in an extended Hilbert space [60]. Kitaev showed that the underlying physics of such a model can be understood by studying a system of Majorana fermions coupled to a static Z_2 gauge field and the ground state turns-out to be a gapless Z_2 QSL with

gapless (or gapped) Majorana fermions (fractionalized excitations) and gapped Z_2 gauge flux excitations. Here, the magnetic flux in the Ising gauge field only takes two values i.e., (0,1) or (1,-1), indicating ground state and excited states [60,69,70]. A brief theoretical description is mentioned in section 3.1. In the 2D model, consist of two gapped particle type of anyonic excitations i.e., (i) ‘ A_e ’ (electric particle), which carries Ising gauge charge and (ii) ‘ A_m ’ (magnetic particle), that carries Ising gauge flux. These two anyons can interact and form a bound state (A_{e-m}), such that the wavefunction sign changes when A_e braids/winds around A_m . Interestingly both ‘ A_e ’ and ‘ A_m ’ follows bosonic statistics but ‘ A_{e-m} ’ which appear due to their mutual braiding follows fermionic statistics. For systems having spin rotation symmetry it has been shown that ‘ A_e ’ particle carries spin-1/2 (bosonic spinon), while ‘ A_m ’ has spin-0 (vison). Their bound state ‘ A_{e-m} ’ carries a spin-1/2 and known as fermionic spinon [71-73].

An analogy of the excitations in Kitaev model can be found in Bardeen-Cooper-Schrieffer superconductor, where excitations are Bogoliubov quasiparticle (broken Cooper pair) and quantized magnetic flux ($h/2e$) vortices [74]. In search of high-temperature superconductivity in doped-Mott insulators [20], Z_2 quantum spin liquids can be considered as a phase-disordered version of superconductors where the fermionic spinon can be identified similar to the Bogoliubov quasiparticle and visons as the quantized magnetic flux vortex [75,76].

In a general approach, it can be extended to more complicated gauge structures to classify a range of spin liquid states. The mean field approach predicts four families of spin liquids in (2+1) dimensions, which are characterized by the nature of the energy gap between the ground state, spinon, and the gauge excitations. For instance, **(a)** Rigid spin liquids: these are topologically ordered, where both spinon excitations and the excitation in the gauge field have a non-zero energy gap.

Table I: Quantum Spin Liquid candidates.

Material	T_{mag}	Structure	Notes	Ref.
1T-TaS ₂	< 20 mK	Triangular	Gapped Z_2 or Dirac spin liquid	[77-79]
YbMgGaO ₄	< 40 mK	Triangular	Gapless U(1) QSL	[80-82]
KYbSe ₂	290 mK	Triangular	Gapped Z_2 QSL	[83-85]
κ -(BEDTTTF) ₂ Cu ₂ (CN) ₃	< 32 mK	Triangular	Gapped valence bond glass	[86-88]
ZnCu ₃ (OH) ₆ Cl ₂	< 50 mK	Kagome	Gap closes under applied magnetic field	[89,90]
Cu ₃ Zn(OH) ₆ FBr	< 20 mK	Kagome	Gapped Z_2 QSL	[26,91]
Na ₄ Ir ₃ O ₈	< 75 mK	Hyperkagome	Gapped Z_2 QSL	[92,93]
PbCuTe ₂ O ₆	< 20 mK	Hyperkagome	Gapless fermionic magnetic excitations	[94]
Ce ₂ Zr ₂ O ₇	< 35 mK	Pyrochlore	U(1) QSL	[95,96]
Pr ₂ Zr ₂ O ₇	< 100 mK	Pyrochlore	Gapless U(1) QSL	[97,98]
YbBr ₃	< 100 mK	Honeycomb	Plaquette-type fluctuations in the absence of Kitaev-type interactions	[99]
VPS ₃	< 60 K	Honeycomb	Signature of enhanced fractionalized excitations in low dimensions.	[100-103]
Na ₂ IrO ₃	15 K	Honeycomb	Gapped to a gapless KSL on application of the magnetic field	[104,105]
α -Li ₂ IrO ₃	15 K	Honeycomb	Pressure dependence of structure and magnetic phase.	[104,106-108]
β -Li ₂ IrO ₃	38 K	Hyperhoneycomb	KSL and topological Weyl States	[109,110]
γ -Li ₂ IrO ₃	39.5 K	Stripyhoneycomb	3D Kitaev–Heisenberg spin system	[109,111,112]
α -RuCl ₃	8 K	Honeycomb	The nature of excitation can be tuned via external magnetic field and pressure.	[113-115]
Cu ₂ IrO ₃	2.7 K	Honeycomb	Proximate KSL	[116,117]
H ₃ LiIr ₂ O ₆	< 50 mK	Honeycomb	Gapless KSL	[118,119]
Na ₂ Co ₂ TeO ₆	< 30 K	Honeycomb	Magnetic ground state still under debate	[120-123]
Na ₃ Co ₂ SbO ₆	< 5 K	Honeycomb	Application of pressure, magnetic field, and doping tunes the KSL state	[124-126]
TbInO ₃	< 0.4 K	Triangular-honeycomb	QSL and ferroelectric phase coexists	[127-130]

Hence, low-energy excitations are absent, which stabilizes the QSL phase, as also observed for Z_2 -gapped liquids and chiral liquids [49]. **(b)** Bose spin liquids: in this class of spin liquids, the spinon excitations have an energy gap, whereas gapless $U(1)$ gauge-boson excitations are present. However, these states are not stable in (2+1) dimensions [131]. **(c)** Fermi spin liquids are gapless, where short-range ($S=1/2$) spinon excitations are present. In addition to that, the electronic excitations also remain gapless. Some of the examples are Z_2 - quadratic, Z_2 - gapless liquids; here, classification refers to the nature of spinon dispersion [33,132,133]. Finally, **(d)** Algebraic spin liquids, which feature excitations where the massless fermions are coupled to a $U(1)$ gauge field, for e.g., $U(1)$ -linear liquids [134]. A general list of Quantum spin liquid candidates on various lattices is mentioned in **Table I**.

For more detailed approach to the theoretical aspect, we would like to propose the reader to refer some of the review articles [1,22,33,135-137].

3. Kitaev Spin Liquids (KSL)

3.1. Theoretical Framework

In 2006 Alexei Kitaev [60], proposed an exactly solvable $S=1/2$ spin model on a 2D Honeycomb lattice as shown in **Figure 3 (d)**. Here, the geometrical frustration factor is absent; in fact, the anisotropic interaction between spin-pairs on different honeycomb lattice bonds induces a conflict giving rise to strong frustration and a spin-liquid ground state. The presence of fractionalized excitation, i.e., Majorana fermions, naturally comes out of the solution of this model. These topological excitations are fault-resistant in nature and can be utilized for quantum technologies [61]. The potential signature of Kitaev spin liquid has been evidence for numerous candidates such as Na_2IrO_3 [138], (α , β and γ) - Li_2IrO_3 [104,109,139], α - $RuCl_3$ [140], VPS_3 [100,102] and $H_3LiIr_2O_6$ [141]. All these materials are known to exhibit Mott insulating behavior. A clear signature of long-range ordering is also observed in these materials except $H_3LiIr_2O_6$. However, the ordering temperature is around one order of

magnitude lower than the interaction energy scale, which is unlike Curie-Weiss behavior and indicates the presence of magnetic frustration. A family of spin-orbit-assisted Kitaev materials where local, spin-orbit-coupled (SOC) $j=1/2$ moments form bond-dependent Ising interactions. These materials are often referred to as “spin-orbit assisted Mott insulators”. The interplay of U , λ (atomic SOC), and t leads to a rich phase diagram as shown in **Figure 6**. The narrow bands generated by the SOC are more susceptible to Mott localization by U .

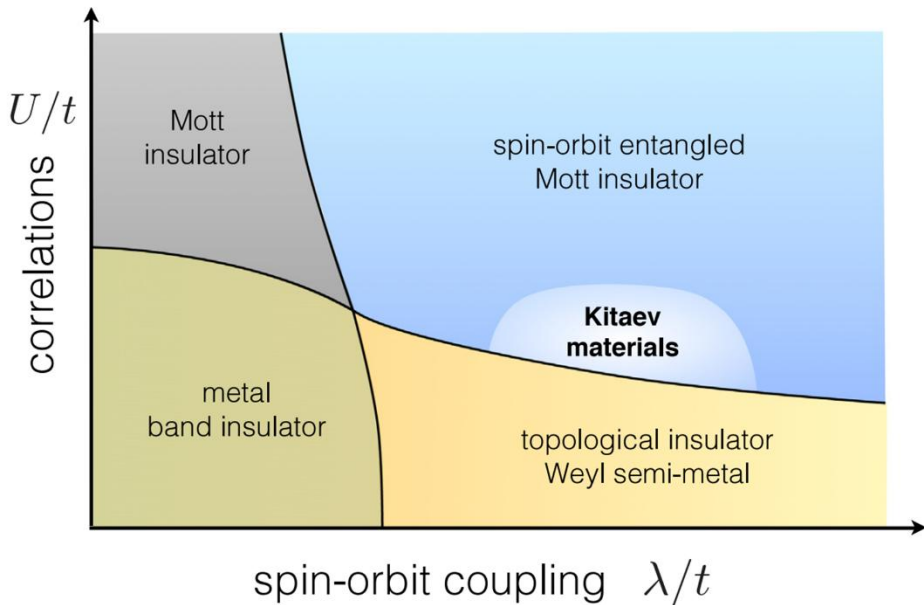


Figure 6: Phase diagram for quantum materials in terms of the interaction strength U/t and spin-orbit coupling λ/t . From Trebst et al., 2022 [142].

The interaction Hamiltonian for the Kitaev model on a honeycomb lattice with Ising-type nearest-neighbor interactions, as shown in **Figure 7**, is given as follows [60] :

$$H = - \sum_{\langle mn \rangle_\gamma} K_\gamma S_m^\gamma S_n^\gamma \quad - 5$$

Here $\langle mn \rangle_\gamma$ is a γ (x, y and z type) bond and the summation is taken over all the bonds around the hexagonal (honeycomb) lattice. K_γ is the nearest neighbor bond-dependent exchange coupling constant, $S = (S_m^x, S_m^y, S_m^z)$ is the spin-1/2 operator at m^{th} site. If we try to align all the spins along a specific direction, let's say the z -axis, $S_m^x S_n^x, S_m^y S_n^y$ and $S_m^z S_n^z$, do not commute and the bond energies along other directions (x and y) are not minimized. Consequently, spins cannot satisfy three different configurations simultaneously and lead to frustration as shown in **Figure 7**. This geometric magnetic frustration is inherent to lattices like Honeycomb, Kagome [143], and pyrochlore [144]. The ground state of the Kitaev model is highly degenerate even in the classical limit, where quantum spin is treated as vectors [145,146]. When quantum fluctuations are in effect, the system starts a transition between degenerate states, which can be considered as the superposition of all possible classical configurations.

The plaquette flux operator W defined over each hexagon of the honeycomb lattice commutes with the Hamiltonian, which is written as:

$$W = \sigma_1^x \sigma_2^x \sigma_3^x \sigma_4^x \sigma_5^x \sigma_6^x \quad -6$$

Here $\sigma_m^\gamma = 2S_m^\gamma$ are the Pauli matrices on m^{th} site, $\hbar=1$. The flux operator has quantized eigenvalues, i.e., ± 1 , which is the Z_2 flux through the hexagon, and different flux operators commute with each other, which further simplifies the problem, as this divides the Hilbert space into sectors of W eigenspaces. Majorana fermions are self-adjoint, which means they are their own antiparticle. Hence, any fermion mode gives rise to two Majorana modes, for instance, $M_1 = (a + a^\dagger)$ and $M_2 = (a - a^\dagger)$ where a^\dagger and a are creation and annihilation operators. Further, the exact solution of the Kitaev model is achieved by fractionalizing the spin degree of freedom, i.e., replacing the spin operator with four Majorana operators, such as

$\sigma_m^\gamma = i b_m^\gamma c_m$, where $\gamma = x, y, z$, b_m and c_m are Majorana operators that satisfy $c_m^2 = 1$, $c_m c_n = -c_n c_m$ ($m \neq n$). The constraint $b_m^x b_m^y b_m^z c_m = 1$, preserves both the $S-1/2$ algebra and the local 2D Hilbert space.

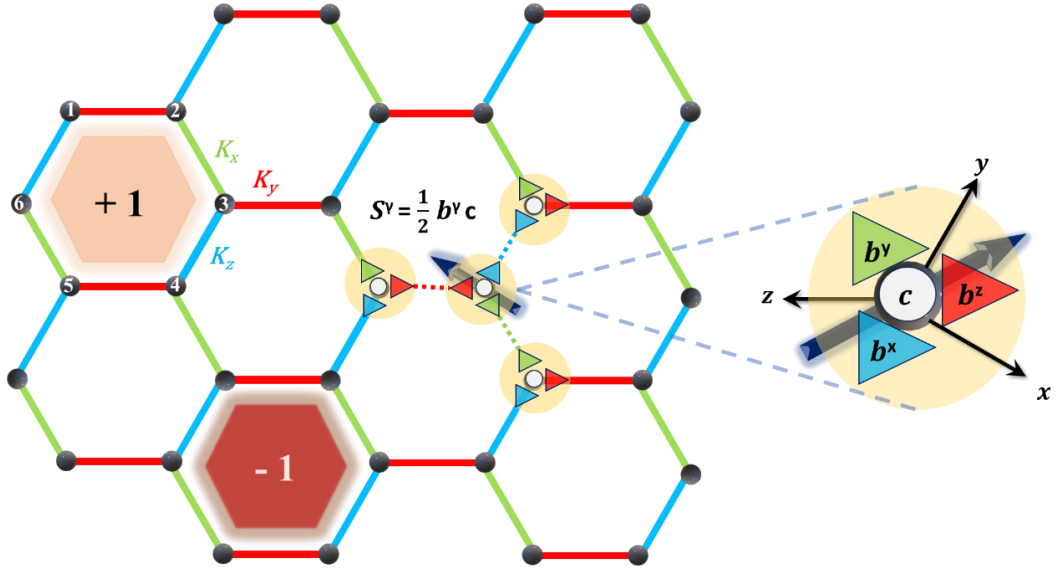


Figure 7: Spin interaction on a Honeycomb structure having bond-dependent Ising interactions as shown in green, red, and blue bonds with interaction strengths K_x , K_y , K_z , respectively. W is the Plaquette flux operator having conserved eigenvalues (± 1) as discussed in the text. The fractionalization of a single spin into localized b^γ and itinerant c Majorana Fermions as shown in the zoomed illustration.

Hence, the revised form of Hamiltonian for this model is written as:

$$H = -\frac{1}{4} \sum_{\langle mn \rangle_\gamma} K_\gamma u_{mn}^\gamma c_m c_n \quad -7$$

Here $u_{mn}^\gamma = b_m^\gamma b_n^\gamma$ is the nearest neighbour bond operator and have an eigenvalue $\pm i$ as also shown in **Figure 7**. u_{mn}^γ operator also commutes with the Hamiltonian, hence is conserved, and the Hilbert space is divided into two eigen spaces of u_{mn}^γ , then it can be replaced by a number, and finally, the solution corresponds to free Majorana fermions (MFs), which correspond to c . As there are four MFs assigned to each spin-1/2, another physical subspace

is introduced by gauge field transformation, where itinerant MFs combine to form a static Z_2 gauge field that is associated with b^γ and the restricted eigenvalue of the W operator given as $w = \pm 1$. $w = 1$ corresponds to the vortex-free ground state, and $w = -1$ is regarded excited state Z_2 vortex, as also shown in **Figure 7**. Hence, u_{mn}^γ , leads to an emergent Z_2 gauge field and dictates the phase of the nearest neighbour tunnelling integral of c -MFs, and are also termed as matter fermions. Magnetic anisotropy dictates the ground state phase of the Kitaev magnets. The energy spectrum is gapless for weakly anisotropic coupling constants K_γ . However, the gap appears if one of the couplings is greater than the other two combined. In the case of the gapless phase, the Dirac point can acquire a finite gap on the application of an external magnetic field, and this topological phase transition is driven by broken time-reversal symmetry perturbations. This gives rise to a chiral spin liquid phase, which has non-zero Chern invariants, also termed as Majorana Chern Insulators. For instance, in the presence of an external magnetic field H , a Majorana gap is induced, which is $\Delta \approx H_x H_y H_z / K^2$, where all the exchange couplings are kept constant or isotropic ($K_x = K_y = K_z = K$) [60]. For the case of isotropic exchange interactions, the spins fractionalize into gapless itinerant Majorana fermions forming gapless Dirac cones with linear dispersion at the K-points of the honeycomb Brillouin zone and a gapped Z_2 vortices, also known as visons [147,148].

3.2 Proximate and Beyond-ideal Kitaev Materials

The Kitaev model is an exactly solvable spin liquid state, having a spin $S=1/2$ (local magnetic moment) on a two-dimensional honeycomb lattice. Here, quantum spins are fractionalized into itinerant Majorana fermions and localized Z_2 fluxes, and various related physical observables such as the dynamic spin structure factor [149] and Raman response [150,151] have been computed exactly. The localized low-energy spin excitations consist of

both itinerant and immobile Majorana fermions (visons) and are reflected in the Q-independent spin response with an excitation gap in the spin structure factor [149].

The putative three-dimensional or quasi-2D Kitaev materials, such as α -RuCl₃ [152], A₂IrO₃ (A = Na, Li) [104], H₃LiIr₂O₆ [153] have been very well studied both theoretically [149] and experimentally [154]. However, the magnetic properties at low temperatures in the putative Kitaev materials were not well understood by the pure two-dimensional Kitaev model. It has been observed that the candidate materials show a long-range magnetic ordering at low temperatures [155], and a star-shaped low-energy feature is observed in inelastic neutron scattering experiments [140,156]. In general, the SOC leads to coupling between the spin-orbit wavefunction and anisotropic spin interactions. However, the presence of Jahn-Teller effect in most of the systems lifts the orbital degeneracy that partially inactivates SOC and leads to dominant XY or Ising anisotropic spin interactions/models. In systems where t_{2g} orbitals are partially filled, they are separated from higher energy e_g orbitals by octahedral crystal fields in the presence of SOC and form total angular momenta $j_{\text{eff}} = \frac{1}{2}$, interacting via entangled spin-orbit exchange interactions. Jackeli and Khaliullin proposed that the Kitaev model could be realized in Mott insulators with strong spin-orbit coupling along with a specific crystal structure, where the localized moments ($j_{\text{eff}} = \frac{1}{2}$) are interacting via superexchange coupling interactions. So, Heisenberg interactions are also present in addition to the Kitaev interactions, and because of that, there are various magnetic ordering states possible, depending on the relative strength and sign of the Kitaev and Heisenberg interactions [138].

Further, in 2014, Rau, Lee, and Kee found out another bond-dependent interaction known as the Gamma (Γ) interaction, which has the form of XY bond-dependent interaction that leads to further frustration of the Kitaev interactions [157], which enhances the complexity and interplay of multiple interactions of the underlying physics. The resultant Hamiltonian for

n.n. (nearest neighbour) sites n and m on a bond of type γ ($= x, y, z$) in an ideal octahedral environment have the following form:

$$H_{\langle n,m \rangle, \gamma} = J \vec{S}_n \cdot \vec{S}_m + K_\gamma S_n^\gamma S_m^\gamma + \Gamma (S_n^\alpha S_m^\beta + S_n^\beta S_m^\alpha) + \Gamma' (S_n^\alpha S_m^\gamma + S_n^\gamma S_m^\alpha + S_n^\beta S_m^\gamma + S_n^\gamma S_m^\beta) \quad -8$$

Here $(\alpha, \beta) = (y, z), (z, x)$, and (x, y) for $\gamma = x, y$ (and y'), and z , respectively, and Γ' appears due to the trigonal distortion [157].

The effect of non-Kitaev terms can be understood as the honeycomb lattice is a bipartite lattice, the Heisenberg interaction results in a magnetic order, and the Kitaev QSL is bound to a pure Kitaev limit. It was shown that when antiferromagnetic Heisenberg interaction, i.e. $J > 0$, is larger than $|K|$, AFM ordering occurs, while for $J < 0$ ferromagnetic order occurs.

However when $J \leq K$ with $J, K > 0$, a zig-zag kind of spin pattern appears; while, for $|J| \leq |K|$ and $J, K < 0$, a stripe type of ordering is found to appear [158]. Γ and Γ' interactions, in contrast, only add to the frustration. In the case where K and Γ dominate a transition between Kitaev QSL and other QSL phases can be achieved [159]. Interestingly, a hidden $SU(2)$ symmetry emerges via a six-site transformation which results in a magnetically ordered state when $K = \Gamma$ [160]. The system becomes more frustrated whenever these interactions have opposite signs. Γ' , the bond-dependent interaction is allowed when one of the C_2 symmetries is broken via trigonal distortion or layer stackings. It was shown that a zigzag magnetic order establishes via $FM\Gamma'$ near FM Kitaev limit [157]. In addition to that, the contribution from other than nearest neighbor interactions is found to contribute to the zig-zag order [161].

3.3. Effect of Dimensionality

The real proximate Kitaev materials have a finite extension in all three spatial dimensions. The effect of dimensionality comes into the picture, as quantum confinement enhances the quantum fluctuations, consequently destabilizing order. According to the Mermin-Wagner-

Hohenberg theorem, continuous symmetries cannot be simultaneously broken at a finite temperature in systems with dimension $d \leq 2$, having short-range or long-range interactions that decay fast with distance [162]. However, Heisenberg magnets (Ferro/anti-ferromagnets) do order at absolute zero temperature, in two dimensions.

The dimensionality of the Kitaev candidates plays an important role in determining the underlying physics. For instance, layered α -RuCl₃, KSL is present when an in-plane moderate external magnetic field (B) is applied. At the same time, the behavior is relatively contrary to theoretical expectations of QSL present only in out-of-plane fields. Recently in a report by Yang et al., in their layer-dependent study of magnons, magnetic anisotropy, structure and exchange coupling in thin α -RuCl₃, reported signatures of average off-diagonal exchange terms changes in the monolayer, due to picoscale distortions, which leads to a reversal of spin anisotropy to easy-axis anisotropy and simultaneously enhances the Kitaev interactions [163].

The effect of the stacking structure (order) has been studied for α -RuCl₃ and H₃LiIr₂O₆ [153,164]. In addition to that, the investigation of interlayer coupling for a bilayer Kitaev model, where two honeycomb layers are coupled by Heisenberg kind of interaction, the results indicate towards existence of a first-order quantum phase transition between a KSL and a dimer-singlet state. This suggests that KSL is a stable state in the presence of such an interlayer interference [165]. Another theoretical study on the fate of KSL in differently stacked bilayer version, showed that increasing the strength of J_{\perp} and the intralayer Kitaev coupling (K), destroys the topological spin liquid and instead favours a paramagnetic dimer phase [166]. The effect of interlayer coupling were further analysed by Merino et al. [167], where the Abrikosov fermion mean-field theory was employed to study the magnetic property of a multilayer (arbitrary number) Kitaev model, where honeycomb layers are stacked on top of each other and are coupled by Heisenberg interaction. Interestingly, the obtained solutions

are gapped and ungapped for even and odd layered systems respectively, and are attributed to the spontaneous symmetry breaking (non-breaking) for the inversion symmetry of the multilayer system. In addition, they found that the Kitaev gapped chiral spin liquid induced by an external magnetic field is stabilized by AFM interlayer coupling [167].

3.4. Effect of High-Spin and Disorder

The Kitaev spin liquid hosts nonlocal fractionalized excitations that include Ising anyons with Majorana zero modes, which follow non-Abelian statistics and may enable fault-tolerant topological quantum computation [59,61]. Originally exactly solvable Kitaev model was formulated for $S = \frac{1}{2}$ systems, however the Kitaev-type bond-dependent interactions have been realized for higher spin configurations. As the flux operator on each hexagon has been proposed to be conserved (Z_2) even for arbitrary spin-S Kitaev models [145]. For instance, in case of cobalt-based honeycomb materials with $3d^7$ where the perturbation processes via e_g orbitals suppresses non-Kitaev interactions, have been proposed and experimentally investigated as a putative Kitaev candidates [168-172]. Even the f-electron systems have also shown signatures of Kitaev coupling (antiferromagnetic) [173-175]. Interestingly, a double peak structure has also been reported for higher-spin Kitaev candidates, suggesting the presence of thermal fractionalization of Spin-S into two distinct quasiparticles [176-179]. Just like the $S = 1/2$ Kitaev model, for $S = 3/2$ using $SO(6)$ Majorana representation also results in itinerant Majorana fermion and Z_2 fluxes. However, unlike $S = 1/2$ case an additional interaction term between itinerant Majorana fermions are present for $S = 3/2$. Further, a qualitative difference has been observed between integer and half-integer spins, which appears in the anisotropic limit ($K_z \gg K_x, K_y$). Interestingly, the topological order is found only in the half-integer Spin configuration. Further, in recent years, a search for a stable QSL ground state for general spin (S), in the presence of other additional interactions, has taken centre stage as it is inevitable in the real candidate materials [179,180].

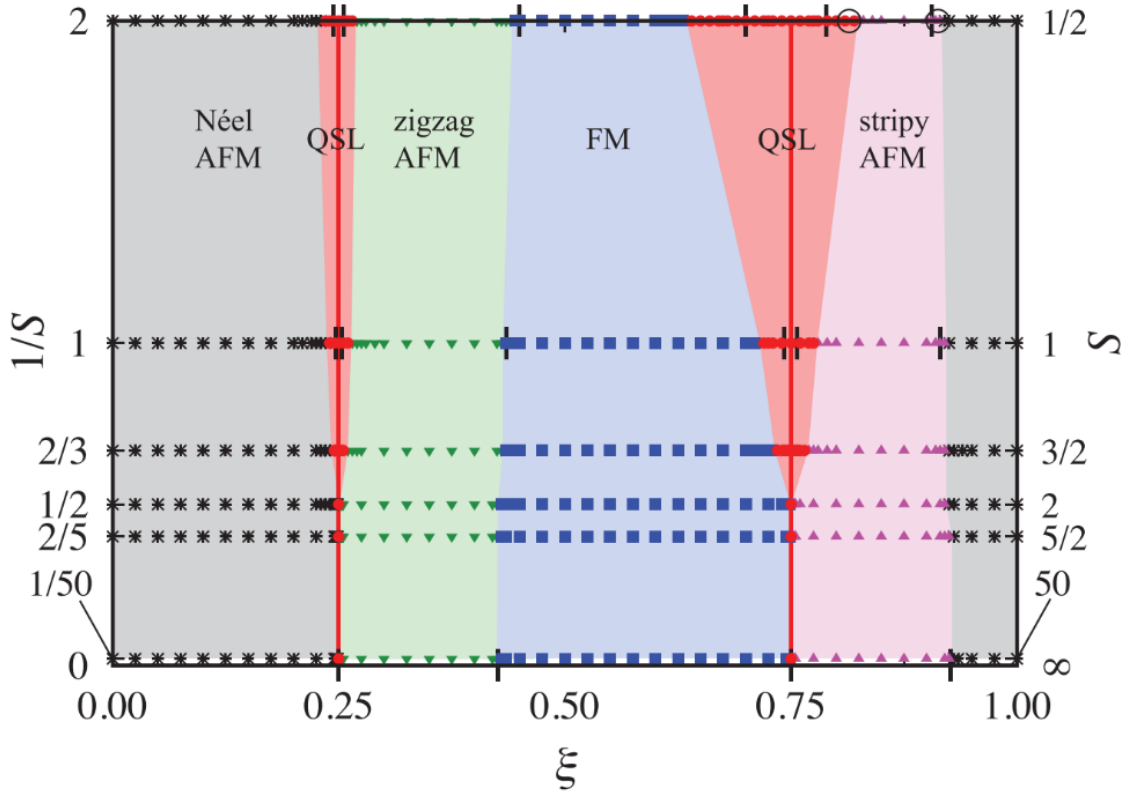


Figure 8: Ground-state phase diagram of the spin- S Kitaev-Heisenberg models. The two open circles in the results for $S=1/2$ indicate the phase boundaries obtained by the previous PFFRG study[181], while the vertical ticks for $S=1/2$, 1, and ∞ indicate the results obtained in the previous studies by the ED [158], DMRG [182], and classical MC [183] calculations, respectively. From Fukui et al., 2022 [184].

A spin- S Kitaev-Heisenberg models for the generalized spin- S honeycomb lattice, whose Hamiltonian can be described as: $H = (1/4S^2) \sum_{t=x,y,z} \sum_{\langle n,m \rangle_t} [2KS_n^t S_m^t + JS_n \cdot S_m]$, here the summation is over the pairs of nearest-neighbor sites n and m connected by t bond, and S_n^t is the t^{th} component of the spin- S operator at the n^{th} site. The first and second terms signify the Kitaev (K) and Heisenberg (J) interactions, whose coupling strength can be parametrized as $K = \sin(2\pi\xi)$ and $J = \cos(2\pi\xi)$ respectively, where $\xi \in [0,1]$ and unit of energy is taken as $\sqrt{K^2 + J^2} = 1$ [184].

The ground-state phase diagram of such a spin- S Kitaev-Heisenberg model in **Figure 8** summarizes the results of pseudofermion functional renormalization group (PFFRG) calculations for $S = 1/2$ to $5/2$ and 50. Further the results proposed that, similar to the $S = 1/2$ case, in addition to four magnetically ordered phases, the phase diagram for higher S also shows signatures of QSL phases in the vicinity of the pristine ferromagnetic and antiferromagnetic Kitaev models. For $S \geq 2$, the KSL phase vanishes rapidly, which is expected as one enters classical domains. However, the phase boundaries between the ordered phases remain mostly unperturbed [184]. Surprisingly, a broad continuum in the dynamical spin structure factor is reported even in the classical limit [185,186]. Some of the high spin candidate materials for $S = 1$ are nickel oxides $A_3Ni_2XO_6$ ($X = Bi, Sb, A = Li, Na$) [187], and $Na_2Ni_2TeO_6$ [188,189]. Chromium based compounds such as $CrBr_3$ [190], CrI_3 [191,192], $CrGeTe_3$ [193], and $CrSiTe_3$ [194] have been reported for $S = 3/2$ Kitaev candidate.

In a recent theoretical study on the effect of higher spin impurities ($S = 1$ and $S = 3/2$) in the pure KSL revealed that (i) the local behavior of KSL depends on value of spin i.e., integer or half integer spin ; (ii) Z_2 fluxes binds with the magnetic impurities in the lattice similar to vacancies and quasi-vacancies and (iii) for $S = 3/2$ impurities, a reentrant bound-flux sector was observed which is stable under finite magnetic fields [195]. The flux associated with the impurity site results in the formation of localized Majorana zero modes when the time-reversal symmetry is broken.

It was proposed by A.J. Willans that the vacancy binds a flux and induces a local moment, which can be polarized by an applied field [196]. For the case of a spin-half Heisenberg chain, when no disorder is present, the susceptibility remains finite at low temperatures [197]. However, site dilution creates free chain ends and leads to a Curie contribution [198] to the susceptibility and the disorder in the exchange interaction lead to the formation of random

spin singlets [199], which diverges the low-temperature susceptibility [200]. In higher dimensions, it is found that the vacancy induces a local moment and Curie-like response [201]. Such a local moment around the vacancy can be probed using a local probe such as nuclear magnetic resonance.

The introduction of vacancies into a KSL leads to a spectrum of quasi-zero-energy Majorana modes from which true zero modes emerge [202-205]. Recently, in the inelastic scanning tunnelling microscopic response of a Kitaev spin liquid containing a finite concentration (1% - 4%) of vacancies, a well-defined quasi-zero voltage peak ($eV \ll J$) was observed in the tunnelling conductance, dG/dV , whose voltage and intensity were found to increase with vacancy concentration. The finite amount of vacancy acts as a tunnelling barrier between the tip and the substrate. Such a signal is interpreted as the signature of spin-liquid-based Majorana zero modes [206]. For the pure model (without any vacancies), the ground state is in the zero-flux sector, having $w = +1$ for all the plaquettes throughout the lattice [60,207]. However, the ground state for a site-diluted (small vacancy) model in the presence of weak magnetic fields belongs to a bound-flux sector [196,202-204,208]. Interestingly, in this case, $w = +1$ for the hexagonal plaquettes, but $w = -1$ for enlarged vacancy plaquettes (formed by three hexagonal plaquettes around each vacancy site). $w = -1$, in the enlarged plaquette leads to a non-Abelian Ising anyon [60] and stabilizes a localized Majorana zero mode in the ground state. The low-energy physics of such diluted KSLs is dictated by these vacancy-induced quasi-zero-energy modes, which result in a unique characteristic feature in the dynamical spin correlation functions. Surprisingly, it was found to mirror the single-quasiparticle density of states and showed a quasi-zero-frequency peak [209].

Phonon dynamics of a site-disordered Kitaev candidate was investigated by Dantas et al., via ultrasound measurements, where attenuation of sound provided a signature of spin fractionalization [210]. The disorder in real Kitaev materials leads to localised modes that

dictate the low-energy dynamics. Interestingly, under an applied magnetic field in the disordered system, the quasi-localized modes from quasi vacancies are found to affect the phonon self-energy parameters, but the sound attenuation coefficient remains unaffected and maintains its six-fold symmetry and linear temperature dependence at low temperatures. This highlights the persistent influence of fractionalized excitations, under an external magnetic field, despite disorder [210]. Random hopping of fractionalized excitations has been reported in the diluted Kitaev system α -Ru_{0.8}Ir_{0.2}Cl₃, via magnetic susceptibility, specific heat, and Raman scattering measurements [211]. At intermediate energy range (> 3 meV) of Raman spectra, they observed a linear ω -dependent Majorana-like excitations, obeying Fermi statistics. This indicates robustness of a Kitaev paramagnetic state under spin vacancies. In the lower energy range (< 3 meV), a power law dependence and quantum-critical-like scaling of thermodynamic quantities is observed, which implies the presence of a weakly divergent low-energy density of states [211].

Another instance where Ru-spin vacancies are substituted in the form of Ir³⁺ (Ru_{1-x}Ir_xCl₃), which destabilizes the long-range ordering that arises due to non-Kitaev terms in the Hamiltonian. It was found that with increasing x, the zigzag low-temperature magnetic ordering suppresses and disappears completely for $x > 0.3$, as also shown in **Figure 9 (a)**. In addition to T_{N1} (7 K) zigzag transition of the parent compound, another second feature is observed at $T_{N2} \leq 14$ K for $x > 0$ [black arrow, **Figure 9 (a)** inset] and is attributed to the stacking faults. The low-temperature susceptibility does not decrease monotonically with x, but instead increases over the range $0.07 < x < 0.16$. Such a behavior arises due to non-magnetic impurities. Site-diluted Kitaev model also showed such an increase in local susceptibility [196,208,212].

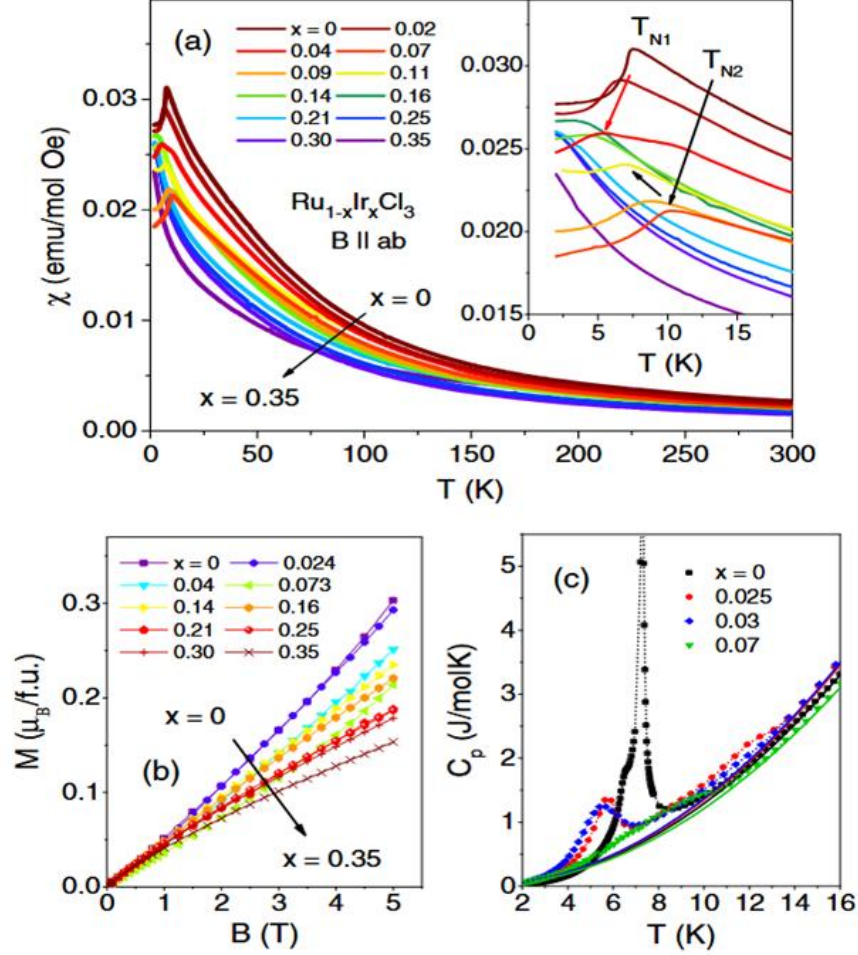


Figure 9: (a) Magnetic susceptibility of $\text{Ru}_{1-x}\text{Ir}_x\text{Cl}_3$ for different x with a magnetic field of $B = 1$ T applied in the ab plane. The inset shows a magnified low-temperature range. Red arrow and black/grey arrows mark the evolution of T_{N1} and T_{N2} , respectively. (b) Field-dependent magnetization at 2 K. (c) Heat capacity curves of crystals with small Ir concentration. Solid lines are an estimate of the lattice contribution. Dotted lines are a guide to the eye. From Kelley et al., 2017 [213].

The field-dependent magnetization at 2 K showed an upward curvature approaching the suppression of the zigzag phase near 7.5 T [214]. For $x > 0.09$, the field-dependent magnetization curves (**Figure 9 (b)**) develop opposite concavity from the clean limit. Interestingly, this coincides with the region of increase in the low-temperature susceptibility. The specific heat measurement showed the absence of a λ -like anomaly, indicating no long-range ordering transition above 2 K, see **Figure 9 (c)**. Further, the signatures of fractionalized

excitations are found over the full range of x , in the inelastic neutron scattering experiment, which indicates the importance of Kitaev physics in the magnetically diluted RuCl_3 [213].

Recently in a Muon spin relaxation investigation of another Kitaev candidate $\text{H}_3\text{LiIr}_2\text{O}_6$, has revealed that even in the presence of finite true vacancies (non-magnetic impurities and quasi-vacancies originated from bond randomness), the Kitaev model can lead to a pileup of low-energy density of states. Also, they did not find any signature of magnetic ordering down to 80 mK, which is an indication of spin fluctuations [215]. The theoretical study by Yatsuta et al., on the vacancies in generic Kitaev spin liquids, found qualitatively that (i) Isolated vacancies carry a magnetic moment and (ii) pairs of vacancies on even or opposite sublattices gap each other with distinct power laws and reveal the presence of emergent gauge flux [216].

4. Experimental Probes for Quantum Spin Liquids

It has been a very challenging job to find candidate QSL materials and probe them experimentally. Still, a lot of progress has been made theoretically and experimentally for 1D, 2D, and 3D (D-dimension) materials. 1D uniform Heisenberg spin-1/2 chain does not have a gap in the triplet excitation spectrum and is in a disordered state for the isotropic case. Any sort of anisotropy may result in long-range ordering at 0K. Very well studied case for 1D is $\text{X}_2\text{Cu}(\text{PO}_4)_2$ ($\text{X}=\text{Sr, Ba}$) [217], KCuF_3 [218]. In 2D materials, the reduced dimensionality increases the quantum fluctuations, for example, in the case of Na_2IrO_3 [219], $\alpha\text{-Li}_2\text{IrO}_3$ [104] and $\alpha\text{-RuCl}_3$ [220], all have a honeycomb crystal structure. There have also been efforts to search for 3D QSL materials such as hyperkagome $\text{Na}_4\text{Ir}_3\text{O}_8$ [221] and $\text{PbCuTe}_2\text{O}_6$ [222], hyperhoneycomb $\beta\text{-Li}_2\text{IrO}_3$ [223], stripy-honeycomb $\gamma\text{-Li}_2\text{IrO}_3$ [112], Triangular $\kappa\text{-(BEDT-TTF)}_2\text{Cu}_2(\text{CN})_3$ [224] and 1T- TaS_2 [79].

Investigating for QSL state down to 0K is not practically possible; however, there are some experimental techniques that can provide some solid signatures. It is often considered that at a temperature below around two orders of magnitude of the magnetic exchange coupling can be taken as representative of the properties at 0K, provided there is no other phase transition present. Some of the experimental probes are discussed below; however, more focus is given on the spectroscopic technique, in particular, Raman scattering in the upcoming sections.

Experimental probes, like Magnetic susceptibility which can provide a crucial hint of magnetic ordering $\chi \approx C / (T - \Theta_{cw})$, here C is the Curie constant and Θ_{cw} is the Curie-Weiss temperature, which is an indication of the strength of exchange interactions. $\Theta_{cw} < 0$ indicates anti-ferromagnetic ordering and $\Theta_{cw} > 0$ indicates ferromagnetic ordering. In frustrated materials, by comparing Θ_{cw} with the temperature where the magnetic order freezes T_c , one can estimate the magnitude of frustration, which is defined by the frustration parameter as $f = |\Theta_{cw}| / T_c$. The value of $f > 5 - 10$, typically indicates strong frustration and the temperature range of $T_c < T < |\Theta_{cw}|$ defines the spin-liquid regime [225]. Some of the geometrically frustrated candidates of spin liquid state are κ -(BEDT-TTF)₂Cu₂(CN)₃ (triangular) with a $J \sim 250$ K, no magnetic order nor spin freezing is observed down to 20 mK, giving rise to a frustration index over 10,000 [224,226]. In the case of 1T-TaS₂ [79] even though the value of Θ_{cw} and J is significantly smaller than those calculated from high-temperature susceptibility in ref. [227]. This system goes under a series of charge density wave transitions on lowering temperatures. In the completely commensurate state below 180K, it forms a star of David cluster. The localised unpaired electron spin ($S = 1/2$) at the centre of the cluster forms a triangular network and adds to geometric frustration [77,228].

Specific heat can provide information about the low-energy density of states (DOS), which can further be verified from the theoretical predictions. In the case of magnetic ordering, it shows a λ -type peak in the specific heat vs temperature curve and reflects the presence of magnetic excitations at low temperatures. But in the case of QSL, such a sharp transition is absent unless a topological phase transition is present [229]. To obtain the residual magnetic entropy, which is an indication of long-range magnetic ordering at low temperatures, one has to carefully subtract the phononic contribution [230,231]. Thermal transport measurement is useful in determining whether the excitations are localized or itinerant [231,232]. The fractionalization of spin is also reflected in the specific heat measurements as two-well separated peaks, where the high temperature one corresponds to itinerant Majorana fermions and the low temperature peak corresponds to the flux ordering of the localized Majorana fermions (Z_2) [60,233,234] which is consistent with the theoretical prediction as well [154,235]. An expected two-stage release of magnetic entropy was reported for α -RuCl₃, γ -Li₂IrO₃ [236], β -Li₂IrO₃ [111].

Spectroscopic investigation via neutron diffraction provides the signature of magnetic ordering in the system [156]. The defining feature of QSL is the presence of fractionalized excitations i.e., spinons, which are deconfined from the lattice and have their own dispersions and become itinerant in the crystal. In U(1) gapless QSL, spinons form a Fermi sea similar to electrons in metals [237]. In order to detect the fractionalized excitations and to classify the QSL on the basis of the nature of correlation and excitation, crucial signatures are obtained from Inelastic and elastic neutron scattering. Inelastic neutron scattering (INS) is a spin-1 process where at least one spinon is excited during spin-flip and the spinon pair follows the energy-momentum conservation rule $E_q = E_s(k) + E_s(q-k)$, here $E_s(k)$ is the dispersion of spinons, and E and q are the transferred energy and momentum respectively. As many possible values of k satisfy this condition, hence a broad magnetic continuum both in

momentum and energy is observed in the excitation spectra. For the case of α -RuCl₃ the inelastic neutron scattering results at low temperature reveals (neutron scattering function $S_{\text{tot.}}(Q, \omega)$) an hour-glass shaped quasielastic excitation spectrum (extending to about 20 meV) centred at Γ -point with strong low-energy excitations around Γ -point and Y-shaped magnetic continuum of high-energy excitations. The low-energy feature in INS reflects on the quasielastic responses associated with the Z₂ flux excitations, and the Y-shaped Q- ω dependence of $S_{\text{tot.}}(Q, \omega)$, in the high-energy region reflects the dispersive itinerant Majorana fermions extending upto $\omega \sim |J_K|$ [140,149,238]. Further, the thermal evolution of $S_{\text{mag}}(Q, \omega)$ reveals that upon increasing temperature upto T~100K (Kitaev paramagnetic phase), the Z2 flux excitations are significantly reduced, whereas the high energy intensity is still maintained. However, that also loses spectral weight on further increase in temperature, and finally a featureless background is left (T >> 240K) as observed in the case of conventional paramagnets [140]. There are numerous reports for observation of broad continuum, such as for ZnCu₃(OH)₆Cl₂ (herbertsmithite) [239], Ca₁₀Cr₇O₂₈ [240], Ba₃NiSb₂O₉ [132], and YbMgGaO₄ [241,242]. This behavior is in contrast to the spin wave excitations in magnetically ordered systems, where a well-defined peak is observed around the ordering wave vector [243].

Another excellent spectroscopic probe is Raman measurements, which is a non-destructive technique that provides the signature of fractionalized low-energy excitations that are embedded in the spectral features [111,244]. A detailed discussion is done in the next section.

There are other various potential techniques as well such as tetra-hertz spectroscopy, where electromagnetic radiation of the frequency range of terahertz is ideal for investigating low-energy excitation. The temperature-dependent absorption across a wide range of frequencies can provide potential signatures of the QSL state [245,246]. In order to probe the dynamic local magnetic environment, Muon spin relaxation (μ SR) and nuclear magnetic resonance

(NMR) can provide a signature of magnetic ordering [227,240]. In addition, electron spin resonance (ESR) can be used to shed light on the dynamics of the spin state of unpaired electrons in the system and provides shreds of evidence of fractionalized excitations [86,247].

5 Inelastic Light Scattering Investigation (Raman)

Atoms and molecules in materials are in continuous motion even at absolute zero temperature, owing to quantum mechanical restrictions. Phonons (quasi-particles) are the quanta of lattice vibrations, just like photons are for light. Phonons emerge as the consequence of the breaking of continuous translational and rotational symmetry in solids. Inside the material, any quantum phenomenon emerges as a collective behavior of the system, and in this process, the underlying lattice does not remain untouched. So, the lattice degrees of freedom can couple with electronic and spin degrees of freedom and can provide vital information about the presence of other quasiparticles, such as magnons, excitons, Majorana Fermions, etc. It is crucial in quantum materials to identify the nature of low-energy excitations (magnetic or electronic) to shed light on the ground state properties. Light is an electromagnetic wave and consists of an oscillating, self-sustaining electric field $\vec{E}(\omega, t)$ and magnetic field $\vec{B}(\omega, t)$. It interacts with the electronic spin via two processes, which are direct and indirect coupling. In direct coupling, there is a magnetic dipole interaction between the oscillating magnetic field of light and the electronic spin of the magnetic ion. In indirect coupling, there is an electric dipole interaction that happens between the oscillating electric field of light and the electrons of magnetic ions, mediated by the spin-orbit coupling [248,249]. Among these two channels of interaction, the strength of indirect coupling is found to be much greater than the direct coupling.

Inelastic light scattering (Raman) measurement can simultaneously provide signatures of scattering from lattice, spin, and charge degrees of freedom via spin-phonon and electron-phonon couplings as shown in **Figure 10 (a)**. The Raman spectral signature for conventional

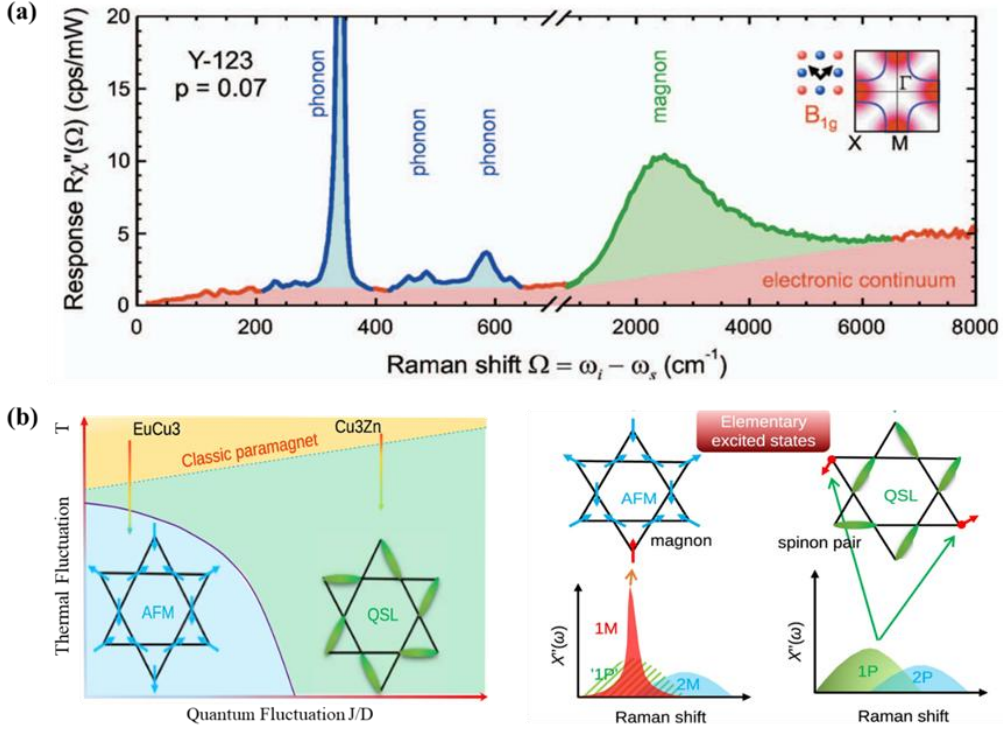


Figure 10: (a) Raman scattering response unveiling different kinds of quasi-particle excitations over a wide range of energy from an underdoped cuprate. Panel (a) is from Devereaux et al., 2007 [250]. (b) Increasing value of J/D drives the Kagome antiferromagnet into a QSL state from a chiral 120° configuration. The schematic compares the Raman responses for the antiferromagnetic and QSL states. 1M and 2M in AFM ordered state denote the one- and two-magnon excitations, whereas 1P and 2P denote the one-pair and two-pair spinon excitations, respectively. Panel (b) is from Fu et al., 2021 [91].

magnetic systems differs considerably from that of the QSLs. Sharp magnon (one/two) peaks are observed for the conventional magnetically ordered systems [251,252]; however, a broad magnetic continuum is a common feature for QSL systems [102,111,253,254], as also illustrated in **Figure 10 (b)**. Raman spectroscopy has proved to be a user-friendly and non-destructive technique based on inelastic light scattering to investigate the exotic features of

quantum materials, which we have discussed in the sections above. Unlike other spectroscopic techniques, such as INS, even a micron-sized sample will serve the purpose. Temperature, field, and polarization-dependent Raman scattering can provide crucial information about material properties such as the presence of structural/magnetic transitions, exotic quasiparticle excitations, etc. This information is embedded in the Raman spectra as background continuum, peak line shape, position, full-width at half maxima (FWHM), and spectral weight or area under the curve of a typical Raman spectrum.

5.1 Magnetic Excitations

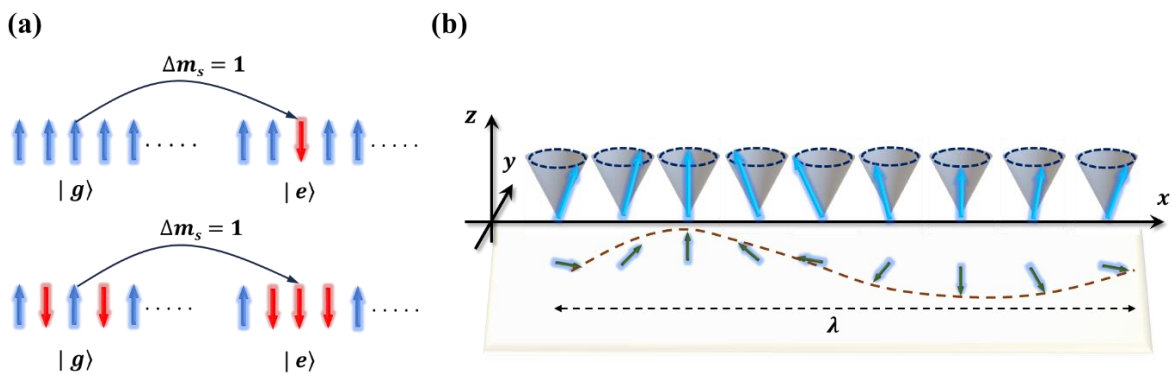


Figure 11: Raman scattering as a probe of magnetic excitations in (a) Ising type 1D Ferro and anti-ferromagnetic ordering and (b) illustration of propagation of a spin-wave of wavelength λ , along with its x-y plane projection.

Raman scattering from magnetic insulators comprises signals from phonons and magnetic excitations. The magnetic excitations in long-range ferro and antiferromagnets are magnons or also known as spin waves. Magnons are bosons with integer spin and obey Bose statistics. Magnons are the excitation that happens via spin flip, as also shown in **Figure 11 (a)** for a perfectly aligned 1D chain of Ferro and antiferromagnet having Ising type interaction, where $|g\rangle$ and $|e\rangle$ are the ground state and excited states, respectively. In the process of spin-flip, the total change in spin is $\Delta m_s = 1$, and it costs energy of $\Delta E = 8|J|S^2$. At any finite temperature, instead of perfect alignment, the spins precess about a quantization axis, which

is the direction of the internal field as shown in **Figure 11 (b)**, along with the x-y projection, where the dotted pattern signifies a propagating spin wave or magnon. The dispersion relation of this spin wave is given as: $\hbar\omega = 4JS[1 - \cos(qa)]$, where a is the lattice constant and q is the wavevector [255].

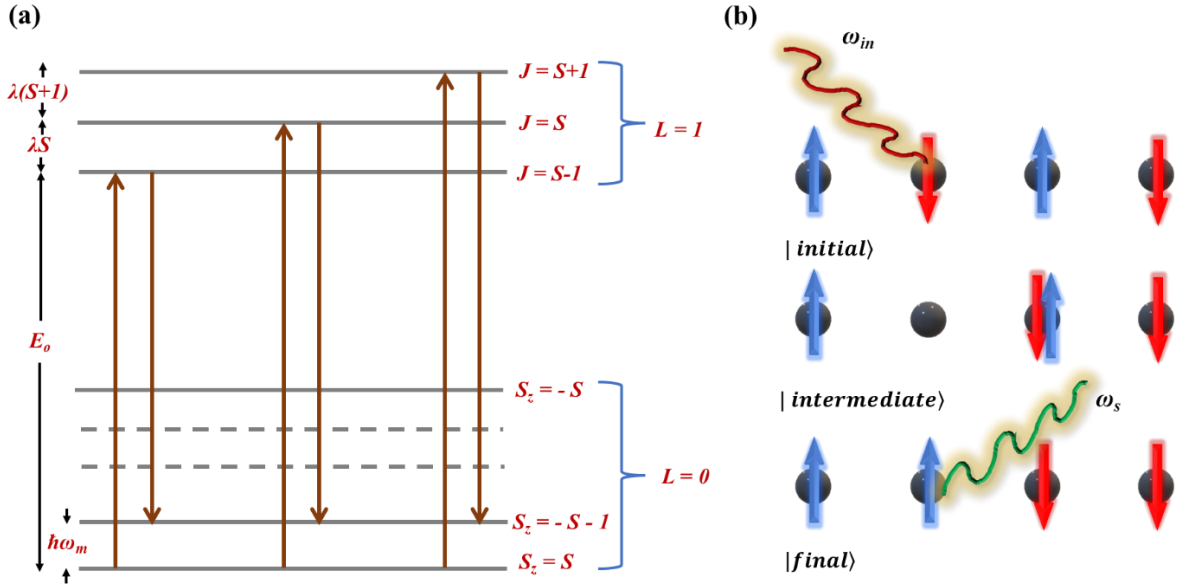


Figure 12: A schematic representation of (a) the principle of one-magnon scattering for a ferromagnet as discussed in the text, (b) a schematic representation of two-magnon scattering for an anti-ferromagnetic spin chain.

The Stokes/anti-Stokes Raman light scattering from one magnon involves two photons and one magnon, while for two magnons pair of magnons is created/annihilated. In terms of energy and momentum conservation, a one-magnon process in Stokes scattering, where an incident photon (ω_i, \mathbf{k}_i) scatters (ω_s, \mathbf{k}_s) after interacting with the spin, and generates a magnon (ω_M, \mathbf{q}) in the system, which can be written as: $\hbar\omega_i = \hbar\omega_s + \hbar\omega_M$ and $\mathbf{k}_i = \mathbf{k}_s + \mathbf{q}$. Here a single flip occurs via a transition from $S^z = S$ ground state to $S^z = S - 1$ via electrical transition with $L = 1$ as the intermediate state due to the presence of spin-orbit coupling $\lambda \mathbf{L} \cdot \mathbf{S}$, here λ is the spin-orbit interaction term, and the process is schematically shown in **Figure 12 (a)**.

In anti-ferromagnetic systems, two-magnon scattering arises from the exchange scattering mechanism which is based on double spin-flip due to coulomb interaction where the total z-component of spins is conserved [256]. Hence, this is a creation or annihilation of an even number of magnons which leads to a larger scattering cross-section as compared to one magnon case. In the case of two magnon, as shown in **Figure 12 (b)**, in Stokes Raman scattering the incident photon generates two magnon for which the energy and momentum conservation can be written as: $\hbar\omega_i = \hbar\omega_s + 2\hbar\omega_M$, $\mathbf{k}_i - \mathbf{k}_s = \mathbf{q}_1 + \mathbf{q}_2$. Generally, the laser used in the Raman scattering experiments which will generate the magnon has a wavelength in the visible range; for instance for a 532 nm the transferred momentum is $k \sim 10^{-3} \text{ \AA}^{-1}$, so one can only probe excitation near the zone center as Brillouin zone boundary is at $\pi \text{ \AA}^{-1}$ for a lattice constant of 1 \AA . The presence of spin waves is reflected in the temperature-dependent Raman spectra as an appearance of new broad or sharp peaks (Magnon) in the spin-solid phase, also it will reflect in the phonon energies and lifetime (FWHM) and line shapes.

Spin excitations affects phonon self-energy, $\Lambda = \Lambda' + i\Lambda''$, here Λ' is the real part of the self-energy and determines the renormalization of phonon frequency whereas the imaginary part Λ'' dictates the lifetime or the line width of the phonon mode. The spin-phonon coupling occurs in the spin-solid phase and affects the phonon dynamics below $\sim T_N$. It is also reflected in the reduced lifetime and broader linewidth in the magnetic systems with significant spin-phonon coupling. Lattice vibrations may lead to the modulation in the exchange interaction and can be expressed as: $J_{ij} = J_0 + \frac{\partial J_{ij}}{\partial q} q_{ij} + \frac{1}{2} \frac{\partial^2 J_{ij}}{\partial q^2} q_{ij}^2$. Here, J_0 is a constant signifying the equilibrium exchange coupling, q_i is the i^{th} atom displacement. The first term gives rise to the bare spin Hamiltonian i.e., $H_{\text{spin}} = \sum_{i,i \neq j} J_0 \vec{S}_i \cdot \vec{S}_j$ and the last two terms signify $H_{\text{spin-phonon}}$. The renormalization of phonon energy occurs due to alteration in

the exchange integral and is proportional to the spin-spin correlation which is given as

$$\Delta\omega = -\frac{1}{2\mu_\alpha\omega_\alpha} \sum_{i,i\neq j} \frac{\partial^2 J_{ij}}{\partial q_\alpha^2} \vec{S}_i \cdot \vec{S}_j \quad [257,258].$$

Here ω_α is the mode frequency, μ_α is the reduced

mass associated with a mode, J_{ij} is the exchange interaction between i^{th} and j^{th} atomic spin, q_α is the atomic displacement associated with a phonon mode, $\vec{S}_i \cdot \vec{S}_j$ determines the spin-spin correlation. One can easily see that only those phonons which modify the underlying exchange interaction contribute to the renormalization process. $\Delta\omega$ can be positive or negative depending on the spin-phonon coupling coefficient, which is dictated by the kind of interaction, i.e., symmetry and amplitude of vibrations of a particular phonon mode.

Raman scattering has been smoking gun evidence for probing the Fractionalized excitation, such as spinons (Majorana fermions), which are the key feature of QSL state. In Kitaev QSL the elementary spin-1/2 fractionalizes into two itinerant MFs and localized Z_2 flux [259,260]. Raman scattered light couples with itinerant MFs either via the creation and annihilation of a pair of fermions or the creation of one and annihilation of another fermion. These features are reflected in the multiparticle continuum background signal, which is due to itinerant MFs, phonon anomalies in frequency, linewidth, and quasi-elastic scattering which comes into the picture due to Z_2 flux and line shapes such as Fano asymmetry. A careful subtraction of the bosonic signal from the raw spectra is needed to obtain the scattering response from the other quasi-particles. Next, we will focus in detail on the investigation of Kitaev quantum spin liquid via Raman spectroscopy.

5.2. Evidence for Kitaev Quantum Spin Liquids

Jackeli and Khaliullin advocated that strong spin-orbit coupled Mott insulators with edge-sharing octahedral geometry could host a Kitaev QSL as their ground state [138]. Thus far, only a limited number of materials - such as the 2D honeycomb lattices A_2IrO_3 ($A = Na, Li$) and $RuCl_3$ [152,261,262] meet these structural and electronic criteria. However, in these

systems, the realization of a true Kitaev QSL is hindered by the emergence of long-range magnetic order at low temperatures, likely driven by interactions beyond the ideal Kitaev model, including Heisenberg-type off-diagonal terms. Intriguingly, despite this magnetic ordering, experimental signatures of spin fractionalization and Majorana-like excitations have been observed through light-scattering techniques. Raman and inelastic neutron scattering measurements reveal a broad continuum [244,263,264], contrasting sharply with the discrete magnon modes typical of conventional magnetically ordered states [91,244,253,265-268]. These findings imply that the magnetically ordered ground state may lie in close proximity to a quantum phase transition into a Kitaev spin liquid. The search is still on for definitive experimental evidence of a genuine Kitaev QSL.

Evidence of a QSL state or its remnant may be uncovered via observation of the quantum fluctuations of the associated spin degrees of freedom and their coupling with the lattice degrees of freedom through spin-phonon coupling. Raman spectroscopy is an excellent probe for investigating and classifying the presence of long-range ordering, symmetry, and statistics of the quasiparticles. In the Raman process for QSLs, the light interacts with underlying gauge field via spin-photon coupling [256]. Raman scattering in low-dimensions has provided evidence of spinons and emergent gauge fields in U(1) Dirac spin liquids [269] and chiral spin liquids [270]. In conventional magnets, there are bosonic spin wave excitations known as magnons. For Mott insulators, where the trivial spin wave picture of low energy excitations is inapplicable, a coupling of dynamically induced electron-hole pair with “two-magnon states” occurs in the Raman scattering process, revealing the underlying magnetic phase [271,272].

In the case of quantum spin liquids, the spins are fractionalized, and the spin operator excites both itinerant Majorana fermion and Z_2 flux simultaneously, and usually it is difficult to observe them separately. Theoretically, in the pure Kitaev model, the magnetic Raman

operator (R) commutes with the Z_2 fluxes (or plaquette operator W). That means Raman response in the pure Kitaev limit provides a direct measure of the continuum of itinerant Majorana fermions only [273,274]. However, it was theoretically proposed for $A_2\text{IrO}_3$ ($A = \text{Na}$ or Li) that the Raman response of a gapless QSL, which is described by Kitaev-Heisenberg model, may exhibit the signatures of both of these excitations [150]. Spin fractionalization into Majorana fermions gives rise to a broad background signal, which reflects their density of states and Z_2 flux, which in contrast shows a sharp feature due to the Heisenberg interaction, which is closer to the real Kitaev materials [150]. Theoretically, it has been proposed that the signatures of Kitaev QSL may reflect in the dynamical response at $T = 0K$ and temperature evolution of thermodynamic quantities [154,229]. However, it has been a challenge to handle quantum and thermal fluctuations simultaneously at finite temperatures. That is where a dynamical correlation function is required in order to hunt the signature of fractionalization at finite temperature. Direct evidence of fermionic excitations in a finite temperature dependent Raman scattering experiment in a two-dimensional material $\alpha\text{-RuCl}_3$, was reported by Nasu et al. [151].

The signature of underlying electronic and magnetic Raman scattering is embedded in the Raman spectral background. Mobile charge carriers in the metallic systems yield a continuum that is weakly energy-dependent, fractionalized excitations in QSL systems, with a broad continuum, follow Fermi-Dirac statistics, and one/two-magnon in conventional magnetically ordered systems often give a sharp/broad Raman peak. Raman spectrum can probe different dynamics within the system simultaneously, such as magnon, orbiton, charge dynamics, and fractionalized excitations [91,102,111,244,250,258,275-283]. Two-magnon spectral signatures generally result in a broad mode, which considerably gains spectral weight in the spin-solid phase. The electronic continuum comes from the dynamics of mobile charges, which are absent in the case of insulators. However, this is not the case for magnetic

insulators, and the Raman background continuum may arise from the spin dynamics, which is different from that for the mobile charge carriers [252,284]. In inelastic light scattering, the measured intensity depends on the symmetry, Fermi's golden rule, and, in the context of the fluctuation-dissipation theorem, is proportional to the Raman susceptibility ($\text{Im}(\chi[\omega, T])$) times a Bose function [250,285]. In the case of conventional magnets, it shows up as a one-magnon peak or broad features of two-magnon joint density of states (*JDos*), or a quasi-elastic response from thermal fluctuations [244,253].

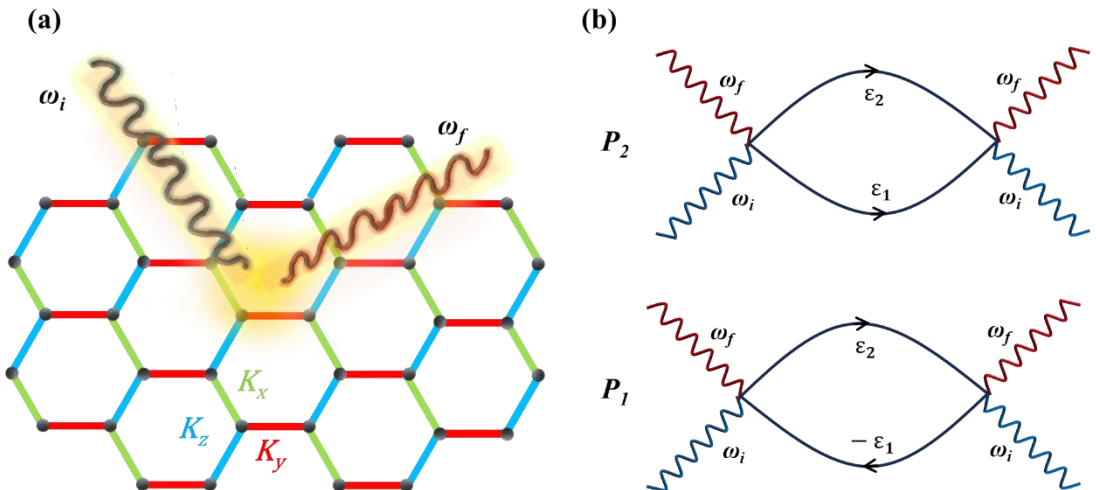


Figure 13: (a) Honeycomb lattice structure. Ising-like interactions between x -, y -, and z -components of the $S = 1/2$ spins are shown by blue, green, and red bonds, respectively. Incoming and outgoing photons (ω_i and ω_f). (b) Feynman diagrams of the Raman scattering processes that correspond to a creation or annihilation of a pair of fermions (P_1), and a combination of creation and annihilation of the matter fermions (P_2) respectively.

In particular, Kitaev materials, where spins are arranged on a quasi-2D honeycomb lattice, due to the presence of bond-dependent anisotropic magnetic interactions, various degenerate states of different spin alignments are equally probable throughout the material, which results in magnetic frustration, and no particular ordering is observed down to even zero kelvin. The characteristic feature of Raman scattering from these systems is the broad background known as continuum scattering or multi-particle scattering, Fano asymmetry in the phonon modes

line-shape, strong quasi-elastic scattering, and phonon anomalies as observed in the case of α -RuCl₃ [244] and β -Li₂IrO₃ [111]. In the framework of Fleury-Loudon-Elliott theory [286], the magnetic Raman scattering intensity in 3D Kitaev systems is given by the density of states of a weighted two-Majorana spinon and is written as: $I(\omega) = \pi \sum_{m,n;k} \delta(\omega - \varepsilon_{m,k} - \varepsilon_{n,k}) |C_{m,n;k}|^2$, where $\varepsilon_{m,k}$ is a Majorana spinon band dispersion with m, n as band indices and $C_{m,n;k}$ is the matrix element creating two Majorana excitations [287]. Whereas bosonic excitations ($bb^\dagger = b^\dagger b + 1$) are obtained by a simple one-particle photon scattering process, which is proportional to $[1 + n(\omega, T)] = 1/[1 - e^{-\hbar\omega_B/k_B T}]$, $n(\omega, T)$ is the Bose distribution function ($\hbar\omega_B$, is the energy of bosons). In the pure Kitaev model only the itinerant Majorana fermions couples with Raman operators, however a perturbed (such as applied external magnetic field) Kitaev model can excite the anyons in pairs and reveal their dynamic interactions and statistics. Further, Yang et al. has proposed a macroscopic Raman scattering formalism for strong-spin orbit coupled Kitaev materials which go beyond Loudon-Fleury approach [288].

The itinerant Majorana fermions contribute in two ways to the inelastic light scattering process. One is the creation or annihilation of a pair of fermions (P₂) and the second is the creation of one fermion and annihilation of the other fermion (P₁). These two processes have a distinct scattering response and the spectral weight of the former one is proportional to $[(1 - f(\omega_1))(1 - f(\omega_2))\delta(\omega - \omega_1 - \omega_2)]$, and for the latter, it is given as $[f(\omega_1)(1 - f(\omega_2))\delta(\omega + \omega_1 - \omega_2)]$ [151]. Here, f is the Fermi-Dirac distribution function $f(\omega, T) = 1/[1 + e^{\hbar\omega/k_B T}]$, ω is the Raman shift and \hbar is Plank's constant, $\hbar\omega_1$ and $\hbar\omega_2$ are the energies of the two fermions. In process (P₂) with increase in temperature the population of high energy fermions diminishes (easier excitation of fermions), whereas process (P₁) vanishes at T = 0 K due to absence of fermions in the ground state. A schematic diagram for a honeycomb lattice for these processes is shown in **Figure 13**.

An unusual broad continuum in the magnetic Raman for β -Li₂IrO₃, (3D Kitaev-Heisenberg system) as shown in **Figure 14 (a)**. The increase in the Raman intensity on lowering temperature (see **Fig. 14 (b)**) cannot be merely explained by bosonic contributions such as phonons and magnons [111]. A similar observation was reported for the case of putative Kitaev QSL candidate α -RuCl₃, in the absence of magnetic field. Sandilands et al. reported a magnetic continuum at 5 K, which persists over a wide temperature range above T_N, attributed to the fractionalized excitations [244]. This is also confirmed from analysis of phonon line width, which shows an anomaly due to phonons decaying into fractionalized excitations, via spin-phonon coupling. Majorana fermions with derived positive frequencies ($\omega_1 > 0$, $\omega_2 > 0$) is a signature of the presence of non-bosonic contributions [151].

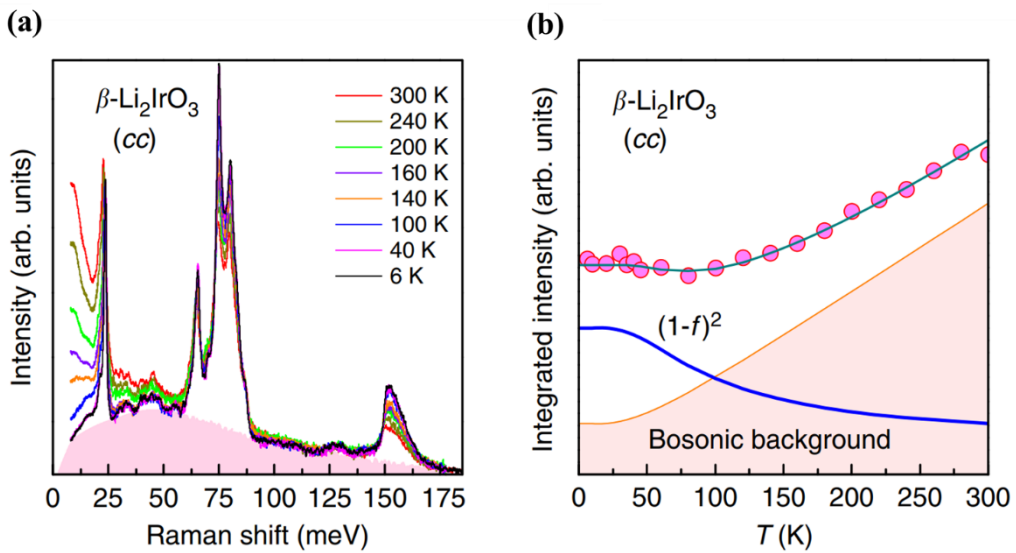


Figure 14: (a) Polarized Raman spectra of β -Li₂IrO₃ at different temperatures. The shaded pink region is the background continuum. (b) variation of the spectral weight of Raman intensity (25 – 51 meV). The shaded region shows the bosonic contribution, and the solid lines are a fit to the two-fermion creation or annihilation process as discussed in the text. From Glamazda et al., 2016 [111].

Glamazda et al. [263] have reported for α -RuCl₃ a similar enhancement of spectral weight of the background continuum below 80K and whose temperature evolution was in line with the

combination of two fermion creation and annihilation process with a bosonic background. In addition to that a hysteric behavior of magnetic excitations was observed over a wide temperature range below the first-order structural transition (from monoclinic to rhombohedral) at ~ 165 K. The magnetic response was found to be stronger in the rhombohedral phase than the monoclinic, which highlights that small variations in bonding geometry significantly affect the Kitaev magnetism and the respective fractionalized excitations [263].

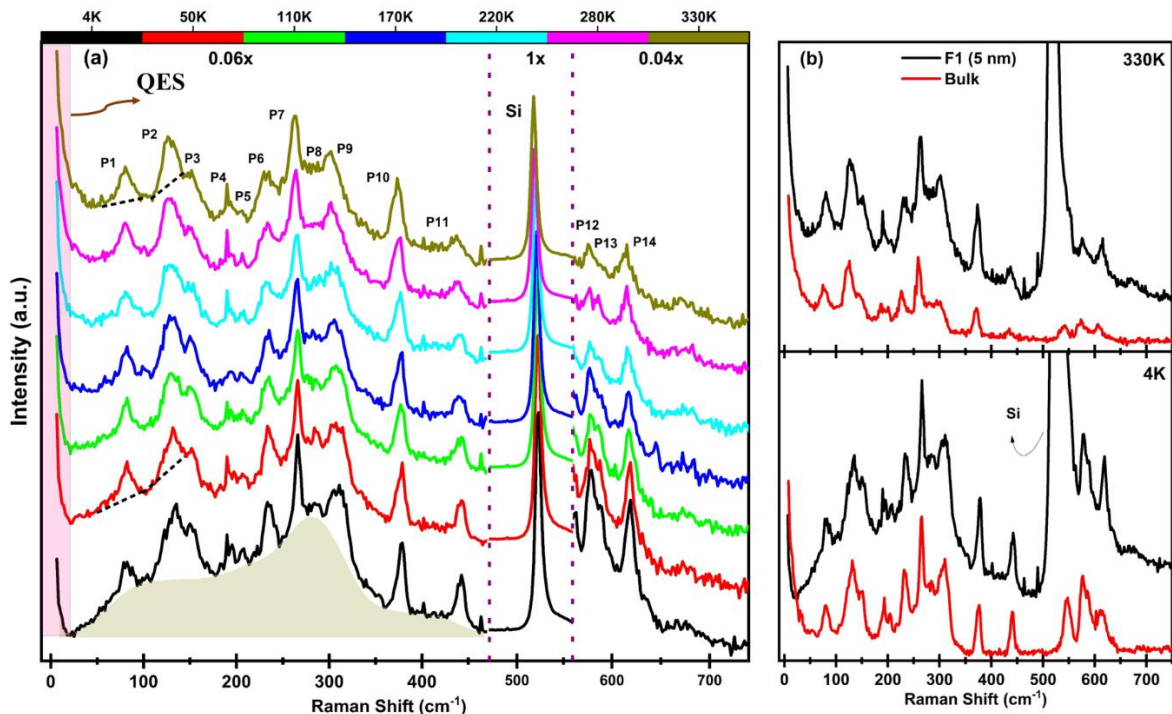


Figure 15: (a) Temperature evolution of the raw spectra for F1 flake (5 nm). Dashed thick black line shows Fano asymmetry for the modes P1 and P2 mode. The pink shaded region shows quasi-elastic region. (b) Comparison of the raw Raman spectra for F1 flake and bulk at 4K and 330K. From Kumar et al., 2025 [103].

Another interesting Raman spectroscopic study on a putative Kitaev candidate $V_{1-x}PS_3$ ($x=0.15$) in its non-stoichiometric composition showed an enhanced background continuum in low thickness regime (~ 8 -9 layers). $V_{1-x}PS_3$ is a well-known Mott-insulator, with $T_N \sim 60$ K [100,102]. The consequence of vacancy defects is that it induces a mixed valency of

vanadium atom V^{3+} , V^{2+} and the corresponding spin value are $S = 1$ and $S = 3/2$, respectively.

Hence, is a candidate for realising KSL physics in a higher spin configuration in the presence of vacancies. The temperature evolution of the Raman spectra for a 5nm flake is shown in

Figure 15 (a). A comparison of Raman spectra at 4K and 330K for 5nm flake and bulk sample is shown in **Figure 15 (b).** The enhanced quantum spin fluctuation (spin-fractionalization) and presence of pure (site) vacancies (favourable for stabilising KSL) is an excellent signature for applications such as quantum computation [103,206].

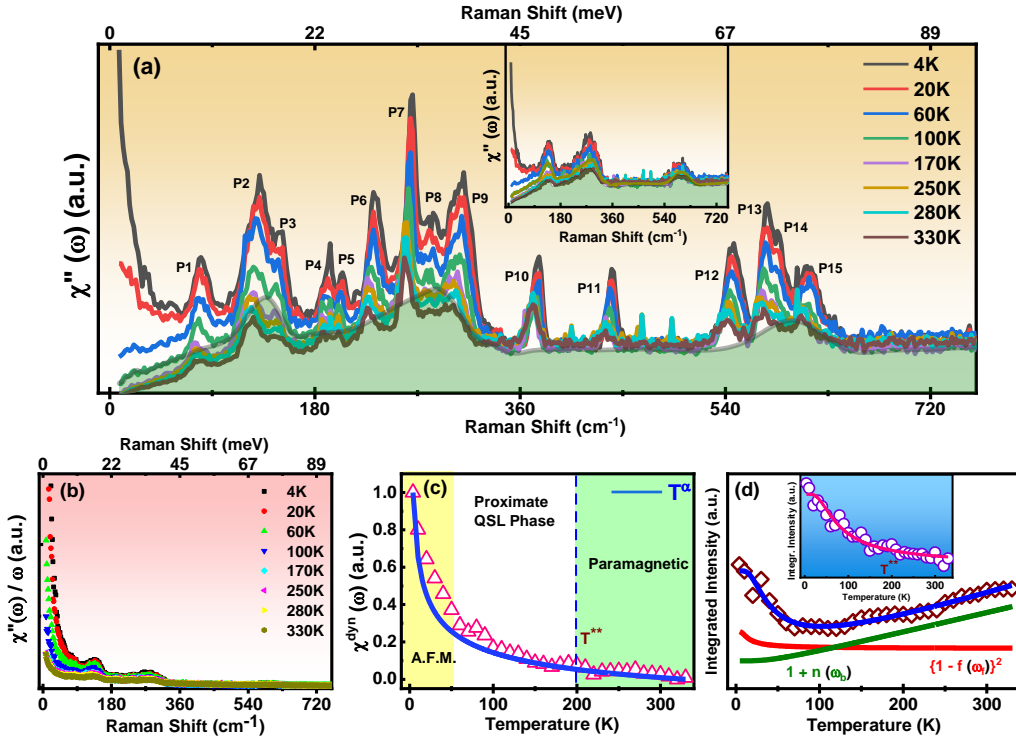
Raman scattering can provide a measure of dynamical spin fluctuations, which can be gauged via dynamic Raman susceptibility, as the magnetic Raman scattering at finite temperatures arises from dynamical spin fluctuations in a quantum paramagnetic state and may provide a qualitative measure of the fractionalization of quantum spins. Generally, the Raman modes are found to be superimposed onto the magnetic background continuum. One has to carefully remove the phononic contribution. To extract the non-bosonic contribution to the Raman spectra, Raman response, $\chi''(\omega, T)$ (Bose corrected spectra) is evaluated. Here χ'' , is the imaginary part of the correlation function of the Raman tensor, $\tau(r, t)$,

$$\chi(\omega) = \int_0^\infty dt \int dr \langle \{\tau(0,0), \tau(r,t)\} \rangle e^{-i\omega t}$$
. A general expression for the Raman tensor can be written in powers of spin-half operators as : $\tau^{ab}(r) = \tau_0^{ab}(r) + \sum_l K_l^{ab} S^l(r) + \sum_{\delta} \sum_{lm} M_{lm}^{ab}(r, \delta) S_r^l(r) S_{r+\delta}^m + \dots$, here the first term shows Rayleigh scattering, the second and the third term indicate the one/two spin-flip process, respectively [150,151,256,289-291]. The complex tensors K and M are the coupling strength of the light to the spin system.

The Raman response, $\chi''(\omega, T)$, is proportional to stokes Raman intensity given as:

$$I(\omega, T) = \int_0^\infty dt e^{i\omega t} \langle R(t) R(0) \rangle \propto [1 + n(\omega, T)] \chi''(\omega, T)$$
; where $R(t)$ is the Raman operator and $[1 + n(\omega, T)]$ is the Bose thermal factor. In Kitaev spin liquids the Raman operator couples to the

dispersing Majorana fermions and extensively projects to two-Majorana fermion density of states [287]. A phonon-subtracted Raman response for $V_{1-x}PS_3$ (bulk) is shown in **Figure 16 (a)**, inset [102]. **Figure 16 (d)** shows the temperature dependence of background raw spectral weight extended up to ~ 95 meV, clearly showing the presence of a fermionic contribution, which is evident from the inset where the spectral weight of the Bose corrected spectra or



Raman response increases with decreasing temperatures [102].

Figure 16: (a) Temperature evolution of the Raman response for bulk $(V_{0.85}PS_3)$ $\chi''(\omega, T)$ [measured raw Raman intensity/ $1 + n(\omega, T)$]. Inset shows the phonons subtracted (P1-P15) Raman response. (b) Temperature dependence Raman conductivity $\chi''(\omega, T) / \omega$. (c) $\chi^{dyn}(T)$, the solid blue line is a power-law fit $\chi^{dyn} \sim T^\alpha$. Background-coloured shading reflects different magnetic phases. (d) The main panel shows integrated raw spectra spectral weight in the energy range 1 to ~ 95 meV, the blue solid line is fitting by a combined bosonic and fermionic function, $[a + b\{1 + n(\omega_b, T)\}] + c\{1 - f(\omega_f, T)\}^2$. Solid green and red line show temperature dependence of bosonic and fermionic function. Inset shows non-bosonic or contribution and T^{**} (~ 200 K) represents the temperature where spin fractionalization starts

building up. The pink solid line represents fitting by the two-fermion scattering function $a+b[1-f(\omega,T)]^2$. From Kumar et al., 2023 [102].

The underlying nature of the dynamical spin fluctuations can be gauged via dynamic Raman susceptibility (χ^{dyn} or χ_R), which is in the dynamic limit of $\chi^{static}=\lim_{k\rightarrow 0}\chi(k,\omega=0)$. It can be calculated at a given temperature by integrating phonon-subtracted Raman conductivity,

$\chi_{cont.}(\omega)/\omega$, and using Kramers - Kronig relation given as: $\chi^{dyn}=\lim_{\omega\rightarrow 0}\chi(k=0,\omega)\equiv\frac{2}{\pi}\int_0^\Omega\frac{\chi''(\omega)}{\omega}d\omega$,

where Ω is the upper cutoff (~ 95 meV) value of integrated frequency, where Raman conductivity shows no change with a further increase in the frequency. The power law dependence of χ^{dyn} even well above the long-range magnetic ordering temperature reflects the slowly decaying correlation inherent to the quantum spin liquid phase and triggers the fractionalization of spins into itinerant fermions around $T^* \sim 200$ K [134,229]. On lowering the temperature χ^{dyn} shows nearly temperature-independent behaviour down to ~ 200 K as expected in a pure paramagnetic phase, on further lowering the temperature, it increases continuously till 4K. For conventional antiferromagnets, as the system attains an ordered phase, dynamical fluctuations should be quenched in the spin-solid phase. An increase in the χ^{dyn} below ~ 200 K reflects the enhancement of Majorana fermion density of states and marks the cross-over from a paramagnetic to the proximate spin liquid state. A similar enhancement in the χ^{dyn} has been observed in Cu_2IrO_3 [116], $\alpha\text{-Li}_2\text{IrO}_3$ [108] and $\alpha\text{-RuCl}_3$ [263].

Another reliable method to hunt for signatures of fractionalized excitations in the case of Kitaev spin liquids, where the Raman process excites a pair of fractional particles, leading to the stokes (energy loss) and anti-Stokes (energy gain) part as $I_S[\omega,T]$ and $I_{AS}[\omega,T]$ respectively, can be given as [150,151,292]:

$$I_S[\omega, T] = \text{Im}(\chi[\omega, T])(n_B[\omega, T] + 1) = JDos[\omega, T](1 - n_F[\omega/2, T])^2$$

$$I_{AS}[\omega, T] = \text{Im}(\chi[\omega, T])(n_B[\omega, T]) = JDos[\omega, T](n_F[\omega/2, T])^2 \quad - 9$$

Here $n_{B/F}[\omega, T]$ are the Bose/Fermi distributions and $JDos[\omega, T]$ reflects approximate Joint Density of states (JDos) from the fractionalized particles. The contribution from non-fractional excitations such as phonons, is an additional term to be added to the susceptibility, without contribution from the Fermi function.

In case of α -RuCl₃, the energy range and temperature boundaries of the non-Kitaev terms and their role in the emergence or suppression of the fractionalized particles were determined by comparing the Raman susceptibility with the Monte Carlo (QMC) results [292]. A new approach was employed, where a reasonable intensity of Raman spectra was recorded for both Stokes and anti-Stokes spectra, as also shown in **Figure 17 (a)** (magnetic continuum is shown in grey shaded region), the Rayleigh scattering half width was reported ~ 2.3 meV. As the Raman intensity contains a Bose factor, Raman susceptibility can be directly measured using $\delta I = I_S[\omega, T] - I_{AS}[\omega, T] = \text{Im}[\chi[\omega, T]]$. This new quantity can be used to provide a measure of non-Kitaev terms. **Figure 17 (b)** shows the comparison of the QMC results for the pure Kitaev limit and the Raman susceptibility at 10 and 40 K. As the magnetic ordering temperature is 7K, the additional susceptibility arises from the non-Kitaev terms, which was also suggested by exact diagonalization calculations [293]. Further the energy and temperature dependence of the non-Kitaev terms, is estimated using $\delta\chi = \chi_{Raman} - \chi_{QMC}$, which is the difference between the measured Raman susceptibility and that of the pure Kitaev model (measured by QMC calculation), plotted in **Figure 17 (c)** (black dots indicate the temperature and energy boundaries which resemble pure Kitaev QSL). A large deviation in the region below 6 meV and 40K, is where the non-Kitaev terms are dominant. However, the response

above 8 meV and 150K can be understood from the QES induced by well known the thermal fluctuations in the frustrated magnets [239,244,263]. That will be discussed in depth in the next section.

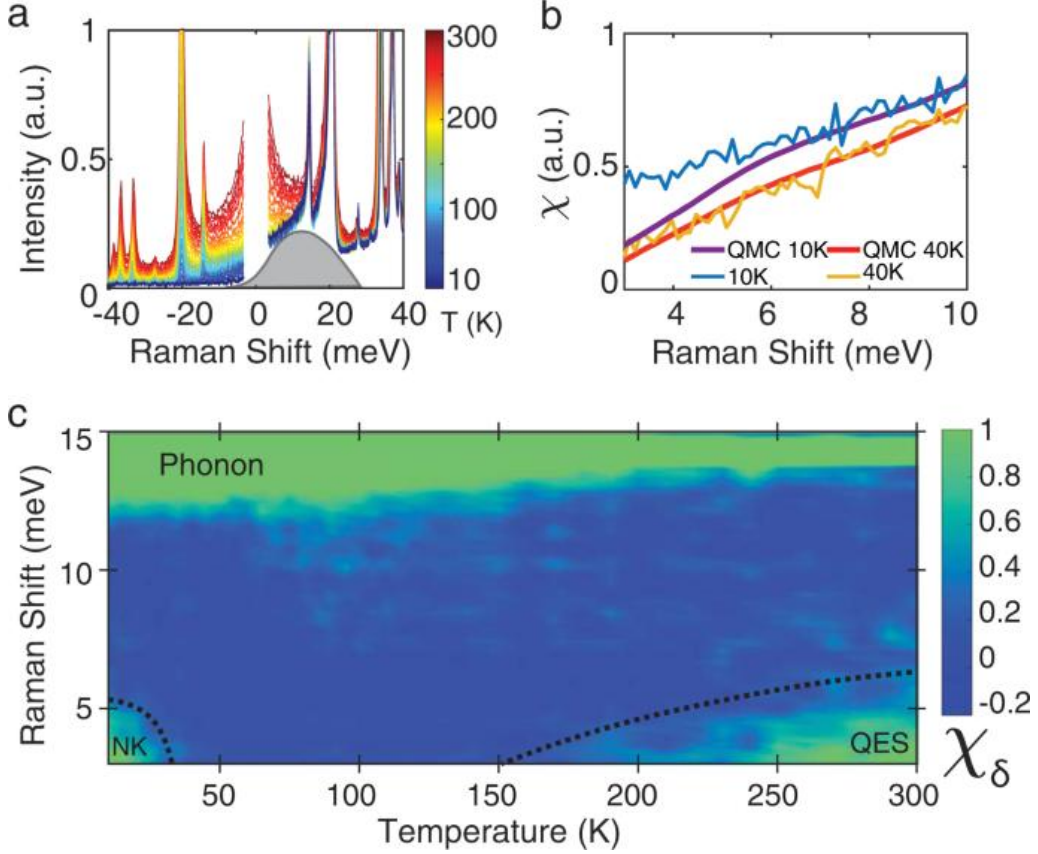


Figure 17: (a) Temperature dependent Raman intensity (Stokes and anti-Stokes) of α -RuCl₃ in XY polarization. The gray shade indicates the magnetic continuum excitation. (b) The measured Raman susceptibility in XY polarization of α -RuCl₃ at 10 K (blue line) compared with the calculated result of the pure Kitaev limit (purple line) at the same temperature. The enhanced signal at low energies results from the non-Kitaev interactions in the system. (c) The temperature and energy dependent map of $\delta\chi = \chi_{\text{Raman}} - \chi_{\text{QMC}}$. From Wang et al., 2020 [292].

5.2.1. Quasi-elastic Scattering

The low-energy excitations in the system are observed close to the energy of the incident light, i.e., quasi-elastic scattering (QES) response. Generally, it is associated with the

relaxation phenomenon and low-frequency molecular dynamics within materials, as in case of disordered systems like glasses and liquids. In quantum magnets, the quasi-elastic part arises from spin energy fluctuations and can be used to extract the magnetic specific heat (C_m), which is very difficult to approximate otherwise [236]. The magnetic Raman scattering at finite temperatures arises from dynamical spin fluctuations in a quantum paramagnetic state and can provide a good measure of the thermal fractionalization of quantum spins. It is attributed to the diffusive fluctuations of a four-spin time correlation function or fluctuations of the magnetic energy density [294].

In magnetic Mott insulators, the Raman scattering can be thought of as a photon-in and photon-out process. As in most of the Mott insulators the photon frequencies lie below the charge gap, and the electronic degrees of freedom can be considered frozen. This fact can be used to formulate a scattering process based on a pure spin Hamiltonian, also known as the Loudon-Fleury approach [256,295,296]. For a Heisenberg interaction spin system, i.e., ($H = J \sum_{\langle i,j \rangle} S_i \cdot S_j$), the corresponding Loudon-Fleury operator (R) for the interaction between light and quantum spins can be written as $R = \sum_{\langle i,j \rangle} (\varepsilon_i \cdot \hat{r}_{ij})(\varepsilon_s \cdot \hat{r}_{ij}) S_i \cdot S_j$, here ε_i and ε_s are the polarization vectors of the incident and the scattered light, respectively, and \hat{r}_{ij} is the unit vector connecting i^{th} and j^{th} sites. Interestingly Raman (Loudon-Fleury) operator (R) has a similar form of the Heisenberg Hamiltonian, as the Coulomb interaction involved in the exchange scattering process and the magnetic exchange interaction are similar [256]. Hence, within this framework, the magnetic Raman intensity can be written as,

$$I(\omega) = \int_{-\infty}^{\infty} dt e^{i\omega t} \langle R(t)R(0) \rangle , \text{ where } R(t) = e^{iHt} \text{ Re}^{-iHt} \text{ and } \omega = \omega_f - \omega_i \text{ is the Raman shift.}$$

Here, the magnetic Raman intensity is determined by using a four-spin time correlation function [236]. This framework has successfully explained the magnetic Raman

spectroscopic scattering from magnons (one/two) as well as fractionalized excitations (spinons), as also picturized in **Figure 18 (a)** [259].

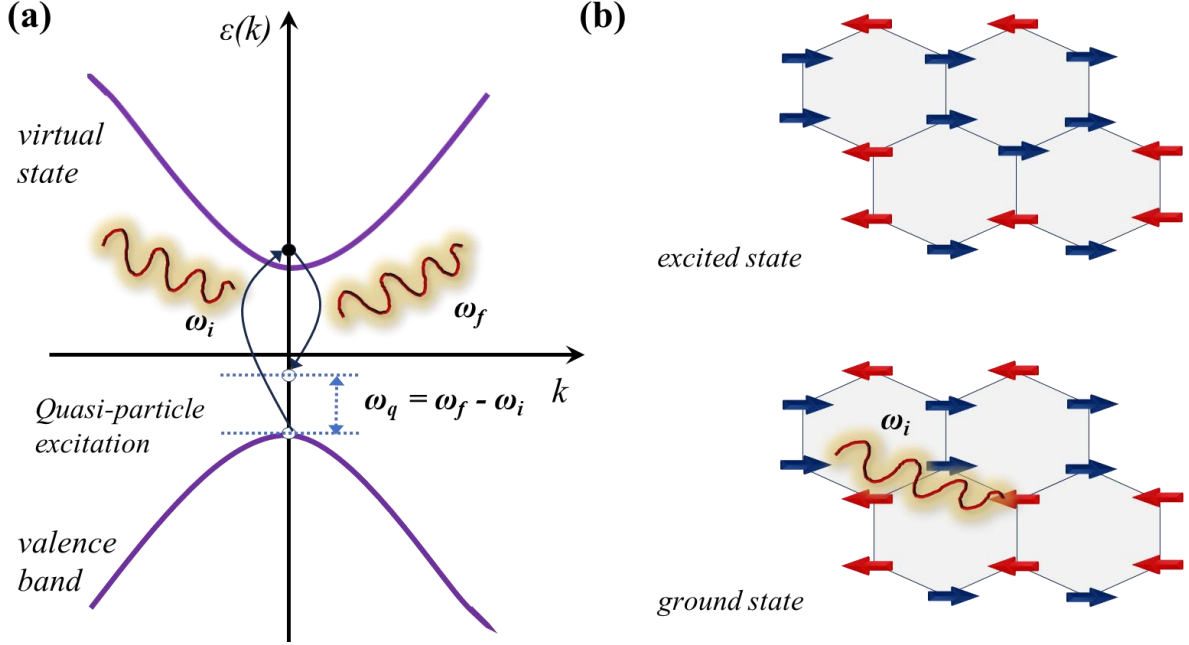


Figure 18: (a) Schematic sketch of Stokes Raman scattering involving the electronic transitions of a third-order light scattering process. (b) Two-magnon excitation in a magnetically ordered system.

Thermal fluctuations interfere with the quasiparticle excitations in conventional magnets (magnons) and spin liquids (spinons). However, light can still be coupled with either diffusive fluctuations of a four-spin time correlation function or fluctuations of magnetic energy density $E(k,t)$, which is the Fourier transform of $E(r) = -\left\langle \sum_{i>j} J S_i \cdot S_j \delta(r - r_i) \right\rangle$, with the position of i^{th} spin at r_i . A Gaussian-type spectral shape for QES appears in the case of diffusive fluctuations [297]. However, on the other hand, Reiter and Halley showed that light couples with the magnetic energy density, leads to the spectral weight of the quasi-elastic scattering via a two-spin process ((as shown in **Figure 18 (b)**) and can be written as: [298-300]:

$$I(\omega) \propto \int_{-\infty}^{\infty} e^{-i\omega t} dt \langle E(k, t) E^*(k, 0) \rangle. \quad -10$$

Here the correlation function $\langle E(k, t) E^*(k, 0) \rangle$ is assumed within hydrodynamic limit and using fluctuation-dissipation theorem the eqn. 10 can be rewritten as:

$$I(\omega) \propto \frac{\omega}{1 - e^{-\beta \hbar \omega}} \frac{C_m T D_T k^2}{\omega^2 + (D_T k^2)^2} \equiv \frac{\chi''(\omega)}{\omega T} \propto C_m \frac{D_T k^2}{\omega^2 + (D_T k^2)^2} \quad -11$$

Here $\beta = 1/k_B T$, C_m is the magnetic specific heat and $D_T = K/C_m$ is the thermal diffusion constant with the magnetic contribution to thermal conductivity K , and $\chi''(\omega)$ is the Raman susceptibility. $\frac{\chi''(\omega)}{\omega T}$ is a magnetic analog of the optical conductivity and has a Lorentzian functional form. It conveys information regarding magnetic specific heat, spin correlation length, and the magnetic part of thermal conductivity. Thermal diffusive constant $D_T(T)$ ($D_T = K/C_m$), is inversely proportional to the magnetic correlation length. The spectroscopically derived K exclusively contains a magnetic contribution and cannot be compared with the thermodynamic counterpart. In the case of magnetic insulators, the thermal conductivity is mostly dominated by phonons, and a small magnetic contribution is very difficult to separate out from the total thermal conductivity. The temperature dependence of the Raman response $\chi''(\omega, T)$ and Raman conductivity $\chi''(\omega, T)/\omega$ for bulk $V_{0.85}PS_3$ is shown in **Figure 19 (a,b)** [102]. The magnetic specific heat (C_m) of Kitaev systems, where spin fractionalization occurs into two kinds of Majorana fermions, leads to a distinct two-peak structure in the temperature dependence of magnetic specific heat [140,229]. At high temperature, the crossover can be related to the development of short-range correlations between nearest neighbour spins; however, at low temperatures, it is attributed to the Z_2 fluxes. That is exactly reflected for hyperhoneycomb iridates, which suggests a proximity to a Kitaev spin liquid phase, as also shown in **Figure 19 (c)** ($\beta\text{-Li}_2\text{IrO}_3$) [111,140]. The onset temperature T^* corresponds to a

crossover from a simple paramagnetic to a Kitaev paramagnetic state, where spin-correlations are confined to nearest neighbor sites due to exchange frustration, and saturates for $T < T^*$ [234], whereas T_N corresponds to the long-range magnetic ordering; 38 K and 39.5 K for β - and γ -Li₂IrO₃, respectively [109,301].

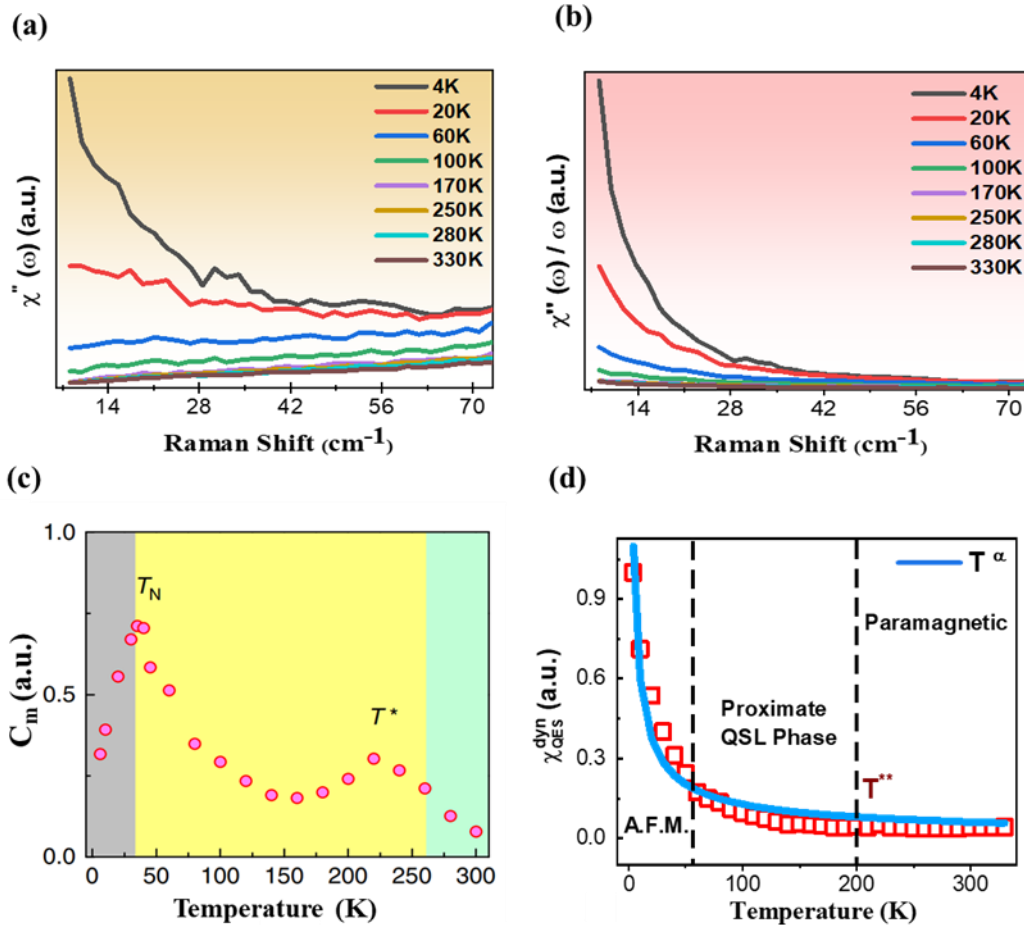


Figure 19: (a,b) shows the temperature dependence of the Raman response $\chi''(\omega, T)$, Raman conductivity $\chi''(\omega, T)/\omega$ for the bulk V_{0.85}PS₃ [102]. (c) Temperature-dependence of the magnetic specific heat C_m derived from the Raman conductivity for Hyperhoneycomb Iridate β -Li₂IrO₃; $T_N = 0.1$ J and $T^* \sim J$ [111]. (d) Shows the temperature dependence of $\chi_{QES}^{\text{dyn}}(T)$ for bulk V_{0.85}PS₃. T^{**} (~ 200 K) represents the temperature where spin fractionalization starts building up. The solid blue line is the power-law fit T^α [102]. Panel (a, b, and d) from Kumar et al., 2023 (ref. 102) and panel (c) from Glazman et al., 2016 (ref. 111).

For γ -Li₂IrO₃, the Raman spectra reported showed signatures of QES, a broad magnetic continuum extends up to ~ 1300 cm⁻¹, which consists of several maxima. γ -Li₂IrO₃ is found to possess three Majorana spinon bands; thereby, the magnetic Raman response emulates Majorana band edges and van Hove singularities [236]. Hence, the maxima of the Lorentzian shapes in $\frac{\chi''(\omega)}{\omega}$ are ascribed to the large density of states of the Majorana spinon multibands [111]. C_m for γ -Li₂IrO₃ also showed a λ -like peak at $T_N \sim 40$ K and a weak high-temperature maximum around $T^* \sim 223$ K [236].

As discussed in section 5.2, Raman scattering doesn't probe the Z_2 flux for ideal Kitaev model but may provide sharp features for a Kitaev-Heisenberg model which is more realistic approach. Z_2 flux excitations has been observed at low-temperatures and low-energies (quasi-elastic part), which is supported by specific heat and INS measurements as discussed in earlier sections. Interestingly, a similar feature has been observed in the temperature dependence of dynamic Raman susceptibility (χ^{dyn}) in the Raman scattering measurement of the bulk V_{0.85}PS₃ [102]. Here, a strong temperature dependence of both broad magnetic continuum and QES (or low frequency region) spectral features was observed, where the onset of thermal fractionalization of spin is marked a crossover temperature at $T^{**} \sim 200$ K, where system goes from paramagnetic to proximate KSL state. However, in comparison to the temperature dependence of continuum ($\chi_{cont.}^{dyn}$) the QES (χ_{QES}^{dyn}) remains mostly independent (constant) till ~ 90 K as also shown in **Figure 19 (d)**. In addition to that, the rate of increase is sharper in case of χ_{QES}^{dyn} than $\chi_{cont.}^{dyn}$ [102]. From here it can be deduced that there is a presence of two different quasiparticle dynamics at different energy scale (QES and broad magnetic continuum), which are actively dominant in different temperature range i.e., low temperature for QES and for broad magnetic continuum it is present throughout the temperature range. Hence, the signature of the dynamics of Z_2 flux excitation may be probed

via investigation of QES and itinerant Majorana fermion can be traced in the broad magnetic continuum spread over large energy range.

5.2.2. Phonon Anomaly

In QSL candidates, the absence of any long-range magnetic ordering may also reflect in the renormalization of phonon self-energy parameters, i.e., line-width and frequency, via spin-phonon coupling. Spin-phonon coupling may lead to a possible Yukawa-type interaction between a Majorana bilinear and the phonon, which is similar to the electron-phonon coupling in superconductivity [116]. The effect of phonons on the exchange interaction is discussed in **section 5.1**. Hamiltonian in the presence of spin-phonon coupling that shows the coupled dynamics of optical phonons and spins can be written as:

$H = H_{spin} + H_{spin-phonon} + H_{phonon}$, here H_{spin} is the bare Kitaev Hamiltonian. Further, $H_{spin-phonon} = H' + H''$, that are the first and second order contributions to the exchange coupling due to lattice vibrations. The renormalization of the phonon frequency and linewidth can be found by calculating the self-energy correction to the phonon propagators arising due to spin-phonon coupling within a single-mode approximation for phonons.

The scattering vertices between the matter fermions and phonons can be obtained using standard Majorana decoupling of spins and are shown in **Figure 20**. Here, Majorana fermions are transformed into the bond matter fermions [302]. The interactions shown in **Figure 20 (a, b)** arise due to first-order interactions (H'), and the (c, d) arise due to second-order (H'') interactions [116]. The phonon decays into the fractionalized excitations in a Kitaev spin liquid and renormalizes both frequency and the linewidth, which are the real and imaginary part of the self-energy of the phonon, respectively. As an additional decay channel is present, one can expect an anomalous broadening of the linewidth on decreasing temperatures.

The second-order interaction (H'') is the leading-order contribution to the frequency renormalization and is given as:

$$\delta\omega \propto N \sum_{i,\nu} \left\langle \bar{J}_K S_i^\nu S_{i+\hat{v}}^\nu \right\rangle_S \quad -12$$

Here ν indicates type of bonds (x, y or z), \hat{v} denotes the three nearest-neighbor vectors of the honeycomb lattice. The averaging is taken over equal-time spin correlations over the thermodynamic ensemble, N is the proportionality constant (in terms of spin-phonon coupling and transformation to the soft phonon modes), which can be assumed as a constant λ .

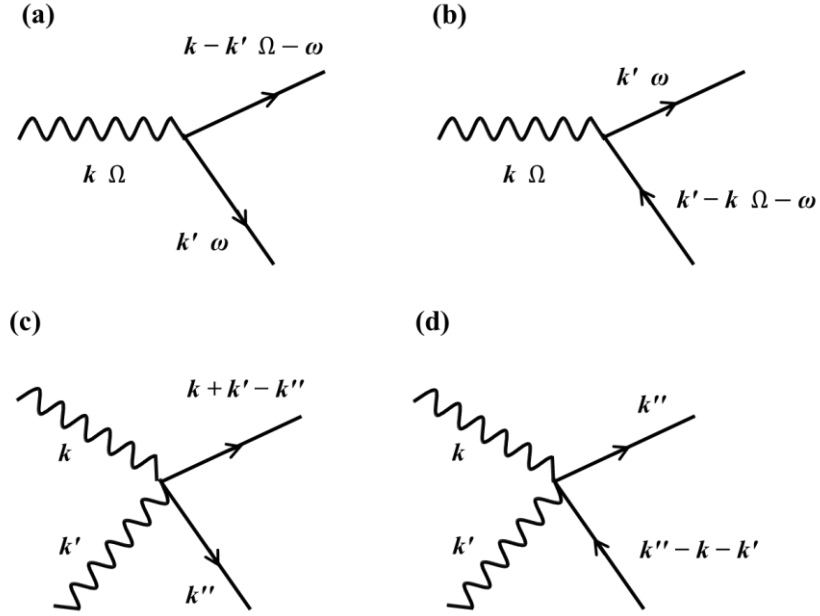


Figure 20: Interaction of phonons with matter fermions arising from first (H') and second order (H'') contributions to the spin-phonon coupling. Adapted from Pal et al., 2021 [116].

The spin energy can be used to estimate the value of $\delta\omega$, in the zero-flux sector within free-Majorana phenomenology, and is given as: $\delta\omega \sim \lambda J_K \sum_k \left\langle \epsilon_k \left(a_k^\dagger a_k - \frac{1}{2} \right) \right\rangle_S$. This indicates

that the spin energy tends to vanish as $T \rightarrow \infty$, takes a gradual non-zero value for $T \sim J_K$ and finally to a constant negative value at absolute zero temperature, reflecting the ground-state energy density of the spins. As the energies are negative, this leads to softening of the phonon with lowering temperatures.

As far as the phonon line-width is concerned, the major contribution arises from the second-order term (H''). In the high temperature regime for a beyond pure Kitaev model, the fermions have a finite lifetime which renormalizes the bandwidth owing to scattering with the Z_2 flux [60]. However, within free Majorana fermions (scattering with the gapped Z_2 fluxes is neglected at very low temperatures), where the matter fermions have been suggested to exist up to finite temperatures. It may exist even up to $T \sim T_h$, where a complete transfer of spectral weight of a coherent itinerant Majorana fermion to an incoherent one occurs (T_h is associated with the van Hove singularity of the completely depleted free Majorana dispersion in the zero-flux sector) [151]. In the context of the free Majorana fermion phenomenology, the imaginary part of the phonon self-energy correction can be given as [116]:

$$\text{Im} \left[\sum(\mathbf{q}, \omega + i0^+) \right] \propto \frac{J_K^2}{N} \sum_k \left[1 - n_F(\varepsilon_{k+q}) \right] \times \left[\delta(\omega + \varepsilon_k + \varepsilon_{k+q}) - \delta(\omega - \varepsilon_k - \varepsilon_{k+q}) \right] \quad -13$$

Here, the proportionality constant depends on the spin-phonon coupling and the normal-mode matrix elements. $n_F(\varepsilon_k)$ shows the occupancy of complex fermionic modes with dispersion ε_k in the zero-flux sector. Such a contribution arises due to the decay of the phonon into two fermions. On increasing temperature ($T \rightarrow \infty$) the Majorana fermions become more and more incoherent, which means the contribution to the line-width is significant at low temperatures as compared to very high temperatures. This behaviour is unlike a typical anharmonic effect, where the linewidth reduces monotonously with decreasing temperature and this anomalous

increase of the linewidth has been reported for different QSL candidates [102,103,116,244].

The interconnection of the line-width and the line shape is discussed in the next section.

5.2.3. Fano Asymmetry

The line shape of the phonon mode can provide a crucial insight into the underlying quasiparticle interactions, as it is directly related to the line width and phonon lifetime. A careful analysis of the line shape can provide information regarding the phase transitions, such as structural, magnetic, etc.. In general, phonon modes (isolated, weakly interacting) show a symmetric Lorentzian line shape for an ideal, bulk, and defect-free crystal. However, in real materials, deviations are observed, which reflect the presence of additional interactions. A Gaussian broadening of the phonon mode arises due to the presence of disorder or inhomogeneity. Anomalous temperature dependence (non-Lorentzian) of linewidth can be an indication of additional interactions such as anharmonic decay or phonon-phonon, electron-phonon interaction, etc. In the case of QSL systems another interesting scenario appears due to the interaction of magnetic energy continuum with the discrete phonon states and leads to an asymmetric line shape known as Fano asymmetry. This type of symmetry basically has its roots in the spin-dependent electron polarizability, which involves spin-photon and spin-phonon coupling [303-305]. In the case of Kitaev spin liquids, the spins are thermally fractionalized into the itinerant Majorana fermions and interact with the lattice dynamics, which leads to the Fano line asymmetry. For the Kitaev spin liquid candidates, recently it was advocated that spin-phonon coupling renormalizes phonon propagators and generates Fano line shape resulting in observable effect of the Majorana fermions and the $Z2$ gauge fluxes, that is a common denominator for a Kitaev quantum spin liquid ground state [306,307].

The Fano function is defined as $F(\omega) = I_0(q + \varepsilon)^2 / (1 + \varepsilon^2)$; where $\varepsilon = (\omega - \omega_0) / \Gamma$ and $1/q$ represents the asymmetry, ω_0 is the bare phonon mode frequency. The asymmetry parameter ($1/q$) characterizes the coupling strength of a phonon to the underlying continuum: a stronger coupling ($1/q \rightarrow \infty$) causes the peak to be more asymmetric, and in the weak-coupling limit ($1/q \rightarrow 0$) the Fano line shape is reduced to a Lorentzian line shape.

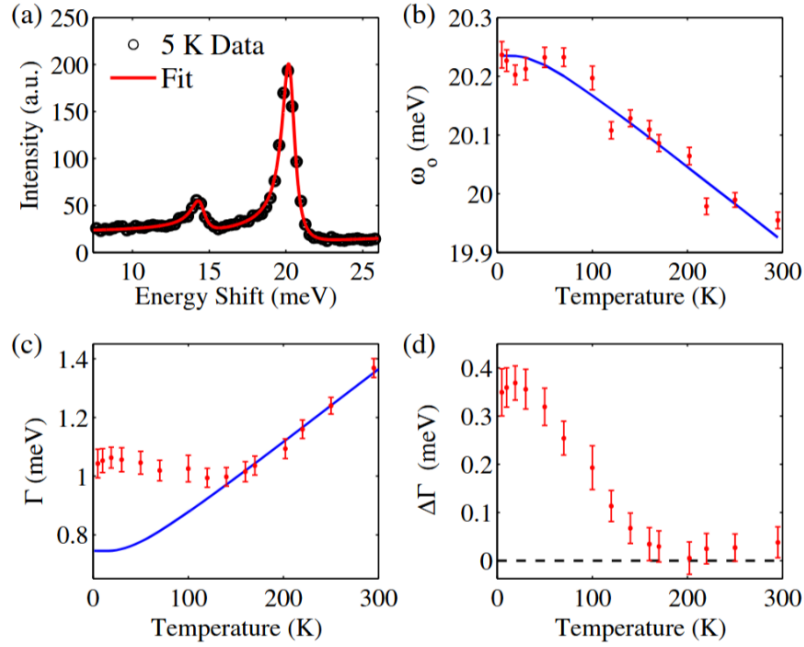


Figure 21. Spin-phonon coupling in α -RuCl₃. (a) Fano fitted 5K spectra. (b,c) Temperature dependence of frequency and line width of 20 meV phonon. (d) Magnetic contribution $\Delta\Gamma$ to the phonon linewidth indicates a coupling between the magnetic continuum and the lattice. From Sandilands et al., 2015 [244].

For α -RuCl₃ [244], it was found that the two lowest energy phonons of E_g symmetry near 14 and 20 meV showed Fano line shapes at low temperatures, as also shown in **Figure 21 (a)**. The typical monotonic (anharmonic) behavior of phonon line width is also compromised as shown in **Figure 21 (c)**, indicating the presence of an additional decay channel, which becomes clearer in **Figure 21 (d)**, where it reveals that the onset of spin fractionalization occurs at \sim 140K. A similar observation was reported for Cu₂IrO₃ [116].

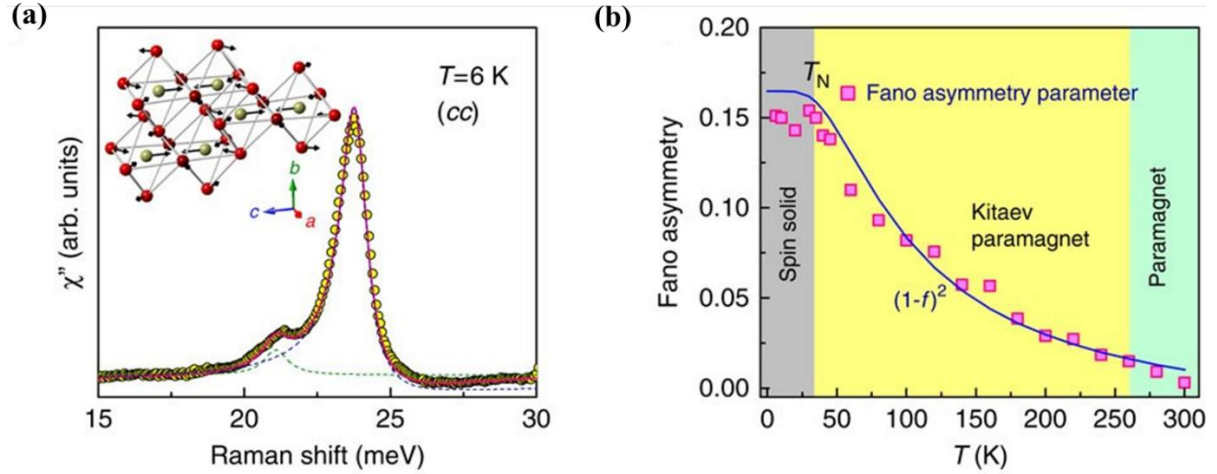


Figure 22: β -Li₂IrO₃, (a) Fit of 24 meV phonon to a Fano profile after subtracting a temperature-dependent magnetic background. The 21 meV phonon on a low-energy side of the Fano resonance is fitted together with a Lorentzian profile. The inset depicts a schematic representation of eigenvector of the 24 meV A_g symmetry mode. The amplitude of the vibrations is represented by the arrow length. Golden balls indicate Ir ions and red balls are O ions. The Li atoms are omitted for simplicity. (b) Temperature dependence of the Fano asymmetry $1/|q|$ plotted together with the two-fermion form $(1-f(\omega))^2$ (solid line). From Glamazda et al., 2016 [111].

In the case of β -Li₂IrO₃, the phonon spectra showed a strong asymmetry for 24 meV mode as shown in **Figure 22 (a)**. With decreasing temperature, the Fano asymmetry, $1/|q|$, increases continuously and then becomes constant below the magnetic ordering temperature. Interestingly, the temperature dependence of $1/|q|$ follows thermal damping of fermionic excitations and matches well with the two-fermion scattering form $(1-f(\omega))^2$ as shown in **Figure 22 (b)** [111]. This was further confirmed theoretically, where the temperature-dependent Fano lineshape was found consistent with the fractionalization of spins into Majorana fermions and Z_2 fluxes [308]. The asymmetry parameter depends on the Kitaev coupling strength J_K ; because the asymmetry depends on the relative position of the phonon peak and the Majorana fermion continuum scales with J_K . A similar observation was found in the case of both bulk and low-thickness flakes of V_{1-x}PS₃. In addition to that, those modes'

line-width showed an anomalous behavior, i.e., an increase with decreasing temperature [102,103], which is again a strong signature of fractionalization of spins.

5.2.4. Effect of Polarization

The symmetry information is very valuable for understanding the symmetry properties and chirality of magnetic excitations and can be effectively probed by utilizing the polarization degree of freedom (light). Polarization-resolved Raman scattering has provided signatures of fractionalized spinon excitations and various spinon bound states [91,309]. The lack of local order may also lead to a very weak polarization dependence of the Raman response is observed in QSLs [253,272]. However, recently, in the Raman spectroscopic investigation of 1D quantum magnet β -VOSO₄, it was revealed that the spectral weight of high-temperature QES exhibits an A_g symmetry, while the low-temperature continuum shows B_g symmetry. Such a typical nature is attributed to the different origins of these two features (QES and continuum) [310].

In the Loudon-Fleury (LF) formalism, the LF operator for the Kitaev model can be written as [150,256]:

$$R = \sum_{\langle ij \rangle_\alpha} (\varepsilon_{in} \cdot d^\alpha) (\varepsilon_{out} \cdot d^\alpha) K_\alpha S_i^\alpha S_j^\alpha \quad -14$$

Here ε_{in} and ε_{out} are the polarization vectors of the incoming and outgoing photons, and d^α is the vector connecting a nearest neighbor, α bond and this can be used to calculate the Raman spectrum using eqn. 14.

The Raman intensity for phonons is given by: $I \propto |\hat{e}_i \cdot \bar{R} \cdot \hat{e}_s|^2$, here \hat{e}_i , \hat{e}_s and \bar{R} are the incident, scattered light polarization vectors and the Raman tensor $\bar{R}(E_L)$ depends on both the crystal structure and electron-phonon coupling, E_L the excitation laser energy [286,311].

Microscopically, the Raman scattering in the optical range of incident laser frequencies is mediated by electronic excitations. The Raman tensor element for the phonon branch depends on the laser excitation energy as follows: [312]:

$$R_{is}^{\mu}(E_L) = \sum_{m,n} \frac{\langle 0 | \hat{e}_s^* \cdot \hat{p} | n \rangle \langle n | H_{el-ph}^{\mu} | m \rangle \langle m | \hat{e}_i^* \cdot \hat{p} | 0 \rangle}{[E_L - E_m + i\Gamma_m][E_L - E_{ph}^{\mu} - E_n + i\Gamma_n]} \quad -15$$

Here $|m\rangle$ and $|n\rangle$ are the eigenstates of the electronic excitations of the crystal (electron-hole pair for example), E_m, E_n are their energies, Γ_m and Γ_n are their damping constant. The light matter interaction is given by the matrix elements of the momentum operator $\langle 0 | \hat{e}_s^* \cdot \hat{p} | n \rangle$, H_{el-ph}^{μ} describe the electron-phonon interaction with the mode μ having energy E_{ph}^{μ} .

In the linear polarized light Raman scattering measurement of α -RuCl₃, (angular dependence of the raw spectra in **Figure 23 (a-c)**) the angular dependence of the spectral weight of A_g^4 , B_g^4 , A_g^5 and B_g^5 phonons is plotted in **Figure 23 (d-g)**, and the solid lines are the group theoretical prediction. In order to measure only the A_g or B_g modes, the incident and scattered light polarizations have to be parallel to either the **a** or **b** axis of the crystal. The intensity of the A_g and B_g phonons is fourfold modulated, and is out of phase with each other as θ (angle between the incoming polarization and the crystal's b axis) changes within the **a-b** plane. In contrast, in the **a-c** plane, B_g phonons are not allowed, and the A_g phonons should only show twofold modulated intensities [313]. The effect of symmetry reduction (D_{3d} to C_{2h}), is found as the splitting of doubly degenerate E_g modes into the nearly degenerate A_g and B_g modes as shown in **Figure 23 (b)**. The symmetry-breaking energy scale is found

to be ~ 1 meV, and arises from weak interlayer coupling or the distortion of each honeycomb layer due to the difference in the strength of the hexagonal bonds [164,314].

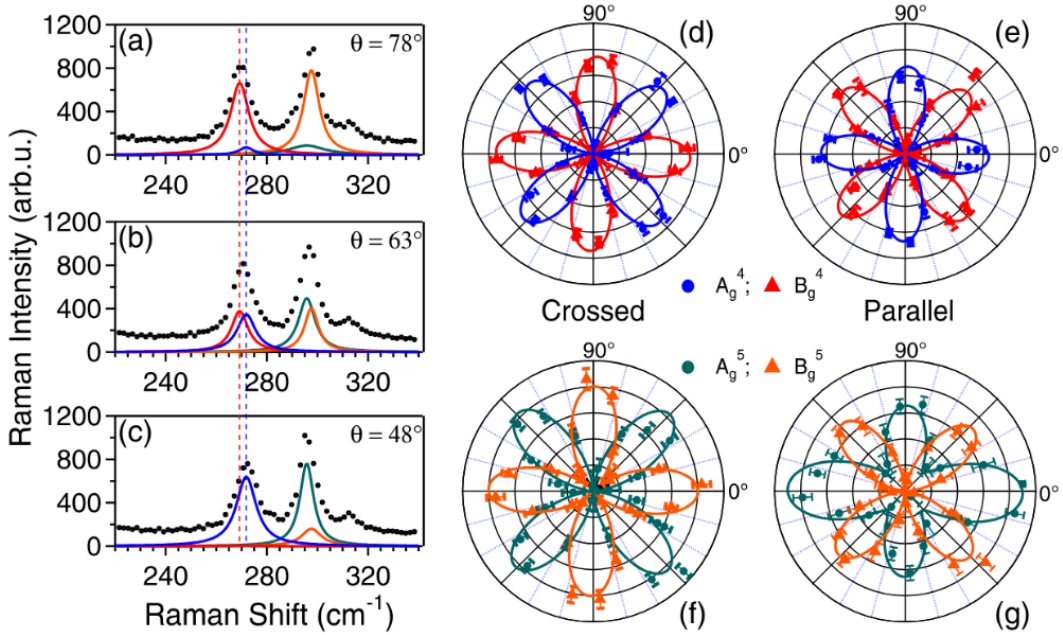


Figure 23: Angular dependence of A_g^4 , B_g^4 , A_g^5 and B_g^5 phonons for α -RuCl₃. (a), (b), (c) show the raw data at certain angles in the crossed polarization configuration. The spectral weight outputs from the data fit are shown in (d) and (e) [(f) and (g)] for A_g^4 and B_g^4 (A_g^5 and B_g^5) for crossed [(d) and (f)] and parallel [(e) and (g)] polarization configurations. The solid lines are the expected behavior. From Mai et al., 2019 [313].

The polarization configuration not only affects the spectral weight of the phonon modes but also the symmetry of the line shape, frequency, and the underlying magnetic continuum as shown in **Figure 24** for the 164 cm⁻¹ mode of α -RuCl₃, where the polarizers are fixed and the sample is rotated, and the spectra are recorded as a function of angle between the laser polarization and crystalline axes. The angular dependence of the asymmetry parameter is plotted in the inset of **Figure 24**. The phonon lineshape asymmetry changes dramatically as a

function of sample orientation angle ϕ (the angle away from the **a** axis for the **a-c** plane measurement). This angle corresponds to the incident and scattered laser polarizations being perpendicular to the **a-b** plane. Interestingly, the asymmetry parameter vanishes $1/|q| \rightarrow 0$; for $\phi = 90^\circ$.

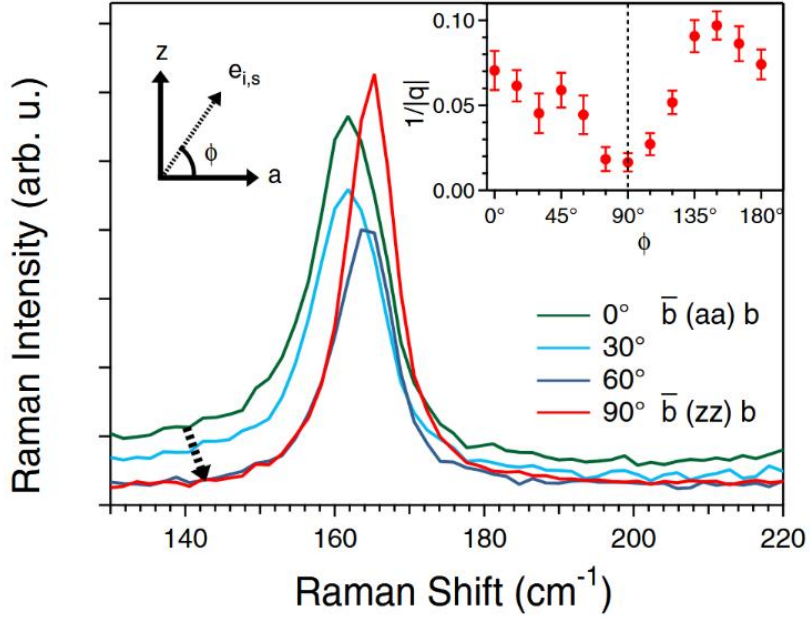


Figure 24: Changes in the asymmetry of the A_g^2 phonon. Here, ϕ is the angle between incoming polarization and the **a**-axis. The dashed arrow highlights both the change in asymmetric line shape and the disappearance of the scattering continuum. The inset shows the Fano parameter $1/|q|$. From Mai et al., 2019 [313].

As the Raman scattering process comes as a measure of itinerant Majorana fermions in Kitaev spin liquids and appear as a broad feature as discussed earlier. In the **a-c** plane as shown in the **Figure 24**, where only the A_g^2 phonon is allowed, an interesting observation in the Raman response as the sample was rotated around the **b**-axis, which is the shift in phonon peak frequency, vanishing of the continuum, and the asymmetry parameter $1/|q|$, when the laser polarization is aligned perpendicular to the honeycomb plane. The Fano line shape and the continuum share the same origin. The large shift in the Fano line shape arises due to comparable energy to the background [303]. Hence, it shows that the continuum observed is a

2D effect and cannot be excited with $e_{i,S} \perp \text{a-b plane}$. The presence of A_g modes, in the absence of the continuum, and the presence of the continuum when B_g phonons are inactive $[\bar{b} (aa) b]$, indicates that the continuum is not coming from the phononic contribution (A_g or B_g). Hence, the single particle excitation from the free electrons can also be ruled out. It was shown that Raman scattering from Kitaev exchange is only absent when incoming and outgoing polarizations are perpendicular to the honeycomb plane. At the same time, the response in the **a-c** plane is not zero if both the threefold symmetry of the perfect honeycomb lattice is broken, and both direct and mediated superexchange are considered in the Kitaev interaction [273]. In a polarization-dependent (varying incident light polarization keeping the analyzer fixed) measurement at 4K and 120K, for $V_{(1-x)}PS_3$, the symmetry of magnetic excitations (continuum, QES) was found to be A_g . Such type of symmetry is expected for antiferromagnetic fluctuations in a monoclinic system [103,315].

The interaction of linearly polarized light is sensitive to symmetric spin correlations and can probe conventional exchange channels. However, the circularly polarized light can provide information about antisymmetric and chiral correlations. In contrast to the conventional picture of phonons where vibrational modes are linearly polarized subjected to symmetry constraints such as time-reversal and inversion restrict the presence of angular momentum, though chiral phonons have been proposed theoretically and observed experimentally [316-321]. Chirality is an inherent property of an object not identical to its mirror image. The helicity of phonons has its roots in spin-phonon coupling, which invokes Berry curvature into phonon bands and introduces topological aspects and phenomena such as phonon hall effect [322,323]. Raman circular dichroism (RCD) or helicity resolved Raman scattering, has proved to be a smoking gun evidence for chiral phonons. [319,324,325].

In the context of Kitaev spin liquids, it is theoretically proposed that coupling of chiral spin excitation continuum with lattice degree of freedom under applied magnetic field renormalizes phonon propagator induces complex superposition of polarization eigenvectors with a non-zero angular momentum. Such a modification is expected to reflect in the Fano line-shape [326]. The effectiveness of RCD has also been proposed to probe chiral U(1) QSL on triangular lattice and other related candidate materials [327]. In another study the low-energy Raman response arising due mobile interacting Ising anyons in chiral Kitaev spin liquid under external magnetic field, showed a power law scaling of intensity at 0K (two-anyon continuum): $I(\omega) \sim (\omega - E_{2\sigma}^0)^{1/8}$, for linear and parallel-circular polarization channels, where $E_{2\sigma}^0$ is the two-particle gap. The scaling for the cross-circularly polarized channels is given as: $I(\omega) \sim (\omega - E_{2\sigma}^0)^{|m \pm 1/8|}$, here $m = 0,1,2$ and is dictated by number of minima in the single anyon dispersion. The exponents can be directly associated to the topological spin of Ising anyons and describe the underlying exchange statistics [328].

Figure 25 (a,b) shows incident and scattered circularly polarized light on α -RuCl₃. The light polarization is defined with respect to z-axis. Left (+ \hbar) and right (- \hbar) circular helicity is denoted by σ^+ and σ^- respectively. The Raman intensity corresponding to two different geometries are denoted as $I_{+-} [z(\sigma^+ \sigma^-) \bar{z}]$, and $I_{-+} [z(\sigma^- \sigma^+) \bar{z}]$. The field (B > B_C) and helicity-dependent Raman response is shown in **figure 25 (c)**. In addition to broad magnetic multi-particle continuum M0 (MB in ref. [329], M1, M2 and, M3 peaks are observed to exhibit helicity-dependent chiral behaviour. Peak M0, M1, and M2 are attributed to the singlet Majorana bound state, spin-flip $|\Delta S|=1$ excitation, and two-particle bound state respectively [329,330]. M3 has been suggested to be associated with, either two-particle excitation as its energy is approximately twice to that of M1 [330] or three-particle bound state [329].

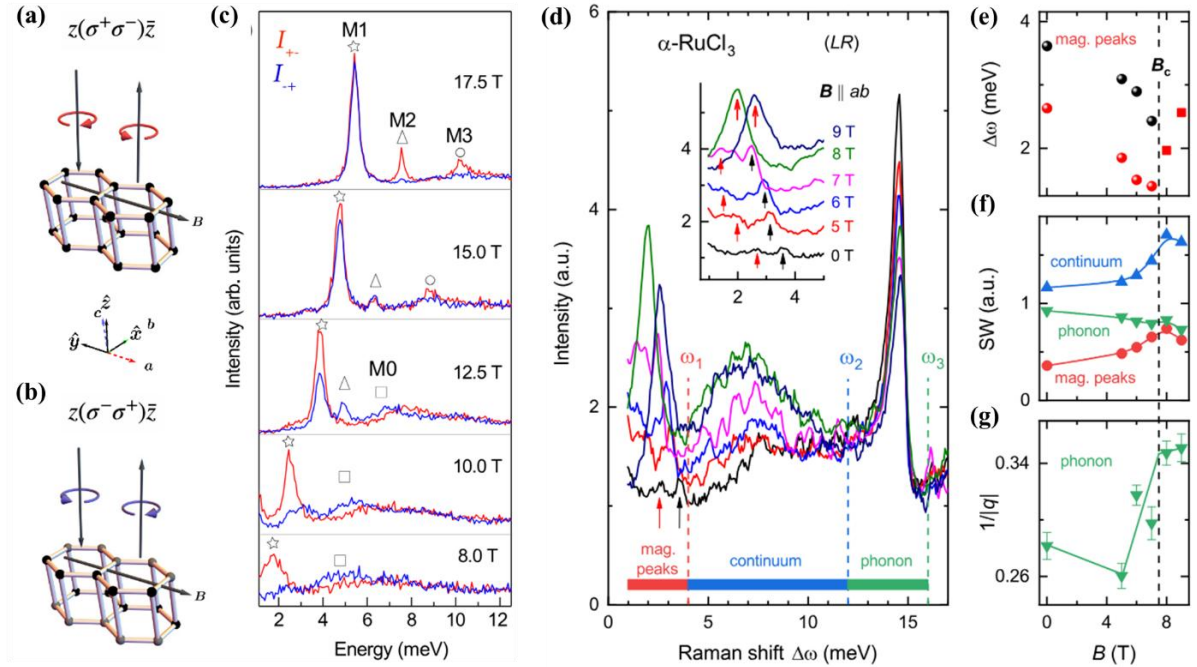


Figure 25: Schematic representation of polarization (circular) resolved Raman scattering (a) I_{+} and (b) I_{-} . The Porto's notation describes the experimental geometry. (c) Helicity dependent Raman response for $B > B_c$ (7.5 T). [331]. (d) Field-dependent circularly polarized (LR – Left/Right circularly polarized light) Raman spectra at 1.7 K, with low power ($\sim 10 \mu\text{W}$). Dashed line separates three different frequency regions in the Raman spectra. Arrows in inset indicate the low-energy magnetic excitations. (e) field-dependent energy transfer of magnetic excitation. (f) field-dependent spectral weight of different frequency regions. (g) variation of Fano asymmetry parameter ($1/|q|$) with applied external field. Dashed line indicates the critical field $B_c = 7.5 \text{ T}$. [330].

The field-dependent (upto 9T) Raman spectra at 1.7 K, in the LR circularly polarized channel is shown in **Figure 25 (d)** [330]. The two-magnetic peaks at 2.7 and 3.6 meV, identified as single-magnon excitation at Γ - point are observed to shift to lower energies with an increase in magnetic field, as shown in **Figure 25 (e)**. These features are observed at very low laser-power $\sim 10 \mu\text{W}$. The field-dependent spectral weight of different frequency ranges indicated by dashed lines in **figure 25 (d)**, containing continuum, phonon mode and magnetic peaks is shown in **figure 25 (f)**. In contrast to the 15-meV phonon mode, the field dependence of

spectral weight for both low-energy excitations and the mid-frequency continuum enhances while approaching B_C . Further, the phonon mode at 15 meV shows line shape asymmetry (Fano), and the asymmetry parameter ($1/|q|$) is shown in **figure 25 (g)**. A sudden increase in the asymmetry is observed as B approaches B_C , owing to increase in continuum scattering strength and its coupling with the phonon modulating Ru-Ru bond [263,330]. The effect of magnetic field on the spin liquid state is further discussed in detail the next section (5.2.5).

5.2.5 Effect of Magnetic Field

Kitaev model theoretically predicts non-Abelian statistics for Z_2 vortices (visons) in presence of external magnetic field (\mathbf{H}) [60], emerging out of non-local entanglement and underlying gauge dictating the quantum correlations inherent to the system. The application of magnetic field introduces time-reversal symmetry-breaking and can alter the excitation spectrum considerably and may lead to chiral spin liquid state. Itinerant Majorana fermion on a honeycomb lattice exhibits a Dirac cone-like excitation spectrum in absence of magnetic field (at K and K' points). However, a topological gap is acquired and is subjected to the direction of the applied external magnetic field. For a 2D honeycomb lattice the energy gap appears and the Chirality of in-plane thermal edge currents is reversed when the direction of field is changed from $\mathbf{H} \parallel \mathbf{a}$ to $-\mathbf{a}$ axis (along antibonding direction of hexagonal lattice). However, when $\mathbf{H} \parallel \mathbf{b}$ -axis the both energy gap and chiral currents disappears [332].

As also seen in above sections most of the candidate materials show long range ordering at low temperatures for e.g., α -RuCl₃ and Na₂IrO₂ [142,333,334]. However, interestingly on the application of external magnetic field the magnetic order is observed to disappear. For example, in case of α -RuCl₃ , with in-plane field strength above 8T, the zigzag magnetic ordering is interrupted and a field-induced quantum-disordered (FIQD) is observed to emerge [214,314,335-338]. A highly disordered and broad response has been observed in neutron-scattering experiments at high temperatures above magnetic ordering [115,264]. A half-

quantized thermal Hall effect further confirmed the presence of Majorana fermions on application of an external magnetic field [339,340]. Morampudi et al., proposed the potential of spectroscopic techniques to provide signatures of anionic fractionalized excitations, where the low-energy onset of spectral functions near the threshold follows universal power laws and the exponent depends only on the statistics of the underlying anionic excitations and hence can characterize topologically ordered states such as gapped quantum spin liquids and fractional Chern insulators [341].

The excitations in a generic Kitaev spin liquid in the chiral phase, having mobile anyons as the low-energy degree of freedom is shown in **figure 26**. In comparison to the pure Kitaev model, where excitations are gapless Majorana fermions (dashed blue lines) and immobile Z_2 fluxes or visons (dashed orange lines), a topological gap Δ_m appears in the Majorana fermion spectrum; whereas the Z_2 fluxes transform into Ising anyons that become dynamical degrees of freedom for generic Kitaev spin liquids[328].

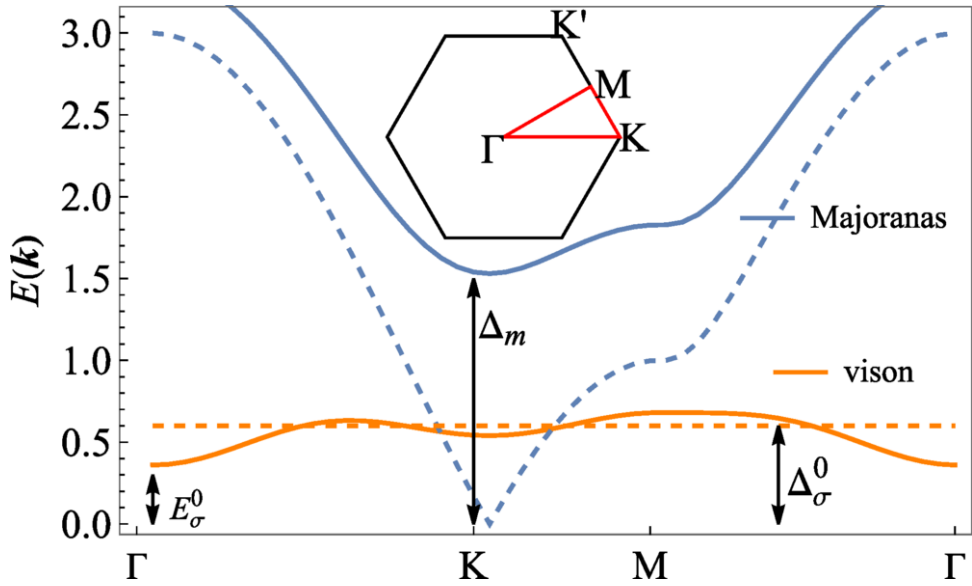


Figure 26: Excitations in a generic Kitaev spin liquid under applied external field (chiral phase) [328].

In the magnetic field dependent Raman experiments in addition to the emergence of a gapped-continuum, multiple sharp peaks have been observed for e.g., α –RuCl₃, and have been attributed to the anionic excitations and their bound states[329]. Further these sharp peaks are found to be sensitive to the handedness (circular polarization) of light indicating the chiral nature of the excitations present in the system. Sahasrabudhe et al., in their high-field Raman and tetrahertz spectroscopy measurements reported a quantum disordered state in α –RuCl₃, observed spin flips, bound states, and multiparticle Raman continuum. Interestingly in addition to the broad Raman continuum, two magnon-like features at 2.7 and 3.6 meV were observed, as also discussed in section 5.2.4. However, the spectral strength of the continuum was observed to increase on application of a magnetic field as the long-range magnetic order is suppressed. Further, at \sim 7.5 T, a gapped multi-particle continuum is observed out of which two-particle bound states emerged with a well-defined single-particle excitation at lower energy. Such features have been attributed to the contribution of off-diagonal exchange terms in the Loudon-Fleury operator [330]. The presence of Chiral excitations in the intermediate magnetic field strength range (7.5 – 10.5 T) was recently reported in the helicity-dependent Raman scattering measurement as a function of temperature and magnetic field [331].

Wulferding et al., in their magnetic field (B = 0 - 29 T) and temperature-dependent Raman spectroscopic (circularly polarized, E_g symmetry channel) study of α –RuCl₃, observed low-energy quasi-particle excitations emerging out of the Raman continuum of fractionalized excitations at intermediate fields, which are in contrast to the conventional magnon excitations. The peculiar temperature dependence of these excitations pointed towards the formation of bound states out of the fractionalized excitations [329]. It was suggested that the application of a magnetic field may lead to the possibility of an Ising topological quantum spin liquid in Kitaev materials. In the case of α –RuCl₃, this transition happens at B_C \sim 6-7 T

[337,342]. However, the intermediate field ($7 - 10$ T) melts the magnetic order into a quantum disordered state, and a half-integer quantized thermal Hall conductance has been observed [339]. Higher magnetic fields lead to a trivial polarized state. **Figure 27 (a-c)** shows the field dependence of Raman spectra at 5K, with magnetic field aligned along the crystallographic a -axis [$B \parallel (100)$]. At fields $B < B_C$ and low temperature ($T < T_N$), along with continuum (fractionalized excitations), signature of magnons is also observed. At $B = 0$, peak $M1$ (~ 2.5 meV) arises from one-magnon scattering and is useful to find the gap of excitations at the Γ -point as a function of field. Weakly bound state occurs in the intermediate phase where spectral weight transfer from the fractionalized continuum happens through an isosbestic point (~ 8.75 meV) and does not transit to the high-field magnon bound state smoothly. For $B > 10$ T, a topological gap opens in the continuum (spectral width becomes narrow) and the spectral weight is shifted to well defined sharp excitations attributing to one/multi-magnon bound states and making a transition to a polarized phase. The opening of the gap is traced by the dashed curve in **figure 27 (d)** [329].

The appearance of spectral features till 29 T is shown in **figure 27 (d-f)**. 2M (orange line; two magnon bound state) separates from M1 for $B > 12$ T, and the 3M (red line; three magnon or a van Hove singularity of the gapped continuum) appears above 10-14T. These features have been realised as one-magnon or magnon-bound states in various experiments [115,245,343]. The field direction-dependent spectra are shown in **figure 27 (g-i)** for directions along (100), (010), and (110), respectively. The anisotropy of magnetic excitations is shown in **figure 27 (j)**. Interestingly, the field-dependent Raman spectra at 2K revealed new sharp peaks M2 (5 meV; two-magnon) and M3 (7.5 meV) in addition to M1 and continuum. Further, as B_C is approached, a new low-energy mode MB appears out of the low-field M2 mode. This new emergent feature in the intermediate phase has been tentatively attributed to the Majorana bound state [115]. The field dependence of MB mode, along with other spin-wave excitations

observed in the zig-zag ordered phase and high-field polarized phase, is plotted in **figure 27 (k)**.

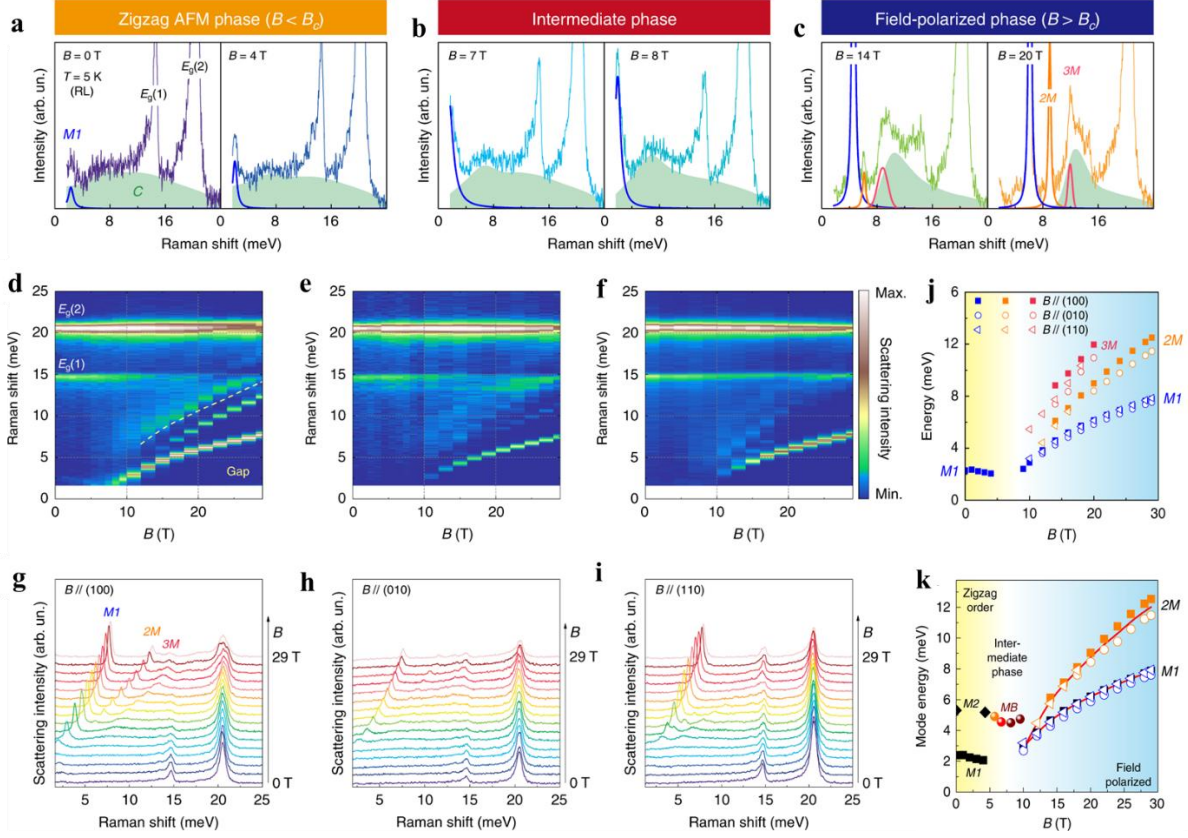


Figure 27: (a-c) Magnetic field-dependent Raman Spectra at 5K. Well-defined phonon, magnon peaks are present on top of the broad Raman continuum (green shade). (d-f) contour plots showing magnetic field direction-dependence [(110), (010), and (100)] of Raman intensity. The magnetic field-dependent gap of the fractionalized excitation continuum is denoted by the dashed line in (d) panel. (g-i) shows the respective raw Raman spectra. (j) field direction-dependence of low-energy excitations (M1, 2M and 3M). (k) field-dependence of various excitations i.e., spin waves at low and high magnetic fields; MB at intermediate strengths (spheres) [329].

The strength of the external magnetic field indeed dictates the dynamics and nature of the underlying quasi-particle excitation. A non-trivial crossover from a magnetically ordered state to a reconfiguration of magnetic fractionalized continuum via an increase in field strength. Further, it will be interesting to investigate the connection between observed Majorana-bound

states and angle dependence of external magnetic field with respect to crystal plane. The application of magnetic field may provide an excellent opportunity to tune non-abelian nature of anionic excitations and realize topologically protected quantum applications.

5.2.6. Effect of Pressure

Pressure, internal via chemical doping or external, is an important parameter to potentially tune the magnetic ordering in putative QSL candidates and may help in realizing the true Kitaev QSL material. External perturbations, such as pressure, affect the underlying physics of the Kitaev system. Huimei et al, in their study of exchange interactions and resulting magnetic phases in the honeycomb cobaltate ($\text{Na}_3\text{Co}_2\text{SbO}_6$), found that the non-Kitaev terms nearly vanish for small values of a trigonal field ($\Delta \sim 20$ meV), which can be achieved via strain or pressure, leads to a spin liquid ground state owing to the localized nature of magnetic electrons in 3d compounds [125]. **Figure 28** shows various magnetic phases of spin-orbit entangled pseudospin-1/2 Co^{2+} ions on a honeycomb lattice. The phase diagram is shown as a function of trigonal field (Δ), and the ratio of Coulomb repulsion U and the charge-transfer gap Δ_{pd} (in a window relevant for honeycomb cobaltates) [125]. Such a result is very interesting and indicates that strong SOC is not a necessary condition for Kitaev physics to be realized. In the pressure-dependent magnetization measurement for Li_2RhO_3 , along with a decrease in the magnitude of nearest-neighbour ferromagnetic Kitaev coupling K_1 the corresponding increase in the antiferromagnetic, off-diagonal anisotropy Γ_1 was observed. The interplay between these terms, along with weak third-neighbor coupling J_3 (stabilize zigzag ordering) adds to magnetic frustration. In this system negative pressure enhances the Kitaev term and reduces the $\Gamma_1 / |K_1|$, hence bringing it closer to the ideal Kitaev limit [344].

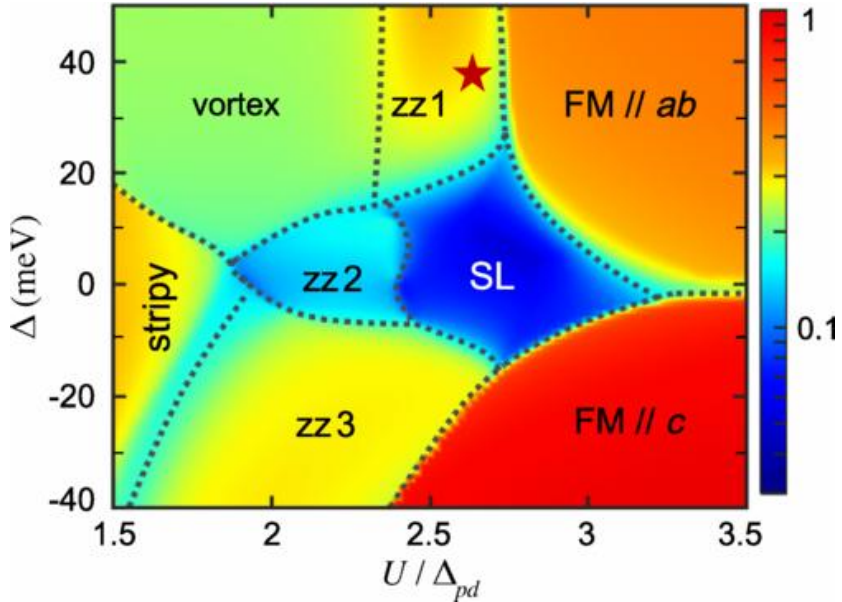


Figure 28: Magnetic phase diagram of honeycomb cobaltates. The Kitaev SL (spin liquid) phase is surrounded by ferromagnetic (FM) states with moments in the honeycomb *ab* plane and along the *c* axis, zigzag-type states with moments in the *ab* plane (zz1), along Co-O bonds (zz2), and in the *ac* plane (zz3). Vortex- and stripy-type phases take over at smaller U/Δ_{pd} . The color map shows the second-NN spin correlation strength, which drops sharply in the SL phase. The star indicates the rough position of $\text{Na}_3\text{Co}_2\text{SbO}_6$. From Liu et al., 2020 [125].

Pressure affects the structure and magnetic ordering in the case of α -RuCl₃ [345,346]. Raman measurements are sensitive to pressure and can simultaneously provide information on phononic and magnetic excitations, as seen in the discussion in earlier sections. In a room-temperature, pressure-dependent study [347] of α -RuCl₃, increasing pressures showed a different structural and magnetic behavior at transition pressure, $p_1 = 1.1$ GPa and $p_2 = 1.7$ GPa. At p_1 appearance of new Raman modes has been observed, as also shown in **Figure 29 (c)**, owing to broken inversion symmetry and variation in the stacking order. Previously, three low-temperature structures have been reported in the literature: the monoclinic *C2/m*, the trigonal *P3₁12*, and the rhombohedral *R-3* [348]. However, here the system changes from the monoclinic (*C2/m*) to the trigonal (*P3₁12*), which is also supported by Raman and SHG (second harmonic generation) data. This pressure-dependent structural transition can be

linked with that reported phase due to a decrease in temperature [263]. At p_2 , the in-plane Ru-Ru bond dimerizes, which is also accompanied by a collapse in the Mott state and is driven to a correlated band insulator. This effect is also visible in the pressure dependence of dynamic Raman susceptibility χ_R , as shown in **Figure 29 (b)**. As χ_R contains the contribution from one/multi-spin susceptibility corresponding to one/multi-spin flip processes. Hence, the drastic increase in the χ_R with increasing pressure till p_1 is attributed to the multispin flip processes. After p_2 , on further increase in pressure, it decreases, which is consistent with the dimerized nonmagnetic scenario.

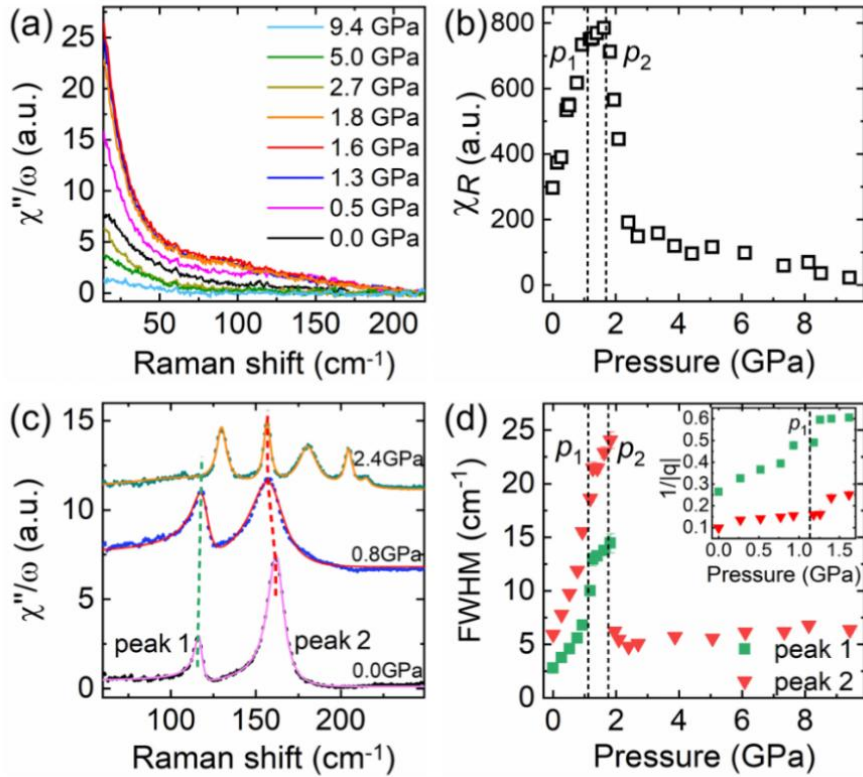


Figure 29: Pressure dependence of the Raman conductivity χ''/ω and the dynamic Raman susceptibility χ_R , in (a) and (b), respectively. (c) The phonon Raman spectra (after subtracting the magnetic continuum) for the 116 cm^{-1} mode (peak 1) and the 161 cm^{-1} mode (peak 2) at different pressures. (d) Pressure dependence of the linewidth and the Fano asymmetry parameter $1/|q|$ (inset) for peak 1 and 2. The vertical dash lines in (b) and (d) indicate the critical pressures. From Li et al., 2019 [347].

The effect of pressure is also seen in the Fano asymmetry and FWHM (**Figure 29 (d)**) of the phonon modes at 116 and 161 cm⁻¹. The coupling strength is reflected in the FWHM and Fano asymmetry parameter (1/|q|) and is consistent with the evolution of χ_R . A similar observation of dimerization (Ir-Ir) and magnetic collapse under pressure has also been reported for α -Li₂IrO₃ and β -Li₂IrO₃, where the critical pressure reported is 4.1 GPa, above which the system turns into a correlated band insulator [108,349].

6. Outlook

Exactly solvable pure Kitaev model for spin-½ was proposed nearly two decades ago; however, hitherto there is no evidence of an ideal Kitaev quantum system. However, the inclusion of more realistic elements (exchange interactions) is bridging the gap between the ideal theoretically proposed model and the material realization. As in most of the putative KQSL candidates have also shown a signature of long-range ordering. The modifiability of Majorana excitations in real materials, at higher temperatures, can bring a breakthrough and the onset of a third quantum revolution. Kitaev physics is no longer bound to just strong spin-orbit coupling. Along with the 4d (α -RuCl₃) and 5d (Ir-based) electron systems, 3d (VPS₃) based systems are also showing experimental signatures of fractionalized excitations.

The Raman signatures of KSL observed are: magnetic continuum (non-bosonic excitation), quasi-elastic scattering, Fano line shape, and anomalies in phonon dynamics. It was found that a finite vacancy binds a flux to the site and, in fact, stabilises the ground state fractionalized excitations. In that context, V_(1-x)PS₃ may turn out to be an ideal candidate, as the existence of fractionalized excitations was observed at ~ 200 K, and the magnetic continuum was found to be enhanced in reduced dimensionality. Pressure, strain in the case of Na₃Co₂SbO₆, provided another controllable parameter that could turn on the quantum spin

liquid behavior. The likes of α -RuCl₃ still remain an elusive candidate with rich phases it exhibits under various environmental conditions.

To conclude, this review article provides a brief historical and theoretical perspective, along with inelastic light scattering, i.e., Raman spectroscopic evidence, and classification of the exotic quasiparticle excitation. Incident light energy, polarization configuration has provided a trustworthy lens to probe the underlying physics of such quantum systems as a function of temperature, pressure, external magnetic field, higher spin-S and thickness (stacking order and interlayer coupling), again highlighting the usefulness of the Raman technique in quantum exploration. There are still open quests for the realization and identification of Majorana modes in real materials, and how they are connected to the ideal model. The exploration of the underlying gauge and topology in the real Kitaev candidates is still an open challenge for the community.

Data availability statement

No new data were created or analysed in this study.

Author contribution statement

Both authors contributed equally to this work.

Declaration of competing interest

The authors declare no competing interests.

Acknowledgment

Authors acknowledge financial support from SERB (CRG/2023/002069), India.

References

- [1] T. Lancaster. Quantum spin liquids. *Contemp. Phys.* **64**, 127 (2023).
- [2] D. Pesin and L. Balents. Mott physics and band topology in materials with strong spin–orbit interaction. *Nat. Phys.* **6**, 376 (2010).
- [3] X.-G. Wen. Colloquium: Zoo of quantum-topological phases of matter. *Rev. Mod. Phys.* **89**, 041004 (2017).
- [4] X.-G. Wen, *Quantum Field Theory of Many-Body Systems: From the Origin of Sound to an Origin of Light and Electrons* (Oxford University Press, 2007).
- [5] L. D. Landau, E. M. Lifshits, L. P. Pitaevskii, J. B. Sykes and M. J. Kearsley, *Statistical Physics* (Pergamon Press, Oxford, 1980), Course of theoretical physics.
- [6] P. Anderson, *Basic Notions of Condensed Matter Physics* (CRC Press, Boca Raton, 2018).
- [7] H. L. Stormer, D. C. Tsui and A. C. Gossard. The fractional quantum Hall effect. *Rev. Mod. Phys.* **71**, S298 (1999).
- [8] W. Heisenberg. Zur Theorie des Ferromagnetismus. *Z. Phys.* **49**, 619 (1928).
- [9] J. Hubbard and B. H. Flowers. Electron correlations in narrow energy bands. *Proc. R. Soc. London, Ser. A* **276**, 238 (1963).
- [10] V. Celebonovic. The Hubbard Model: Basic Ideas and Some Results. *ACS Omega* **8**, 26645 (2023).
- [11] E. Fradkin, *Field Theories Of Condensed Matter Systems* (Addison-Wesley, United States of America, 1991), Vol. 82, *Frontiers In Physics*.
- [12] D. Sen and R. Chitra. Large-U limit of a Hubbard model in a magnetic field: Chiral spin interactions and paramagnetism. *Phys. Rev. B* **51**, 1922 (1995).
- [13] T. Li. What does the giant thermal Hall effect observed in the high temperature superconductors imply? *arXiv:1911.03979 [cond-mat.str-el]* (2019).
- [14] A. Mazurenko, C. S. Chiu, G. Ji, M. F. Parsons, M. Kanasz-Nagy, R. Schmidt, F. Grusdt, E. Demler, D. Greif and M. Greiner. A cold-atom Fermi-Hubbard antiferromagnet. *Nature* **545**, 462 (2017).
- [15] P. A. Lee, N. Nagaosa and X.-G. Wen. Doping a Mott insulator: Physics of high-temperature superconductivity. *Rev. Mod. Phys.* **78**, 17 (2006).
- [16] L. Néel. Propriétés magnétiques de l'état métallique et énergie d'interaction entre atomes magnétiques. *Ann. Phys.* **11**, 232 (1936).

[17] P. W. Anderson, Concepts in solids : lectures on the theory of solids (World Scientific, Singapore, 1923).

[18] A. Auerbach, Interacting electrons and quantum magnetism (Springer-Verlag, New York, 1994).

[19] P. W. Anderson. Resonating valence bonds: A new kind of insulator? Mater. Res. Bull. **8**, 153 (1973).

[20] P. W. Anderson. The Resonating Valence Bond State in La_2CuO_4 and Superconductivity. Science **235**, 1196 (1987).

[21] M. Hermanns, I. Kimchi and J. Knolle. Physics of the Kitaev Model: Fractionalization, Dynamic Correlations, and Material Connections. Annu. Rev. of Condens. Matter Phys. **9**, 17 (2018).

[22] L. Balents. Spin liquids in frustrated magnets. Nature **464**, 199 (2010).

[23] B. Bernu, P. Lecheminant, C. Lhuillier and L. Pierre. Exact spectra, spin susceptibilities, and order parameter of the quantum Heisenberg antiferromagnet on the triangular lattice. Phys. Rev. B **50**, 10048 (1994).

[24] D. A. Huse and V. Elser. Simple Variational Wave Functions for Two-Dimensional Heisenberg Spin-1/2 Antiferromagnets. Phys. Rev. Lett. **60**, 2531 (1988).

[25] S. Yan, D. A. Huse and S. R. White. Spin-Liquid Ground State of the $S = 1/2$ Kagome Heisenberg Antiferromagnet. Science **332**, 1173 (2011).

[26] J.-W. Mei, J.-Y. Chen, H. He and X.-G. Wen. Gapped spin liquid with Z_2 topological order for the kagome Heisenberg model. Phys. Rev. B **95**, 235107 (2017).

[27] H. J. Liao, Z. Y. Xie, J. Chen, Z. Y. Liu, H. D. Xie, R. Z. Huang, B. Normand and T. Xiang. Gapless Spin-Liquid Ground State in the $S=1/2$ Kagome Antiferromagnet. Phys. Rev. Lett. **118**, 137202 (2017).

[28] S. Sachdev. Kagome' - and triangular-lattice Heisenberg antiferromagnets: Ordering from quantum fluctuations and quantum-disordered ground states with unconfined bosonic spinons. Phys. Rev. B **45**, 12377 (1992).

[29] J. Wen, S.-L. Yu, S. Li, W. Yu and J.-X. Li. Experimental identification of quantum spin liquids. npj Quantum Mater. **4**, 12 (2019).

[30] H. Iwase, M. Isobe, Y. Ueda and H. Yasuoka. Observation of Spin Gap in CaV_2O_5 by NMR. J. Phys. Soc. Jpn. **65**, 2397 (1996).

[31] M. Azuma, Z. Hiroi, M. Takano, K. Ishida and Y. Kitaoka. Observation of a Spin Gap in SrCu_2O_3 Comprising Spin-1/2 Quasi-1D Two-Leg Ladders. Phys. Rev. Lett. **73**, 3463 (1994).

[32] H. Kageyama, K. Yoshimura, R. Stern, N. V. Mushnikov, K. Onizuka, M. Kato, K. Kosuge, C. P. Slichter, T. Goto and Y. Ueda. Exact Dimer Ground State and Quantized Magnetization Plateaus in the Two-Dimensional Spin System $\text{SrCu}_2(\text{BO}_3)_2$. *Phys. Rev. Lett.* **82**, 3168 (1999).

[33] L. Savary and L. Balents. Quantum spin liquids: a review. *Rep. Prog. Phys.* **80**, 016502 (2017).

[34] I. Affleck and J. B. Marston. Large- n limit of the Heisenberg-Hubbard model: Implications for high- T_c superconductors. *Phys. Rev. B* **37**, 3774 (1988).

[35] N. Read and S. Sachdev. Large- N expansion for frustrated quantum antiferromagnets. *Phys. Rev. Lett.* **66**, 1773 (1991).

[36] W. Rantner and X.-G. Wen. Electron Spectral Function and Algebraic Spin Liquid for the Normal State of Underdoped High T_c Superconductors. *Phys. Rev. Lett.* **86**, 3871 (2001).

[37] X.-G. Wen. Quantum orders and symmetric spin liquids. *Phys. Rev. B* **65**, 165113 (2002).

[38] X. G. Wen. Topological Orders in Rigid States. *Int. J. Mod. Phys. B* **04**, 239 (1990).

[39] X. G. Wen. Mean-field theory of spin-liquid states with finite energy gap and topological orders. *Phys. Rev. B* **44**, 2664 (1991).

[40] D. S. Simon, *Tying Light in Knots* (Morgan & Claypool Publishers, 2018), Applying topology to optics.

[41] K. v. Klitzing, G. Dorda and M. Pepper. New Method for High-Accuracy Determination of the Fine-Structure Constant Based on Quantized Hall Resistance. *Phys. Rev. Lett.* **45**, 494 (1980).

[42] A. S. T. Pires, *A Brief Introduction to Topology and Differential Geometry in Condensed Matter Physics* (Second Edition) (IOP Publishing, Bristol, 2021).

[43] D. J. Thouless, M. Kohmoto, M. P. Nightingale and M. den Nijs. Quantized Hall Conductance in a Two-Dimensional Periodic Potential. *Phys. Rev. Lett.* **49**, 405 (1982).

[44] F. D. M. Haldane. Model for a Quantum Hall Effect without Landau Levels: Condensed-Matter Realization of the "Parity Anomaly". *Phys. Rev. Lett.* **61**, 2015 (1988).

[45] A. Einstein, B. Podolsky and N. Rosen. Can Quantum-Mechanical Description of Physical Reality Be Considered Complete? *Phys. Rev.* **47**, 777 (1935).

[46] F. J. Duarte, *Fundamentals of Quantum Entanglement* (Second Edition) (IOP Publishing, Bristol, 2022).

[47] N. Laflorencie. Quantum entanglement in condensed matter systems. *Phys. Rep.* **646**, 1 (2016).

[48] T. Giamarchi, Quantum Physics in One Dimension (Oxford University Press, New York, 2003).

[49] A. Ralko and J. Merino. Chiral bosonic quantum spin liquid in the integer-spin Heisenberg-Kitaev model. *Phys. Rev. B* **110**, 134402 (2024).

[50] L. D. a. L. Landau, E.M., Quantum Mechanics (Non-Relativistic Theory) (Pergamon Press, Oxford, 1977), 3rd edn., Vol. 3.

[51] C. Cohen-Tannoudji, Diu, B. and Laloe, F., Quantum Mechanics (Wiley, New York, 1977), Vol. 2.

[52] F. Wilczek. Quantum Mechanics of Fractional-Spin Particles. *Phys. Rev. Lett.* **49**, 957 (1982).

[53] Z. Wang and K. R. A. Hazzard. Particle exchange statistics beyond fermions and bosons. *Nature* **637**, 314 (2025).

[54] L. R. Feynman RP, Sands M., The Feynman lectures on physics. Vol. I. (Pearson Addison Wesley, San Francisco, 2006).

[55] J. M. Leinaas and J. Myrheim. On the theory of identical particles. *Nuovo Cimento B* **37**, 1 (1977).

[56] N. Read and D. Green. Paired states of fermions in two dimensions with breaking of parity and time-reversal symmetries and the fractional quantum Hall effect. *Phys. Rev. B* **61**, 10267 (2000).

[57] F. Wilczek. Anyons for anyone. *Physics World* **4**, 40 (1991).

[58] B. Field and T. Simula. Introduction to topological quantum computation with non-Abelian anyons. *Quantum Sci. Technol.* **3**, 045004 (2018).

[59] C. Nayak, S. H. Simon, A. Stern, M. Freedman and S. Das Sarma. Non-Abelian anyons and topological quantum computation. *Rev. Mod. Phys.* **80**, 1083 (2008).

[60] A. Kitaev. Anyons in an exactly solved model and beyond. *Ann. Phys.* **321**, 2 (2006).

[61] A. Y. Kitaev. Fault-tolerant quantum computation by anyons. *Ann. Phys.* **303**, 2 (2003).

[62] A. G. Williams, Introduction to quantum field theory: classical mechanics to gauge field theories (Cambridge University Press, Cambridge, 2023).

[63] S. Liang, B. Doucot and P. W. Anderson. Some New Variational Resonating-Valence-Bond-Type Wave Functions for the Spin-1/2 Antiferromagnetic Heisenberg Model on a Square Lattice. *Phys. Rev. Lett.* **61**, 365 (1988).

[64] J. B. Kogut. An introduction to lattice gauge theory and spin systems. *Rev. Mod. Phys.* **51**, 659 (1979).

[65] M. E. Peskin and D. V. Schroeder, *An Introduction To Quantum Field Theory* (Westview Press, New York, 1995).

[66] M. D. Schwartz, *Quantum Field Theory and the Standard Model* (Cambridge University Press, Cambridge, UK, 2014).

[67] G. Chen. Dirac's "magnetic monopoles" in pyrochlore ice $U(1)$ spin liquids: Spectrum and classification. *Phys. Rev. B* **96**, 195127 (2017).

[68] C. Castelnovo, R. Moessner and S. L. Sondhi. Spin Ice, Fractionalization, and Topological Order. *Annu. Rev. Condens. Matter Phys.* **3**, 35 (2012).

[69] G. Ravikumar, V. C. Sahni, A. K. Grover, S. Ramakrishnan, P. L. Gammel, D. J. Bishop, E. Bucher, M. J. Higgins and S. Bhattacharya. Stable and metastable vortex states and the first-order transition across the peak-effect region in weakly pinned 2H-NbSe₂. *Phys. Rev. B* **63**, 024505 (2000).

[70] T. Senthil and M. P. A. Fisher. Z_2 gauge theory of electron fractionalization in strongly correlated systems. *Phys. Rev. B* **62**, 7850 (2000).

[71] N. Read and B. Chakraborty. Statistics of the excitations of the resonating-valence-bond state. *Phys. Rev. B* **40**, 7133 (1989).

[72] S. Kivelson. Statistics of holons in the quantum hard-core dimer gas. *Phys. Rev. B* **39**, 259 (1989).

[73] C. Broholm, R. J. Cava, S. A. Kivelson, D. G. Nocera, M. R. Norman and T. Senthil. Quantum spin liquids. *Science* **367** (2020).

[74] J. Bardeen, L. N. Cooper and J. R. Schrieffer. Theory of superconductivity. *Phys. Rev.* **108**, 1175 (1957).

[75] S. A. Kivelson and D. S. Rokhsar. Bogoliubov quasiparticles, spinons, and spin-charge decoupling in superconductors. *Phys. Rev. B* **41**, 11693 (1990).

[76] T. H. Hansson, V. Oganesyan and S. L. Sondhi. Superconductors are topologically ordered. *Ann. Phys.* **313**, 497 (2004).

[77] K. T. Law and P. A. Lee. 1T-TaS₂ as a quantum spin liquid. *Proc. Natl. Acad. Sci.* **114**, 6996 (2017).

[78] S. Mañas-Valero, B. M. Huddart, T. Lancaster, E. Coronado and F. L. Pratt. Quantum phases and spin liquid properties of 1T-TaS₂. *npj Quantum Mater.* **6**, 69 (2021).

[79] A. Ribak, I. Silber, C. Baines, K. Chashka, Z. Salman, Y. Dagan and A. Kanigel. Gapless excitations in the ground state of 1T-TaS₂. *Phys. Rev. B* **96**, 195131 (2017).

[80] Y. Li. YbMgGaO₄: A Triangular-Lattice Quantum Spin Liquid Candidate. *Adv. Quantum Technol.* **2**, 1900089 (2019).

[81] Y. Li, D. Adroja, P. K. Biswas, P. J. Baker, Q. Zhang, J. Liu, A. A. Tsirlin, P. Gegenwart and Q. Zhang. Muon Spin Relaxation Evidence for the $U(1)$ Quantum Spin-Liquid Ground State in the Triangular Antiferromagnet YbMgGaO_4 . *Phys. Rev. Lett.* **117**, 097201 (2016).

[82] J. A. M. Paddison, M. Daum, Z. Dun, G. Ehlers, Y. Liu, Matthew B. Stone, H. Zhou and M. Mourigal. Continuous excitations of the triangular-lattice quantum spin liquid YbMgGaO_4 . *Nat. Phys.* **13**, 117 (2017).

[83] A. O. Scheie, E. A. Ghioldi, J. Xing, J. A. M. Paddison, N. E. Sherman, M. Dupont, L. D. Sanjeeva, S. Lee, A. J. Woods, D. Abernathy, D. M. Pajerowski, T. J. Williams, S.-S. Zhang, L. O. Manuel, A. E. Trumper, C. D. Pemmaraju, A. S. Sefat, D. S. Parker, T. P. Devereaux, R. Movshovich, J. E. Moore, C. D. Batista and D. A. Tennant. Proximate spin liquid and fractionalization in the triangular antiferromagnet KYbSe_2 . *Nat. Phys.* **20**, 74 (2024).

[84] A. O. Scheie, Y. Kamiya, H. Zhang, S. Lee, A. J. Woods, M. O. Ajesh, M. G. Gonzalez, B. Bernu, J. W. Villanova, J. Xing, Q. Huang, Q. Zhang, J. Ma, E. S. Choi, D. M. Pajerowski, H. Zhou, A. S. Sefat, S. Okamoto, T. Berlijn, L. Messio, R. Movshovich, C. D. Batista and D. A. Tennant. Nonlinear magnons and exchange Hamiltonians of the delafossite proximate quantum spin liquid candidates KYbSe_2 and NaYbSe_2 . *Phys. Rev. B* **109**, 014425 (2024).

[85] S. Lee, A. J. Woods, M. Lee, S. Zhang, E. S. Choi, A. O. Scheie, D. A. Tennant, J. Xing, A. S. Sefat and R. Movshovich. Magnetic field-temperature phase diagram of the spin-1/2 triangular lattice antiferromagnet KYbSe_2 . *Phys. Rev. B* **109**, 155129 (2024).

[86] B. Miksch, A. Pustogow, M. J. Rahim, A. A. Bardin, K. Kanoda, J. A. Schlueter, R. Hübner, M. Scheffler and M. Dressel. Gapped magnetic ground state in quantum spin liquid candidate $k\text{-(BEDT-TTF)}_2\text{Cu}_2(\text{CN})_3$. *Science* **372**, 276 (2021).

[87] T. Isono, T. Terashima, K. Miyagawa, K. Kanoda and S. Uji. Quantum criticality in an organic spin-liquid insulator $k\text{-(BEDT-TTF)}_2\text{Cu}_2(\text{CN})_3$. *Nat. Commun.* **7**, 13494 (2016).

[88] M. Lang, R. S. Manna, M. de Souza, A. Brühl and J. A. Schlueter. Phase transition and lattice distortion in the proposed spin-liquid system $\kappa\text{-(BEDT-TTF)}_2\text{Cu}_2(\text{CN})_3$. *Physica B: Condensed Matter* **405**, S182 (2010).

[89] J. S. Helton, K. Matan, M. P. Shores, E. A. Nytko, B. M. Bartlett, Y. Yoshida, Y. Takano, A. Suslov, Y. Qiu, J. H. Chung, D. G. Nocera and Y. S. Lee. Spin dynamics of the spin-1/2 kagome lattice antiferromagnet $\text{ZnCu}_3(\text{OH})_6\text{Cl}_2$. *Phys. Rev. Lett.* **98**, 107204 (2007).

[90] M. Fu, T. Imai, T.-H. Han and Y. S. Lee. Evidence for a gapped spin-liquid ground state in a kagome Heisenberg antiferromagnet. *Science* **350**, 655 (2015).

[91] Y. Fu, M. L. Lin, L. Wang, Q. Liu, L. Huang, W. Jiang, Z. Hao, C. Liu, H. Zhang, X. Shi, J. Zhang, J. Dai, D. Yu, F. Ye, P. A. Lee, P. H. Tan and J. W. Mei. Dynamic fingerprint of fractionalized excitations in single-crystalline $\text{Cu}_3\text{Zn}(\text{OH})_6\text{FBr}$. *Nat. Commun.* **12**, 3048 (2021).

[92] Y. Singh, Y. Tokiwa, J. Dong and P. Gegenwart. Spin liquid close to a quantum critical point in $\text{Na}_4\text{Ir}_3\text{O}_8$. *Phys. Rev. B* **88**, 220413 (2013).

[93] M. J. Lawler, H.-Y. Kee, Y. B. Kim and A. Vishwanath. Topological Spin Liquid on the Hyperkagome Lattice of $\text{Na}_4\text{Ir}_3\text{O}_8$. *Phys. Rev. Lett.* **100**, 227201 (2008).

[94] P. Khuntia, F. Bert, P. Mendels, B. Koteswararao, A. V. Mahajan, M. Baenitz, F. C. Chou, C. Baines, A. Amato and Y. Furukawa. Spin Liquid State in the 3D Frustrated Antiferromagnet $\text{PbCuTe}_2\text{O}_6$: NMR and Muon Spin Relaxation Studies. *Phys. Rev. Lett.* **116**, 107203 (2016).

[95] K. C. Sahu and S. Sanyal. U(1) quantum spin liquids in dipolar-octupolar pyrochlore magnets: A fermionic parton approach. *Phys. Rev. B* **110**, 115144 (2024).

[96] E. M. Smith, O. Benton, D. R. Yahne, B. Placke, R. Schäfer, J. Gaudet, J. Dudemaine, A. Fitterman, J. Beare, A. R. Wildes, S. Bhattacharya, T. DeLazzer, C. R. C. Buhariwalla, N. P. Butch, R. Movshovich, J. D. Garrett, C. A. Marjerrison, J. P. Clancy, E. Kermarrec, G. M. Luke, A. D. Bianchi, K. A. Ross and B. D. Gaulin. Case for a $U(1)\}_{\pi}$ Quantum Spin Liquid Ground State in the Dipole-Octupole Pyrochlore $\text{Ce}_2\text{Zr}_2\text{O}_7$. *Phys. Rev. X* **12**, 021015 (2022).

[97] K. Kimura, S. Nakatsuji, J. J. Wen, C. Broholm, M. B. Stone, E. Nishibori and H. Sawa. Quantum fluctuations in spin-ice-like $\text{Pr}_2\text{Zr}_2\text{O}_7$. *Nat. Commun.* **4**, 1934 (2013).

[98] M. J. P. Gingras and P. A. McClarty. Quantum spin ice: a search for gapless quantum spin liquids in pyrochlore magnets. *Rep. Prog. Phys.* **77**, 056501 (2014).

[99] C. Wessler, B. Roessli, K. W. Krämer, B. Delley, O. Waldmann, L. Keller, D. Cheptiakov, H. B. Braun and M. Kenzelmann. Observation of plaquette fluctuations in the spin-1/2 honeycomb lattice. *npj Quantum Mater.* **5**, 85 (2020).

[100] M. J. Coak, S. Son, D. Daisenberger, H. Hamidov, C. R. S. Haines, P. L. Alireza, A. R. Wildes, C. Liu, S. S. Saxena and J.-G. Park. Isostructural Mott transition in 2D honeycomb antiferromagnet $\text{V}_{0.9}\text{PS}_3$. *npj Quantum Mater.* **4**, 38 (2019).

[101] C. Liu, Z. Li, J. Hu, H. Duan, C. Wang, L. Cai, S. Feng, Y. Wang, R. Liu, D. Hou, C. Liu, R. Zhang, L. Zhu, Y. Niu, A. A. Zakharov, Z. Sheng and W. Yan. Probing the Néel-Type Antiferromagnetic Order and Coherent Magnon–Exciton Coupling in Van Der Waals VPS_3 . *Adv. Mater.* **35**, 2300247 (2023).

[102] V. Kumar, D. Kumar, B. Singh, Y. Shemerliuk, M. Behnami, B. Büchner, S. Aswartham and P. Kumar. Fluctuating fractionalized spins in quasi-two-dimensional magnetic $V_{0.85}PS_3$. *Phys. Rev. B* **107**, 094417 (2023).

[103] V. Kumar, Y. Shemerliuk, M. Behnami, B. Büchner, S. Aswartham and P. Kumar. Dynamics of phonons and magnetic continuum in thin flakes of $V_{1-x}PS_3$. *Phys. Rev. Mater.* **9**, 076201 (2025).

[104] Y. Singh, S. Manni, J. Reuther, T. Berlijn, R. Thomale, W. Ku, S. Trebst and P. Gegenwart. Relevance of the Heisenberg-Kitaev model for the honeycomb lattice iridates A_2IrO_3 . *Phys. Rev. Lett.* **108**, 127203 (2012).

[105] N. D. Patel and N. Trivedi. Magnetic field-induced intermediate quantum spin liquid with a spinon Fermi surface. *Proc. Natl. Acad. Sci. U.S.A.* **116**, 12199 (2019).

[106] S. C. Williams, R. D. Johnson, F. Freund, S. Choi, A. Jesche, I. Kimchi, S. Manni, A. Bombardi, P. Manuel, P. Gegenwart and R. Coldea. Incommensurate counterrotating magnetic order stabilized by Kitaev interactions in the layered honeycomb β - Li_2IrO_3 . *Phys. Rev. B* **93**, 195158 (2016).

[107] A. A. Tsirlin and P. Gegenwart. Kitaev Magnetism through the Prism of Lithium Iridate. *Phys. Status Solidi B* **259**, 2100146 (2022).

[108] G. Li, L.-L. Huang, X. Chen, C. Liu, S. Pei, X. Wang, S. Wang, Y. Zhao, D. Yu, L. Wang, F. Ye, J.-W. Mei and M. Huang. Probing the continuum scattering and magnetic collapse in single-crystalline β - Li_2IrO_3 by Raman spectroscopy. *Phys. Rev. B* **101**, 174436 (2020).

[109] T. Takayama, A. Kato, R. Dinnebier, J. Nuss, H. Kono, L. S. Veiga, G. Fabbris, D. Haskel and H. Takagi. Hyperhoneycomb Iridate β - Li_2IrO_3 as a platform for Kitaev magnetism. *Phys. Rev. Lett.* **114**, 077202 (2015).

[110] V. M. Katukuri, R. Yadav, L. Hozoi, S. Nishimoto and J. van den Brink. The vicinity of hyper-honeycomb β - Li_2IrO_3 to a three-dimensional Kitaev spin liquid state. *Sci. Rep.* **6**, 29585 (2016).

[111] A. Glamazda, P. Lemmens, S. H. Do, Y. S. Choi and K. Y. Choi. Raman spectroscopic signature of fractionalized excitations in the harmonic-honeycomb iridates β - and γ - Li_2IrO_3 . *Nat. Commun.* **7**, 12286 (2016).

[112] A. Biffin, R. D. Johnson, I. Kimchi, R. Morris, A. Bombardi, J. G. Analytis, A. Vishwanath and R. Coldea. Noncoplanar and counterrotating incommensurate magnetic order stabilized by Kitaev interactions in γ - Li_2IrO_3 . *Phys. Rev. Lett.* **113**, 197201 (2014).

[113] H. Li, H.-K. Zhang, J. Wang, H.-Q. Wu, Y. Gao, D.-W. Qu, Z.-X. Liu, S.-S. Gong and W. Li. Identification of magnetic interactions and high-field quantum spin liquid in α -RuCl₃. *Nat. Commun.* **12**, 4007 (2021).

[114] Q. Stahl, T. Ritschel, G. Garbarino, F. Cova, A. Isaeva, T. Doert and J. Geck. Pressure-tuning of α -RuCl₃ towards a quantum spin liquid. *Nat. Commun.* **15**, 8142 (2024).

[115] A. Banerjee, P. Lampen-Kelley, J. Knolle, C. Balz, A. A. Aczel, B. Winn, Y. Liu, D. Pajerowski, J. Yan, C. A. Bridges, A. T. Savici, B. C. Chakoumakos, M. D. Lumsden, D. A. Tennant, R. Moessner, D. G. Mandrus and S. E. Nagler. Excitations in the field-induced quantum spin liquid state of α -RuCl₃. *npj Quantum Mater.* **3** (2018).

[116] S. Pal, A. Seth, P. Sakrikar, A. Ali, S. Bhattacharjee, D. V. S. Muthu, Y. Singh and A. K. Sood. Probing signatures of fractionalization in the candidate quantum spin liquid Cu₂IrO₃ via anomalous Raman scattering. *Phys. Rev. B* **104**, 184420 (2021).

[117] S. Pal, P. Malavi, A. Sinha, A. Ali, P. Sakrikar, B. Joseph, U. V. Waghmare, Y. Singh, D. V. S. Muthu, S. Karmakar and A. K. Sood. Pressure tuning of structure, magnetic frustration, and carrier conduction in the Kitaev spin liquid candidate Cu₂IrO₃. *Phys. Rev. B* **107**, 085105 (2023).

[118] K. Slagle, W. Choi, L. E. Chern and Y. B. Kim. Theory of a quantum spin liquid in the hydrogen-intercalated honeycomb iridate H₃LiIr₂O₆. *Phys. Rev. B* **97**, 115159 (2018).

[119] K. Kitagawa, T. Takayama, Y. Matsumoto, A. Kato, R. Takano, Y. Kishimoto, S. Bette, R. Dinnebier, G. Jackeli and H. Takagi. A spin-orbital-entangled quantum liquid on a honeycomb lattice. *Nature* **554**, 341 (2018).

[120] G. Lin, J. Jeong, C. Kim, Y. Wang, Q. Huang, T. Masuda, S. Asai, S. Itoh, G. Günther, M. Russina, Z. Lu, J. Sheng, L. Wang, J. Wang, G. Wang, Q. Ren, C. Xi, W. Tong, L. Ling, Z. Liu, L. Wu, J. Mei, Z. Qu, H. Zhou, X. Wang, J.-G. Park, Y. Wan and J. Ma. Field-induced quantum spin disordered state in spin-1/2 honeycomb magnet Na₂Co₂TeO₆. *Nat. Commun.* **12**, 5559 (2021).

[121] S. Zhang, S. Lee, E. Brosha, Q. Huang, H. Zhou, V. S. Zapf and M. Lee. Out-of-plane magnetic phase diagram of the Kitaev quantum magnet Na₂Co₂TeO₆. *Phys. Rev. B* **110**, 144431 (2024).

[122] S. Fang, K. Imamura, Y. Mizukami, R. Namba, K. Ishihara, K. Hashimoto and T. Shibauchi. Field-Angle-Resolved Specific Heat in Na₂Co₂TeO₆: Evidence against Kitaev Quantum Spin Liquid. *Phys. Rev. Lett.* **134**, 106701 (2025).

[123] A. G. Chakkar, C. B. Auti, D. Kumar, N. Jana, K. Pal and P. Kumar. Raman signature of multiple phase transitions and quasiparticle excitations in the putative Kitaev spin liquid candidate $\text{Na}_2\text{Co}_2\text{TeO}_6$. *Phys. Rev. B* **112**, 144417 (2025).

[124] J. Q. Yan, S. Okamoto, Y. Wu, Q. Zheng, H. D. Zhou, H. B. Cao and M. A. McGuire. Magnetic order in single crystals of $\text{Na}_3\text{Co}_2\text{SbO}_6$ with a honeycomb arrangement of $3d^7\text{ Co}^{2+}$ ions. *Phys. Rev. Mater.* **3**, 074405 (2019).

[125] H. Liu, J. Chaloupka and G. Khaliullin. Kitaev Spin Liquid in 3d Transition Metal Compounds. *Phys. Rev. Lett.* **125**, 047201 (2020).

[126] Z. Fu, R. Xu, Y. Chen, S. Bao, H. Du, J. Min, S. Zheng, Y. Zhang, M. Liu, X. Wang, H. Li, R. Zhong, H. Luo, J.-M. Liu, Z. Ma and J. Wen. Signatures of a gapless quantum spin liquid in the Kitaev material $\text{Na}_3\text{Co}_{2-x}\text{Zn}_x\text{O}_6$. *Phys. Rev. B* **107**, 165143 (2023).

[127] J. Nordlander, M. A. Anderson, T. Chiang, A. Kaczmarek, N. Pokhrel, K. Talit, S. Doyle, E. Mercer, C. Tzschaschel, J.-H. Son, H. El-Sherif, C. M. Brooks, E.-A. Kim, A. de la Torre, I. El Baggari, E. A. Nowadnick, K. C. Nowack, J. T. Heron and J. A. Mundy. Signatures of quantum spin liquid state and unconventional transport in thin film TbInO_3 . *Nat. Commun.* **16**, 9469 (2025).

[128] C. J. Ridley, A. H. Abdeldaim, C. L. Bull, K. Tustain and L. Clark. Pressure-induced tuning of the triangular-honeycomb structure of ferroelectric quantum spin liquid candidate, TbInO_3 . *Dalton Trans.* **54**, 15696 (2025).

[129] L. Clark, G. Sala, D. D. Maharaj, M. B. Stone, K. S. Knight, M. T. F. Telling, X. Wang, X. Xu, J. Kim, Y. Li, S.-W. Cheong and B. D. Gaulin. Two-dimensional spin liquid behaviour in the triangular-honeycomb antiferromagnet TbInO_3 . *Nat. Phys.* **15**, 262 (2019).

[130] J. Kim, X. Wang, F.-T. Huang, Y. Wang, X. Fang, X. Luo, Y. Li, M. Wu, S. Mori, D. Kwok, E. D. Mun, V. S. Zapf and S.-W. Cheong. Spin Liquid State and Topological Structural Defects in Hexagonal TbInO_3 . *Phys. Rev. X* **9**, 031005 (2019).

[131] S.-S. Lee. Stability of the $U(1)$ spin liquid with a spinon Fermi surface in 2+1 dimensions. *Phys. Rev. B* **78**, 085129 (2008).

[132] B. Fåk, S. Bieri, E. Canévet, L. Messio, C. Payen, M. Viaud, C. Guillot-Deudon, C. Darie, J. Ollivier and P. Mendels. Evidence for a spinon Fermi surface in the triangular $S=1$ quantum spin liquid $\text{Ba}_3\text{NiSb}_2\text{O}_9$. *Phys. Rev. B* **95**, 060402(R) (2017).

[133] P.-L. Dai, G. Zhang, Y. Xie, C. Duan, Y. Gao, Z. Zhu, E. Feng, Z. Tao, C.-L. Huang, H. Cao, A. Podlesnyak, G. E. Granroth, M. S. Everett, J. C. Neufeind, D. Voneshen, S. Wang, G. Tan, E. Morosan, X. Wang, H.-Q. Lin, L. Shu, G. Chen, Y. Guo, X. Lu and P. Dai. Spinon

Fermi Surface Spin Liquid in a Triangular Lattice Antiferromagnet NaYbSe_2 . *Phys. Rev. X* **11**, 021044 (2021).

[134] M. Hermele, Y. Ran, P. A. Lee and X.-G. Wen. Properties of an algebraic spin liquid on the kagome lattice. *Phys. Rev. B* **77**, 224413 (2008).

[135] Y. Zhou, K. Kanoda and T.-K. Ng. Quantum spin liquid states. *Rev. Mod. Phys.* **89**, 025003 (2017).

[136] J. Knolle and R. Moessner. A Field Guide to Spin Liquids. *Annu. Rev. Condens. Matter Phys.* **10**, 451 (2019).

[137] M. Dressel and A. Pustogow. Electrodynamics of quantum spin liquids. *J Phys Condens Matter* **30**, 203001 (2018).

[138] G. Jackeli and G. Khaliullin. Mott Insulators in the Strong Spin-Orbit Coupling Limit: From Heisenberg to a Quantum Compass and Kitaev Models. *Phys. Rev. Lett.* **102**, 017205 (2009).

[139] K. A. Modic, T. E. Smidt, I. Kimchi, N. P. Breznay, A. Biffin, S. Choi, R. D. Johnson, R. Coldea, P. Watkins-Curry, G. T. McCandless, J. Y. Chan, F. Gandara, Z. Islam, A. Vishwanath, A. Shekhter, R. D. McDonald and J. G. Analytis. Realization of a three-dimensional spin-anisotropic harmonic honeycomb iridate. *Nat. Commun.* **5**, 4203 (2014).

[140] S.-H. Do, S.-Y. Park, J. Yoshitake, J. Nasu, Y. Motome, Yong S. Kwon, D. T. Adroja, D. J. Voneshen, K. Kim, T. H. Jang, J. H. Park, K.-Y. Choi and S. Ji. Majorana fermions in the Kitaev quantum spin system $\alpha\text{-RuCl}_3$. *Nat. Phys.* **13**, 1079 (2017).

[141] A. de la Torre, B. Zager, F. Bahrami, M. H. Upton, J. Kim, G. Fabbris, G. H. Lee, W. Yang, D. Haskel, F. Tafti and K. W. Plumb. Momentum-independent magnetic excitation continuum in the honeycomb iridate $\text{H}_3\text{LiIr}_2\text{O}_6$. *Nat. Commun.* **14**, 5018 (2023).

[142] S. Trebst and C. Hickey. Kitaev materials. *Phys. Rep.* **950**, 1 (2022).

[143] P. Lecheminant, B. Bernu, C. Lhuillier, L. Pierre and P. Sindzingre. Order versus disorder in the quantum Heisenberg antiferromagnet on the kagomé lattice using exact spectra analysis. *Phys. Rev. B* **56**, 2521 (1997).

[144] R. Moessner and J. T. Chalker. Properties of a Classical Spin Liquid: The Heisenberg Pyrochlore Antiferromagnet. *Phys. Rev. Lett.* **80**, 2929 (1998).

[145] G. Baskaran, D. Sen and R. Shankar. Spin-SKitaev model: Classical ground states, order from disorder, and exact correlation functions. *Phys. Rev. B* **78**, 115116 (2008).

[146] I. Rousouchatzakis, Y. Sizuk and N. B. Perkins. Quantum spin liquid in the semiclassical regime. *Nat. Commun.* **9**, 1575 (2018).

[147] A. Agarwala, S. Bhattacharjee, J. Knolle and R. Moessner. Gapless state of interacting Majorana fermions in a strain-induced Landau level. *Phys. Rev. B* **103**, 134427 (2021).

[148] P. Rao, R. Moessner and J. Knolle. Dynamical response theory of interacting Majorana fermions and its application to generic Kitaev quantum spin liquids in a field. *Phys. Rev. B* **112**, 024440 (2025).

[149] J. Knolle, D. L. Kovrizhin, J. T. Chalker and R. Moessner. Dynamics of a Two-Dimensional Quantum Spin Liquid: Signatures of Emergent Majorana Fermions and Fluxes. *Phys. Rev. Lett.* **112**, 207203 (2014).

[150] J. Knolle, G.-W. Chern, D. L. Kovrizhin, R. Moessner and N. B. Perkins. Raman Scattering Signatures of Kitaev Spin Liquids in $A_2\text{IrO}_3$ Iridates with $A = \text{Na}$ or Li . *Phys. Rev. Lett.* **113**, 187201 (2014).

[151] J. Nasu, J. Knolle, D. L. Kovrizhin, Y. Motome and R. Moessner. Fermionic response from fractionalization in an insulating two-dimensional magnet. *Nat. Phys.* **12**, 912 (2016).

[152] K. W. Plumb, J. P. Clancy, L. J. Sandilands, V. V. Shankar, Y. F. Hu, K. S. Burch, H.-Y. Kee and Y.-J. Kim. α -RuCl₃: A spin-orbit assisted Mott insulator on a honeycomb lattice. *Phys. Rev. B* **90**, 041112(R) (2014).

[153] S. Bette, T. Takayama, K. Kitagawa, R. Takano, H. Takagi and R. E. Dinnebier. Solution of the heavily stacking faulted crystal structure of the honeycomb iridate H₃LiIr₂O₆. *Dalton Trans.* **46**, 15216 (2017).

[154] J. Nasu, M. Udagawa and Y. Motome. Thermal fractionalization of quantum spins in a Kitaev model: Temperature-linear specific heat and coherent transport of Majorana fermions. *Phys. Rev. B* **92**, 115122 (2015).

[155] H. Suzuki, H. Liu, J. Bertinshaw, K. Ueda, H. Kim, S. Laha, D. Weber, Z. Yang, L. Wang, H. Takahashi, K. Fürsich, M. Minola, B. V. Lotsch, B. J. Kim, H. Yavaş, M. Daghofer, J. Chaloupka, G. Khaliullin, H. Gretarsson and B. Keimer. Proximate ferromagnetic state in the Kitaev model material α -RuCl₃. *Nat. Commun.* **12**, 4512 (2021).

[156] A. Banerjee, J. Yan, J. Knolle, C. A. Bridges, M. B. Stone, M. D. Lumsden, D. G. Mandrus, D. A. Tennant, R. Moessner and S. E. Nagler. Neutron scattering in the proximate quantum spin liquid α -RuCl₃. *Science* **356**, 1055 (2017).

[157] J. G. Rau, E. K.-H. Lee and H.-Y. Kee. Generic Spin Model for the Honeycomb Iridates beyond the Kitaev Limit. *Phys. Rev. Lett.* **112**, 077204 (2014).

[158] J. Chaloupka, G. Jackeli and G. Khaliullin. Zigzag Magnetic Order in the Iridium Oxide Na₂IrO₃. *Phys. Rev. Lett.* **110**, 097204 (2013).

[159] J. S. Gordon, A. Catuneanu, E. S. Sørensen and H.-Y. Kee. Theory of the field-revealed Kitaev spin liquid. *Nat. Commun.* **10**, 2470 (2019).

[160] J. Chaloupka and G. Khaliullin. Hidden symmetries of the extended Kitaev-Heisenberg model: Implications for the honeycomb-lattice iridates $A_2\text{IrO}_3$. *Phys. Rev. B* **92**, 024413 (2015).

[161] S. M. Winter, Y. Li, H. O. Jeschke and R. Valentí. Challenges in design of Kitaev materials: Magnetic interactions from competing energy scales. *Phys. Rev. B* **93**, 214431 (2016).

[162] N. D. Mermin and H. Wagner. Absence of Ferromagnetism or Antiferromagnetism in One- or Two-Dimensional Isotropic Heisenberg Models. *Phys. Rev. Lett.* **17**, 1133 (1966).

[163] B. Yang, Y. M. Goh, S. H. Sung, G. Ye, S. Biswas, D. A. S. Kaib, R. Dhakal, S. Yan, C. Li, S. Jiang, F. Chen, H. Lei, R. He, R. Valentí, S. M. Winter, R. Hovden and A. W. Tsien. Magnetic anisotropy reversal driven by structural symmetry-breaking in monolayer α -RuCl₃. *Nat. Mater.* **22**, 50 (2023).

[164] H. B. Cao, A. Banerjee, J. Q. Yan, C. A. Bridges, M. D. Lumsden, D. G. Mandrus, D. A. Tennant, B. C. Chakoumakos and S. E. Nagler. Low-temperature crystal and magnetic structure of α -RuCl₃. *Phys. Rev. B* **93**, 134423 (2016).

[165] H. Tomishige, J. Nasu and A. Koga. Interlayer coupling effect on a bilayer Kitaev model. *Phys. Rev. B* **97**, 094403 (2018).

[166] U. F. P. Seifert, J. Gritsch, E. Wagner, D. G. Joshi, W. Brenig, M. Vojta and K. P. Schmidt. Bilayer Kitaev models: Phase diagrams and novel phases. *Phys. Rev. B* **98**, 155101 (2018).

[167] J. Merino and A. Ralko. Even-odd effect in multilayer Kitaev honeycomb magnets. *Phys. Rev. B* **111**, 085152 (2025).

[168] H. Liu and G. Khaliullin. Pseudospin exchange interactions in d⁷ cobalt compounds: Possible realization of the Kitaev model. *Phys. Rev. B* **97**, 014407 (2018).

[169] R. Sano, Y. Kato and Y. Motome. Kitaev-Heisenberg Hamiltonian for high-spin d⁷ Mott insulators. *Phys. Rev. B* **97**, 014408 (2018).

[170] R. Zhong, M. Chung, T. Kong, L. T. Nguyen, S. Lei and R. J. Cava. Field-induced spin-liquid-like state in a magnetic honeycomb lattice. *Phys. Rev. B* **98**, 220407 (2018).

[171] H. S. Nair, J. M. Brown, E. Coldren, G. Hester, M. P. Gelfand, A. Podlesnyak, Q. Huang and K. A. Ross. Short-range order in the quantum XXZ honeycomb lattice material BaCo₂(PO₄)₂. *Phys. Rev. B* **97**, 134409 (2018).

[172] A. K. Bera, S. M. Yusuf, A. Kumar and C. Ritter. Zigzag antiferromagnetic ground state with anisotropic correlation lengths in the quasi-two-dimensional honeycomb lattice compound $\text{Na}_2\text{Co}_2\text{TeO}_6$. *Phys. Rev. B* **95**, 094424 (2017).

[173] S.-H. Jang, R. Sano, Y. Kato and Y. Motome. Antiferromagnetic Kitaev interaction in $\$f\$$ -electron based honeycomb magnets. *Phys. Rev. B* **99**, 241106 (2019).

[174] J. Xing, E. Feng, Y. Liu, E. Emmanouilidou, C. Hu, J. Liu, D. Graf, A. P. Ramirez, G. Chen, H. Cao and N. Ni. N'eel-type antiferromagnetic order and magnetic field--temperature phase diagram in the spin-1/2 rare-earth honeycomb compound YbCl_3 . *Phys. Rev. B* **102**, 014427 (2020).

[175] M. J. Daum, A. Ramanathan, A. I. Kolesnikov, S. Calder, M. Mourigal and H. S. La Pierre. Collective excitations in the tetravalent lanthanide honeycomb antiferromagnet Na_2PrO_3 . *Phys. Rev. B* **103**, L121109 (2021).

[176] T. Suzuki and Y. Yamaji. Thermal properties of spin-S Kitaev-Heisenberg model on a honeycomb lattice. *Physica B: Condensed Matter* **536**, 637 (2018).

[177] A. Koga, H. Tomishige and J. Nasu. Ground-state and Thermodynamic Properties of an $S = 1$ Kitaev Model. *J. Phys. Soc. Jpn.* **87**, 063703 (2018).

[178] J. Oitmaa, A. Koga and R. R. P. Singh. Incipient and well-developed entropy plateaus in spin-S Kitaev models. *Phys. Rev. B* **98**, 214404 (2018).

[179] H.-K. Jin, W. M. H. Natori, F. Pollmann and J. Knolle. Unveiling the $S=3/2$ Kitaev honeycomb spin liquids. *Nat. Commun.* **13**, 3813 (2022).

[180] I. Khait, P. P. Stavropoulos, H.-Y. Kee and Y. B. Kim. Characterizing spin-one Kitaev quantum spin liquids. *Phys. Rev. Res.* **3**, 013160 (2021).

[181] J. Reuther, R. Thomale and S. Trebst. Finite-temperature phase diagram of the Heisenberg-Kitaev model. *Phys. Rev. B* **84**, 100406(R) (2011).

[182] X.-Y. Dong and D. N. Sheng. Spin-1 Kitaev-Heisenberg model on a honeycomb lattice. *Phys. Rev. B* **102**, 121102(R) (2020).

[183] C. Price and N. B. Perkins. Finite-temperature phase diagram of the classical Kitaev-Heisenberg model. *Phys. Rev. B* **88**, 024410 (2013).

[184] K. Fukui, Y. Kato, J. Nasu and Y. Motome. Ground-state phase diagram of spin-S Kitaev-Heisenberg models. *Phys. Rev. B* **106**, 174416 (2022).

[185] A. M. Samarakoon, A. Banerjee, S. S. Zhang, Y. Kamiya, S. E. Nagler, D. A. Tennant, S. H. Lee and C. D. Batista. Comprehensive study of the dynamics of a classical Kitaev spin liquid. *Phys. Rev. B* **96**, 134408 (2017).

[186] O. Franke, D. Călugăru, A. Nunnenkamp and J. Knolle. Thermal spin dynamics of Kitaev magnets: Scattering continua and magnetic field induced phases within a stochastic semiclassical approach. *Phys. Rev. B* **106**, 174428 (2022).

[187] P. P. Stavropoulos, D. Pereira and H.-Y. Kee. Microscopic Mechanism for a Higher-Spin Kitaev Model. *Phys. Rev. Lett.* **123**, 037203 (2019).

[188] A. I. Kurbakov, A. N. Korshunov, S. Y. Podchezertsev, M. I. Stratan, G. V. Raganyan and E. A. Zvereva. Long-range and short-range ordering in 2D honeycomb-lattice magnet $\text{Na}_2\text{Ni}_2\text{TeO}_6$. *J. Alloys Compd.* **820**, 153354 (2020).

[189] A. M. Samarakoon, Q. Chen, H. Zhou and V. O. Garlea. Static and dynamic magnetic properties of honeycomb lattice antiferromagnets $\text{Na}_2\text{M}_2\text{TeO}_6$, $\text{M} = \text{Co}$ and Ni . *Phys. Rev. B* **104**, 184415 (2021).

[190] M. Kim, P. Kumaravadivel, J. Birkbeck, W. Kuang, S. G. Xu, D. G. Hopkinson, J. Knolle, P. A. McClarty, A. I. Berdyugin, M. Ben Shalom, R. V. Gorbachev, S. J. Haigh, S. Liu, J. H. Edgar, K. S. Novoselov, I. V. Grigorieva and A. K. Geim. Micromagnetometry of two-dimensional ferromagnets. *Nat. Electron.* **2**, 457 (2019).

[191] P. P. Stavropoulos, X. Liu and H.-Y. Kee. Magnetic anisotropy in spin-3/2 with heavy ligand in honeycomb Mott insulators: Application to CrI_3 . *Phys. Rev. Res.* **3**, 013216 (2021).

[192] I. Lee, F. G. Utermohlen, D. Weber, K. Hwang, C. Zhang, J. van Tol, J. E. Goldberger, N. Trivedi and P. C. Hammel. Fundamental Spin Interactions Underlying the Magnetic Anisotropy in the Kitaev Ferromagnet CrI_3 . *Phys. Rev. Lett.* **124**, 017201 (2020).

[193] C. Xu, J. Feng, H. Xiang and L. Bellaiche. Interplay between Kitaev interaction and single ion anisotropy in ferromagnetic CrI_3 and CrGeTe_3 monolayers. *Npj Comput. Mater.* **4**, 57 (2018).

[194] Z. Zhou, K. Chen, Q. Luo, H.-G. Luo and J. Zhao. Strain-induced phase diagram of the $S=3/2$ Kitaev material CrSiTe_3 . *Phys. Rev. B* **104**, 214425 (2021).

[195] M. O. Takahashi, W.-H. Kao, S. Fujimoto and N. B. Perkins. Z_2 flux binding to higher-spin impurities in the Kitaev spin liquid. *npj Quantum Mater.* **10**, 14 (2025).

[196] A. J. Willans, J. T. Chalker and R. Moessner. Disorder in a Quantum Spin Liquid: Flux Binding and Local Moment Formation. *Phys. Rev. Lett.* **104**, 237203 (2010).

[197] S. Eggert and I. Affleck. Magnetic impurities in half-integer-spin Heisenberg antiferromagnetic chains. *Phys. Rev. B* **46**, 10866 (1992).

[198] J. Sirker, N. Laflorencie, S. Fujimoto, S. Eggert and I. Affleck. Chain Breaks and the Susceptibility of $\text{Sr}_2\text{Cu}_{1-x}\text{Pd}_x\text{O}_{3+\delta}$ and Other Doped Quasi-One-Dimensional Antiferromagnets. *Phys. Rev. Lett.* **98**, 137205 (2007).

[199] R. N. Bhatt and P. A. Lee. Scaling Studies of Highly Disordered Spin-1/2 Antiferromagnetic Systems. *Phys. Rev. Lett.* **48**, 344 (1982).

[200] D. S. Fisher. Random antiferromagnetic quantum spin chains. *Phys. Rev. B* **50**, 3799 (1994).

[201] S. Sachdev, C. Buragohain and M. Vojta. Quantum Impurity in a Nearly Critical Two-Dimensional Antiferromagnet. *Science* **286**, 2479 (1999).

[202] W.-H. Kao, J. Knolle, G. B. Halász, R. Moessner and N. B. Perkins. Vacancy-Induced Low-Energy Density of States in the Kitaev Spin Liquid. *Phys. Rev. X* **11**, 011034 (2021).

[203] W.-H. Kao and N. B. Perkins. Disorder upon disorder: Localization effects in the Kitaev spin liquid. *Ann. Phys.* **435**, 168506 (2021).

[204] V. Dantas and E. C. Andrade. Disorder, Low-Energy Excitations, and Topology in the Kitaev Spin Liquid. *Phys. Rev. Lett.* **129**, 037204 (2022).

[205] M. O. Takahashi, M. G. Yamada, M. Udagawa, T. Mizushima and S. Fujimoto. Nonlocal Spin Correlation as a Signature of Ising Anyons Trapped in Vacancies of the Kitaev Spin Liquid. *Phys. Rev. Lett.* **131**, 236701 (2023).

[206] W. H. Kao, N. B. Perkins and G. B. Halasz. Vacancy Spectroscopy of Non-Abelian Kitaev Spin Liquids. *Phys. Rev. Lett.* **132**, 136503 (2024).

[207] E. H. Lieb. Flux phase of the half-filled band. *Phys. Rev. Lett.* **73**, 2158 (1994).

[208] A. J. Willans, J. T. Chalker and R. Moessner. Site dilution in the Kitaev honeycomb model. *Phys. Rev. B* **84**, 115146 (2011).

[209] W.-H. Kao, G. B. Halász and N. B. Perkins. Dynamics of vacancy-induced modes in the non-Abelian Kitaev spin liquid. *Phys. Rev. B* **109** (2024).

[210] V. Dantas, W.-H. Kao and N. B. Perkins. Phonon dynamics in the site-disordered Kitaev spin liquid. *Phys. Rev. B* **110**, 104425 (2024).

[211] S.-H. Do, C. H. Lee, T. Kihara, Y. S. Choi, S. Yoon, K. Kim, H. Cheong, W.-T. Chen, F. Chou, H. Nojiri and K.-Y. Choi. Randomly Hopping Majorana Fermions in the Diluted Kitaev System α -Ru_{0.8}Ir_{0.2}Cl₃. *Phys. Rev. Lett.* **124**, 047204 (2020).

[212] F. Trouselet, G. Khaliullin and P. Horsch. Effects of spin vacancies on magnetic properties of the Kitaev-Heisenberg model. *Phys. Rev. B* **84**, 054409 (2011).

[213] P. Lampen-Kelley, A. Banerjee, A. A. Aczel, H. B. Cao, M. B. Stone, C. A. Bridges, J. Q. Yan, S. E. Nagler and D. Mandrus. Destabilization of Magnetic Order in a Dilute Kitaev Spin Liquid Candidate. *Phys. Rev. Lett.* **119**, 237203 (2017).

[214] Y. Kubota, H. Tanaka, T. Ono, Y. Narumi and K. Kindo. Successive magnetic phase transitions in α -RuCl₃: XY-like frustrated magnet on the honeycomb lattice. *Phys. Rev. B* **91**, 094422 (2015).

[215] Y.-X. Yang, C.-Y. Jiang, L.-L. Huang, Z.-H. Zhu, C.-S. Chen, Q. Wu, Z.-F. Ding, C. Tan, K.-W. Chen, P. K. Biswas, A. D. Hillier, Y.-G. Shi, C. Liu, L. Wang, F. Ye, J.-W. Mei and L. Shu. Muon spin relaxation study of spin dynamics on a Kitaev honeycomb material H₃LiIr₂O₆. *npj Quantum Mater.* **9**, 77 (2024).

[216] I. Yatsuta and D. F. Mross. Vacancies in Generic Kitaev Spin Liquids. *Phys. Rev. Lett.* **133**, 226501 (2024).

[217] A. Vasiliev, O. Volkova, E. Zvereva and M. Markina. Milestones of low-D quantum magnetism. *npj Quantum Mater.* **3**, 18 (2018).

[218] J. C. T. Lee, S. Yuan, S. Lal, Y. I. Joe, Y. Gan, S. Smadici, K. Finkelstein, Y. Feng, A. Rusydi, P. M. Goldbart, S. Lance Cooper and P. Abbamonte. Two-stage orbital order and dynamical spin frustration in KCuF₃. *Nat. Phys.* **8**, 63 (2011).

[219] Y. Singh and P. Gegenwart. Antiferromagnetic Mott insulating state in single crystals of the honeycomb lattice material Na₂IrO₃. *Phys. Rev. B* **82**, 064412 (2010).

[220] J. A. Sears, M. Songvilay, K. W. Plumb, J. P. Clancy, Y. Qiu, Y. Zhao, D. Parshall and Y.-J. Kim. Magnetic order in β -RuCl₃: A honeycomb-lattice quantum magnet with strong spin-orbit coupling. *Phys. Rev. B* **91**, 144420 (2015).

[221] Y. Okamoto, M. Nohara, H. Aruga-Katori and H. Takagi. Spin-liquid state in the S=1/2 hyperkagome antiferromagnet Na₄Ir₃O₈. *Phys. Rev. Lett.* **99**, 137207 (2007).

[222] B. Koteswararao, R. Kumar, P. Khuntia, S. Bhowal, S. K. Panda, M. R. Rahman, A. V. Mahajan, I. Dasgupta, M. Baenitz, K. H. Kim and F. C. Chou. Magnetic properties and heat capacity of the three-dimensional frustrated S=1/2 antiferromagnet PbCuTe₂O₆. *Phys. Rev. B* **90**, 035141 (2014).

[223] A. Biffin, R. D. Johnson, S. Choi, F. Freund, S. Manni, A. Bombardi, P. Manuel, P. Gegenwart and R. Coldea. Unconventional magnetic order on the hyperhoneycomb Kitaev lattice in β -Li₂IrO₃: Full solution via magnetic resonant x-ray diffraction. *Phys. Rev. B* **90**, 205116 (2014).

[224] Y. Shimizu, K. Miyagawa, K. Kanoda, M. Maesato and G. Saito. Spin liquid state in an organic Mott insulator with a triangular lattice. *Phys. Rev. Lett.* **91**, 107001 (2003).

[225] A. P. Ramirez. Strongly Geometrically Frustrated Magnets. *Annu. Rev. of Mater. Res.* **24**, 453 (1994).

[226] Y. Shimizu, K. Miyagawa, K. Kanoda, M. Maesato and G. Saito. Emergence of inhomogeneous moments from spin liquid in the triangular-lattice Mott insulator κ -(ET)₂Cu₂(CN)₃. *Phys. Rev. B* **73**, 140407 (2006).

[227] M. Klanjšek, A. Zorko, R. Žitko, J. Mravlje, Z. Jagličić, Pabitra K. Biswas, P. Prelovšek, D. Mihailovic and D. Arčon. A high-temperature quantum spin liquid with polaron spins. *Nat. Phys.* **13**, 1130 (2017).

[228] M. Kratochvilova, A. D. Hillier, A. R. Wildes, L. Wang, S.-W. Cheong and J.-G. Park. The low-temperature highly correlated quantum phase in the charge-density-wave 1T-TaS₂ compound. *npj Quantum Mater.* **2**, 42 (2017).

[229] J. Nasu, M. Udagawa and Y. Motome. Vaporization of Kitaev Spin Liquids. *Phys. Rev. Lett.* **113**, 197205 (2014).

[230] Y. Li, H. Liao, Z. Zhang, S. Li, F. Jin, L. Ling, L. Zhang, Y. Zou, L. Pi, Z. Yang, J. Wang, Z. Wu and Q. Zhang. Gapless quantum spin liquid ground state in the two-dimensional spin-1/2 triangular antiferromagnet YbMgGaO₄. *Sci. Rep.* **5**, 16419 (2015).

[231] M. Yamashita, N. Nakata, Y. Senshu, M. Nagata, H. M. Yamamoto, R. Kato, T. Shibauchi and Y. Matsuda. Highly Mobile Gapless Excitations in a Two-Dimensional Candidate Quantum Spin Liquid. *Science* **328**, 1246 (2010).

[232] S. Yamashita, T. Yamamoto, Y. Nakazawa, M. Tamura and R. Kato. Gapless spin liquid of an organic triangular compound evidenced by thermodynamic measurements. *Nat. Commun.* **2**, 275 (2011).

[233] J. Nasu, J. Yoshitake and Y. Motome. Thermal Transport in the Kitaev Model. *Phys. Rev. Lett.* **119**, 127204 (2017).

[234] H. Takagi, T. Takayama, G. Jackeli, G. Khaliullin and S. E. Nagler. Concept and realization of Kitaev quantum spin liquids. *Nat. Rev. Phys.* **1**, 264 (2019).

[235] Y. Yamaji, T. Suzuki, T. Yamada, S.-i. Suga, N. Kawashima and M. Imada. Clues and criteria for designing a Kitaev spin liquid revealed by thermal and spin excitations of the honeycomb iridate Na₂IrO₃. *Phys. Rev. B* **93**, 174425 (2016).

[236] S. Yoon, K.-Y. Choi and H. Nam. Raman Spectroscopic Probe of the Magnetic Specific Heat in Quantum Magnets. *J. Korean Phys. Soc.* **77**, 138 (2020).

[237] M. Hermele, T. Senthil, M. P. A. Fisher, P. A. Lee, N. Nagaosa and X.-G. Wen. Stability of U(1)spin liquids in two dimensions. *Phys. Rev. B* **70**, 214437 (2004).

[238] J. Yoshitake, J. Nasu and Y. Motome. Fractional Spin Fluctuations as a Precursor of Quantum Spin Liquids: Majorana Dynamical Mean-Field Study for the Kitaev Model. *Phys. Rev. Lett.* **117**, 157203 (2016).

[239] T. H. Han, J. S. Helton, S. Chu, D. G. Nocera, J. A. Rodriguez-Rivera, C. Broholm and Y. S. Lee. Fractionalized excitations in the spin-liquid state of a kagome-lattice antiferromagnet. *Nature* **492**, 406 (2012).

[240] C. Balz, B. Lake, J. Reuther, H. Luetkens, R. Schönemann, T. Herrmannsdörfer, Y. Singh, A. T. M. Nazmul Islam, E. M. Wheeler, Jose A. Rodriguez-Rivera, T. Guidi, Giovanna G. Simeoni, C. Baines and H. Ryll. Physical realization of a quantum spin liquid based on a complex frustration mechanism. *Nat. Phys.* **12**, 942 (2016).

[241] Y. Shen, Y. D. Li, H. Wo, Y. Li, S. Shen, B. Pan, Q. Wang, H. C. Walker, P. Steffens, M. Boehm, Y. Hao, D. L. Quintero-Castro, L. W. Harriger, M. D. Frontzek, L. Hao, S. Meng, Q. Zhang, G. Chen and J. Zhao. Evidence for a spinon Fermi surface in a triangular-lattice quantum-spin-liquid candidate. *Nature* **540**, 559 (2016).

[242] J. A. M. Paddison, M. Daum, Z. Dun, G. Ehlers, Y. Liu, Matthew B. Stone, H. Zhou and M. Mourigal. Continuous excitations of the triangular-lattice quantum spin liquid YbMgGaO_4 . *Nat. Phys.* **13**, 117 (2016).

[243] J. K. Clark, V. Yannello, A. M. Samarakoon, C. Ross, M. C. Uible, V. O. Garlea and M. Shatruk. Inelastic Neutron Scattering Study of Magnetic Exchange Pathways in MnS . *J. Phys. Chem. C* **125**, 16183 (2021).

[244] L. J. Sandilands, Y. Tian, K. W. Plumb, Y.-J. Kim and K. S. Burch. Scattering Continuum and Possible Fractionalized Excitations in $\alpha\text{-RuCl}_3$. *Phys. Rev. Lett.* **114**, 147201 (2015).

[245] Z. Wang, S. Reschke, D. Huvonen, S. H. Do, K. Y. Choi, M. Gensch, U. Nagel, T. Room and A. Loidl. Magnetic Excitations and Continuum of a Possibly Field-Induced Quantum Spin Liquid in $\alpha\text{-RuCl}_3$. *Phys. Rev. Lett.* **119**, 227202 (2017).

[246] L. Y. Shi, X. M. Wang, R. D. Zhong, Z. X. Wang, T. C. Hu, S. J. Zhang, Q. M. Liu, T. Dong, F. Wang and N. L. Wang. Magnetic excitations of the field-induced states in $\text{BaCo}_2(\text{AsO}_4)_2$ probed by time-domain terahertz spectroscopy. *Phys. Rev. B* **104**, 144408 (2021).

[247] Z. X. Luo, E. Lake, J. W. Mei and O. A. Starykh. Spinon Magnetic Resonance of Quantum Spin Liquids. *Phys. Rev. Lett.* **120**, 037204 (2018).

[248] R. J. Elliott and R. Loudon. The possible observation of electronic Raman transitions in crystals. *Phys. Lett.* **3**, 189 (1963).

[249] Y. R. Shen. Scattering of Light by Magnons. *J. Appl. Phys.* **38**, 1490 (1967).

[250] T. P. Devereaux and R. Hackl. Inelastic light scattering from correlated electrons. *Rev. Mod. Phys.* **79**, 175 (2007).

[251] K. Y. Choi, P. Lemmens, D. Heydhausen, G. Güntherodt, C. Baumann, R. Klingeler, P. Reutler and B. Büchner. Anomalous orbital dynamics in LaSrMnO_4 observed by Raman spectroscopy. *Phys. Rev. B* **77**, 064415 (2008).

[252] T. Sekine, M. Jouanne, C. Julien and M. Balkanski. Light-scattering study of dynamical behavior of antiferromagnetic spins in the layered magnetic semiconductor FePS_3 . *Phys. Rev. B* **42**, 8382 (1990).

[253] D. Wulferding, P. Lemmens, P. Scheib, J. Röder, P. Mendels, S. Chu, T. Han and Y. S. Lee. Interplay of thermal and quantum spin fluctuations in the kagome lattice compound herbertsmithite. *Phys. Rev. B* **82**, 144412 (2010).

[254] Y. Wang, G. B. Osterhoudt, Y. Tian, P. Lampen-Kelley, A. Banerjee, T. Goldstein, J. Yan, J. Knolle, H. Ji, R. J. Cava, J. Nasu, Y. Motome, S. E. Nagler, D. Mandrus and K. S. Burch. The range of non-Kitaev terms and fractional particles in $\alpha\text{-RuCl}_3$. *npj Quantum Mater.* **5**, 14 (2020).

[255] S. Blundell, *Magnetism in Condensed Matter* (Oxford University Press, New York, 2001).

[256] P. A. Fleury and R. Loudon. Scattering of Light by One- and Two-Magnon Excitations. *Phys. Rev.* **166**, 514 (1968).

[257] E. Granado, A. García, J. A. Sanjurjo, C. Rettori, I. Torriani, F. Prado, R. D. Sánchez, A. Caneiro and S. B. Oseroff. Magnetic ordering effects in the Raman spectra of $\text{La}_{1-x}\text{Mn}_x\text{O}_3$. *Phys. Rev. B* **60**, 11879 (1999).

[258] P. Kumar, A. Bera, D. V. S. Muthu, S. N. Shirodkar, R. Saha, A. Shireen, A. Sundaresan, U. V. Waghmare, A. K. Sood and C. N. R. Rao. Coupled phonons, magnetic excitations, and ferroelectricity in AlFeO_3 : Raman and first-principles studies. *Phys. Rev. B* **85**, 134449 (2012).

[259] D. Wulferding, Y. Choi, W. Lee and K. Y. Choi. Raman spectroscopic diagnostic of quantum spin liquids. *J. Phys.: Condens. Matter* **32**, 043001 (2020).

[260] J. Yoshitake, J. Nasu, Y. Kato and Y. Motome. Majorana dynamical mean-field study of spin dynamics at finite temperatures in the honeycomb Kitaev model. *Phys. Rev. B* **96**, 024438 (2017).

[261] S. K. Choi, R. Coldea, A. N. Kolmogorov, T. Lancaster, I. I. Mazin, S. J. Blundell, P. G. Radaelli, Y. Singh, P. Gegenwart, K. R. Choi, S. W. Cheong, P. J. Baker, C. Stock and J. Taylor. Spin Waves and Revised Crystal Structure of Honeycomb Iridate Na_2IrO_3 . *Phys. Rev. Lett.* **108**, 127204 (2012).

[262] X. Liu, T. Berlijn, W. G. Yin, W. Ku, A. Tsvelik, Y.-J. Kim, H. Gretarsson, Y. Singh, P. Gegenwart and J. P. Hill. Long-range magnetic ordering in Na_2IrO_3 . *Phys. Rev. B* **83**, 220403 (2011).

[263] A. Glamazda, P. Lemmens, S. H. Do, Y. S. Kwon and K. Y. Choi. Relation between Kitaev magnetism and structure in $\alpha\text{-RuCl}_3$. *Phys. Rev. B* **95**, 174429 (2017).

[264] A. Banerjee, C. A. Bridges, J. Q. Yan, A. A. Aczel, L. Li, M. B. Stone, G. E. Granroth, M. D. Lumsden, Y. Yiu, J. Knolle, S. Bhattacharjee, D. L. Kovrizhin, R. Moessner, D. A. Tennant, D. G. Mandrus and S. E. Nagler. Proximate Kitaev quantum spin liquid behaviour in a honeycomb magnet. *Nat. Matter.* **15**, 733 (2016).

[265] T. T. Mai, K. F. Garrity, A. McCreary, J. Argo, J. R. Simpson, V. Doan-Nguyen, R. V. Aguilar and A. R. H. Walker. Magnon-phonon hybridization in 2D antiferromagnet MnPSe_3 . *Sci. Adv.* **7**, eabj3106 (2021).

[266] Y.-J. Sun, Q.-H. Tan, X.-L. Liu, Y.-F. Gao and J. Zhang. Probing the Magnetic Ordering of Antiferromagnetic MnPS_3 by Raman Spectroscopy. *J. Phys. Chem. Lett.* **10**, 3087 (2019).

[267] M. G. Cottam and D. J. Lockwood. One-magnon and two-magnon Raman scattering in MnF_2 . *J. Magn. Magn. Mater.* **54-57**, 1143 (1986).

[268] T. M. H. Nguyen, L. J. Sandilands, C. H. Sohn, C. H. Kim, A. L. Wysocki, I.-S. Yang, S. J. Moon, J.-H. Ko, J. Yamaura, Z. Hiroi and T. W. Noh. Two-magnon scattering in the 5d all-in-all-out pyrochlore magnet $\text{Cd}_2\text{Os}_2\text{O}_7$. *Nat. Commun.* **8**, 251 (2017).

[269] W.-H. Ko, Z.-X. Liu, T.-K. Ng and P. A. Lee. Raman signature of the $U(1)$ Dirac spin-liquid state in the spin-1/2 kagome system. *Phys. Rev. B* **81**, 024414 (2010).

[270] T. Tang, B. Moritz and T. P. Devereaux. Spectra of a gapped quantum spin liquid with a strong chiral excitation on the triangular lattice. *Phys. Rev. B* **106**, 064428 (2022).

[271] M. Sato, H. Katsura and N. Nagaosa. Theory of Raman Scattering in One-Dimensional Quantum Spin-1/2 Antiferromagnets. *Phys. Rev. Lett.* **108**, 237401 (2012).

[272] O. Cépas, J. O. Haerter and C. Lhuillier. Detection of weak emergent broken-symmetries of the kagome antiferromagnet by Raman spectroscopy. *Phys. Rev. B* **77**, 172406 (2008).

[273] B. Perreault, J. Knolle, N. B. Perkins and F. J. Burnell. Resonant Raman scattering theory for Kitaev models and their Majorana fermion boundary modes. *Phys. Rev. B* **94**, 104427 (2016).

[274] J. Nasu. Majorana quasiparticles emergent in Kitaev spin liquid. *Prog. Theor. Exp. Phys.* **2024**, 08C104 (2023).

[275] B. Singh, M. Vogl, S. Wurmehl, S. Aswartham, B. Büchner and P. Kumar. Kitaev magnetism and fractionalized excitations in double perovskite $\text{Sm}_2\text{ZnIrO}_6$. *Phys. Rev. Res.* **2**, 013040 (2020).

[276] E. Saitoh, S. Okamoto, K. T. Takahashi, K. Tobe, K. Yamamoto, T. Kimura, S. Ishihara, S. Maekawa and Y. Tokura. Observation of orbital waves as elementary excitations in a solid. *Nature* **410**, 180 (2001).

[277] B. Singh, G. A. Cansever, T. Dey, A. Maljuk, S. Wurmehl, B. Büchner and P. Kumar. Orbiton–phonon coupling in $\text{Ir}^{5+}(5\text{d}^4)$ double perovskite Ba_2YIrO_6 . *J. Phys.: Condens. Matter* **31**, 065603 (2019).

[278] P. Kumar, A. Bera, D. V. S. Muthu, P. M. Shirage, A. Iyo and A. K. Sood. Superconducting fluctuations and anomalous phonon renormalization much above superconducting transition temperature in $\text{Ca}_4\text{Al}_2\text{O}_{5.7}\text{Fe}_2\text{As}_2$. *Appl. Phys. Lett.* **100**, 222602 (2012).

[279] A. Ghosh, M. Palit, S. Maity, V. Dwij, S. Rana and S. Datta. Spin-phonon coupling and magnon scattering in few-layer antiferromagnetic FePS_3 . *Phys. Rev. B* **103**, 064431 (2021).

[280] R. Krüger, B. Schulz, S. Naler, R. Rauer, D. Budelmann, J. Bäckström, K. H. Kim, S. W. Cheong, V. Perebeinos and M. Rübhausen. Orbital ordering in LaMnO_3 Investigated by Resonance Raman Spectroscopy. *Phys. Rev. Lett.* **92**, 097203 (2004).

[281] K. Y. Choi, P. Lemmens, G. Güntherodt, Y. G. Pashkevich, V. P. Gnezdilov, P. Reutler, L. Pinsard-Gaudart, B. Büchner and A. Revcolevschi. Orbiton-mediated multiphonon scattering in $\text{La}_{1-x}\text{Sr}_x\text{MnO}_3$. *Phys. Rev. B* **72**, 024301 (2005).

[282] W. Zhang, S. Wu, S. Kasahara, T. Shibauchi, Y. Matsuda and G. Blumberg. Quadrupolar charge dynamics in the nonmagnetic $\text{FeSe}_{1-x}\text{S}_x$ superconductors. *Proc. Natl. Acad. Sci. USA* **118**, e2020585118 (2021).

[283] S. Pal, V. Kumar, D. P. Panda, A. Sundaresan, A. V. Mahajan, D. V. S. Muthu and A. K. Sood. Raman fingerprints of fractionalized Majorana excitations in the honeycomb iridate $\text{Ag}_3\text{LiIr}_2\text{O}_6$. *Phys. Rev. B* **105**, 235125 (2022).

[284] N. Khan, D. Kumar, V. Kumar, Y. Shemerliuk, S. Selter, B. Büchner, K. Pal, S. Aswartham and P. Kumar. The interplay of topology and antiferromagnetic order in two-dimensional van der Waals crystals of $(\text{Ni}_x\text{Fe}_{1-x})_2\text{P}_2\text{S}_6$. *2D Mater.* **11**, 035018 (2024).

[285] P. N. Butcher and N. R. Ogg. Fluctuation-dissipation theorems for driven non-linear media at optical frequencies. *Proc. Phys. Soc.* **86**, 699 (1965).

[286] W. Hayes , R. Loudon, *Scattering of Light by Crystals*. (Dover, New York, 2004).

[287] B. Perreault, J. Knolle, N. B. Perkins and F. J. Burnell. Theory of Raman response in three-dimensional Kitaev spin liquids: Application to β - and γ - Li_2IrO_3 compounds. *Phys. Rev. B* **92**, 094439 (2015).

[288] Y. Yang, M. Li, I. Rousochatzakis and N. B. Perkins. Non-Loudon-Fleury Raman scattering in spin-orbit coupled Mott insulators. *Phys. Rev. B* **104**, 144412 (2021).

[289] P. Lemmens, G. Güntherodt and C. Gros. Magnetic light scattering in low-dimensional quantum spin systems. *Phys. Rep.* **375**, 1 (2003).

[290] T. Moriya. Theory of Absorption and Scattering of Light by Magnetic Crystals. *J. Appl. Phys.* **39**, 1042 (1968).

[291] J. Fu, J. G. Rau, M. J. P. Gingras and N. B. Perkins. Fingerprints of quantum spin ice in Raman scattering. *Phys. Rev. B* **96**, 035136 (2017).

[292] Y. Wang, G. B. Osterhoudt, Y. Tian, P. Lampen-Kelley, A. Banerjee, T. Goldstein, J. Yan, J. Knolle, H. Ji, R. J. Cava, J. Nasu, Y. Motome, S. E. Nagler, D. Mandrus and K. S. Burch. The range of non-Kitaev terms and fractional particles in α - RuCl_3 . *npj Quantum Mater.* **5**, 14 (2020).

[293] I. Rousochatzakis, S. Kourtis, J. Knolle, R. Moessner and N. B. Perkins. Quantum spin liquid at finite temperature: Proximate dynamics and persistent typicality. *Phys. Rev. B* **100**, 045117 (2019).

[294] I. Yamada and H. Onda. Light scattering from magnetic-energy fluctuations in the one-dimensional Heisenberg antiferromagnet KCuF_3 . *Phys. Rev. B* **49**, 1048 (1994).

[295] W. Hayes, & Loudon, R. , *Scattering of light by crystals* (Wiley, New York, 1978).

[296] B. S. Shastry and B. I. Shraiman. Theory of Raman scattering in Mott-Hubbard systems. *Phys. Rev. Lett.* **65**, 1068 (1990).

[297] W. J. Brya and P. M. Richards. Frequency moments for two-spin light scattering in antiferromagnets. *Phys. Rev. B* **9**, 2244 (1974).

[298] B. I. Halperin and P. C. Hohenberg. Hydrodynamic Theory of Spin Waves. *Phys. Rev.* **188**, 898 (1969).

[299] G. F. Reiter. Light scattering from energy fluctuations in magnetic insulators. *Phys. Rev. B* **13**, 169 (1976).

[300] J. W. Halley. Light Scattering as a Probe of Dynamical Critical Properties of Antiferromagnets. *Phys. Rev. Lett.* **41**, 1605 (1978).

[301] K. A. Modic, T. E. Smidt, I. Kimchi, N. P. Breznay, A. Biffin, S. Choi, R. D. Johnson, R. Coldea, P. Watkins-Curry, G. T. McCandless, J. Y. Chan, F. Gandara, Z. Islam, A.

Vishwanath, A. Shekhter, R. D. McDonald and J. G. Analytis. Realization of a three-dimensional spin-anisotropic harmonic honeycomb iridate. *Nat. Commun.* **5**, 4203 (2014).

[302] J. Knolle, S. Bhattacharjee and R. Moessner. Dynamics of a quantum spin liquid beyond integrability: The Kitaev-Heisenberg- Γ model in an augmented parton mean-field theory. *Phys. Rev. B* **97**, 134432 (2018).

[303] U. Fano. Effects of Configuration Interaction on Intensities and Phase Shifts. *Phys. Rev.* **124**, 1866 (1961).

[304] T. Moriya. Theory of Light Scattering by Magnetic Crystals. *J. Phys. Soc. Jpn.* **23**, 490 (1967).

[305] H. K. Naoshi Suzuki. Theory of Spin-Dependent Phonon Raman Scattering in Magnetic Crystals. *J. Phys. Soc. Jpn.* **35**, 985 (1973).

[306] K. Feng, S. Swarup and N. B. Perkins. Footprints of Kitaev spin liquid in the Fano lineshape of Raman-active optical phonons. *Phys. Rev. B* **105**, L121108 (2022).

[307] A. Metavitsiadis, W. Natori, J. Knolle and W. Brenig. Optical phonons coupled to a Kitaev spin liquid. *Phys. Rev. B* **105**, 165151 (2022).

[308] S. Swarup, S. Singh and N. B. Perkins. Signatures of fractionalization in the optical phonons of the hyperhoneycomb Kitaev magnet β -Li₂IrO₃. *Phys. Rev. B* **110**, 134421 (2024).

[309] V. Gnezdilov, J. Deisenhofer, P. Lemmens, D. Wulferding, O. Afanasiev, P. Ghigna, A. Loidl and A. Yeremenko. Phononic and magnetic excitations in the quasi-one-dimensional Heisenberg antiferromagnet KCuF₃. *Low Temp. Phys.* **38**, 419 (2012).

[310] D. Wulferding, D. L. Quintero-Castro, P. Laurell, G. Alvarez, E. Dagotto and K.-Y. Choi. Spinon excitations and spin correlations in the one-dimensional quantum magnet β -VOSO₄ probed by Raman spectroscopy. *Commun Phys* **8**, 447 (2025).

[311] G. G. Manuel Cardona, *Light Scattering in Solids II* (Springer Berlin, Heidelberg, 2005).

[312] M. C. Peter Y. Yu *Fundamentals of Semiconductors : Physics and Materials Properties* (Springer Science & Business Media, New York, 2010).

[313] T. T. Mai, A. McCreary, P. Lampen-Kelley, N. Butch, J. R. Simpson, J. Q. Yan, S. E. Nagler, D. Mandrus, A. R. H. Walker and R. V. Aguilar. Polarization-resolved Raman spectroscopy of α -RuCl₃ and evidence of room-temperature two-dimensional magnetic scattering. *Phys. Rev. B* **100**, 134419 (2019).

[314] R. D. Johnson, S. C. Williams, A. A. Haghimirad, J. Singleton, V. Zapf, P. Manuel, I. I. Mazin, Y. Li, H. O. Jeschke, R. Valentí and R. Coldea. Monoclinic crystal structure of α -RuCl₃ and the zigzag antiferromagnetic ground state. *Phys. Rev. B* **92**, 235119 (2015).

[315] M. Ye, H. H. Kung, P. F. S. Rosa, E. D. Bauer, Z. Fisk and G. Blumberg. Raman spectroscopy off-electron metals: An example of CeB₆. *Phys. Rev. Mater.* **3**, 065003 (2019).

[316] T. Wang, H. Sun, X. Li and L. Zhang. Chiral Phonons: Prediction, Verification, and Application. *Nano Letters* **24**, 4311 (2024).

[317] H. Chen, W. Zhang, Q. Niu and L. Zhang. Chiral phonons in two-dimensional materials. *2D Mater.* **6**, 012002 (2019).

[318] M. Che, J. Liang, Y. Cui, H. Li, B. Lu, W. Sang, X. Li, X. Dong, L. Zhao, S. Zhang, T. Sun, W. Jiang, E. Liu, F. Jin, T. Zhang and L. Yang. Magnetic Order Induced Chiral Phonons in a Ferromagnetic Weyl Semimetal. *Phys. Rev. Lett.* **134**, 196906 (2025).

[319] R. Kumar, P. K. Barman, P. K. Nayak and M. S. R. Rao. Chiral phonon and in-plane Raman optical activity of anisotropic layered α -MoO₃. *Phys. Rev. B* **110**, 085423 (2024).

[320] J. Mi, T. Wang, W. Tang, X. Fan, J. Zhou, L. Zhang, L. Li and Z. Xu. Chiral phonons and giant magneto-optical Raman effect in chiral antiferromagnetic CoNb₃S₆. *Appl. Phys. Lett.* **127** (2025).

[321] X. Qin, C. Yang, D. Sun, J. Liu and V. Blum. Chiral Phonon-Induced Spin Transport via Microscopic Barnett Effect. *Phys. Rev. Lett.* **135**, 076703 (2025).

[322] C. Strohm, G. L. J. A. Rikken and P. Wyder. Phenomenological Evidence for the Phonon Hall Effect. *Phys. Rev. Lett.* **95**, 155901 (2005).

[323] L. Zhang, J. Ren, J.-S. Wang and B. Li. Topological Nature of the Phonon Hall Effect. *Phys. Rev. Lett.* **105**, 225901 (2010).

[324] T. Zhang, Z. Huang, Z. Pan, L. Du, G. Zhang and S. Murakami. Weyl Phonons in Chiral Crystals. *Nano Lett.* **23**, 7561 (2023).

[325] K. Ishito, H. Mao, Y. Kousaka, Y. Togawa, S. Iwasaki, T. Zhang, S. Murakami, J.-i. Kishine and T. Satoh. Truly chiral phonons in α -HgS. *Nat. Phys.* **19**, 35 (2022).

[326] E. Koller, S. Swarup, J. Knolle and N. B. Perkins. Spin-lattice coupling induced chiral phonons and their signature in Raman Circular Dichroism. *arXiv preprint arXiv:2511.14902* (2025).

[327] E. Koller, V. Leeb, N. B. Perkins and J. Knolle. Raman Circular Dichroism and Quantum Geometry of Chiral Quantum Spin Liquids. *arXiv preprint arXiv:2503.14091* (2025).

[328] A. P. Joy and A. Rosch. Raman spectroscopy of anyons in generic Kitaev spin liquids. *Phys. Rev. B* **112**, 184411 (2025).

[329] D. Wulferding, Y. Choi, S.-H. Do, C. H. Lee, P. Lemmens, C. Faugeras, Y. Gallais and K.-Y. Choi. Magnon bound states versus anyonic Majorana excitations in the Kitaev honeycomb magnet α -RuCl₃. *Nat. Commun.* **11**, 1603 (2020).

[330] A. Sahasrabudhe, D. A. S. Kaib, S. Reschke, R. German, T. C. Koethe, J. Buhot, D. Kamenskyi, C. Hickey, P. Becker, V. Tsurkan, A. Loidl, S. H. Do, K. Y. Choi, M. Grüninger, S. M. Winter, Z. Wang, R. Valentí and P. H. M. van Loosdrecht. High-field quantum disordered state in α -RuCl₃: Spin flips, bound states, and multiparticle continuum. *Phys. Rev. B* **101**, 140410 (2020).

[331] A. Sahasrabudhe, M. A. Prosnikov, T. C. Koethe, P. Stein, V. Tsurkan, A. Loidl, M. Grüninger, H. Hedayat and P. H. M. van Loosdrecht. Chiral excitations and the intermediate-field regime in the Kitaev magnet α -RuCl₃. *Phys. Rev. Res.* **6**, L022005 (2024).

[332] Y. Matsuda, T. Shibauchi and H.-Y. Kee. Kitaev quantum spin liquids. *Rev. Mod. Phys.* **97**, 045003 (2025).

[333] N. Janša, A. Zorko, M. Gomilšek, M. Pregelj, K. W. Krämer, D. Biner, A. Biffin, C. Rüegg and M. Klanjšek. Observation of two types of fractional excitation in the Kitaev honeycomb magnet. *Nat. Phys.* **14**, 786 (2018).

[334] A. Revelli, M. Moretti Sala, G. Monaco, C. Hickey, P. Becker, F. Freund, A. Jesche, P. Gegenwart, T. Eschmann, F. L. Buessen, S. Trebst, P. H. M. van Loosdrecht, J. van den Brink and M. Grüninger. Fingerprints of Kitaev physics in the magnetic excitations of honeycomb iridates. *Phys. Rev. Res.* **2**, 043094 (2020).

[335] I. A. Leahy, C. A. Pocs, P. E. Siegfried, D. Graf, S. H. Do, K.-Y. Choi, B. Normand and M. Lee. Anomalous Thermal Conductivity and Magnetic Torque Response in the Honeycomb Magnet α -RuCl₃. *Phys. Rev. Lett.* **118**, 187203 (2017).

[336] J. A. Sears, Y. Zhao, Z. Xu, J. W. Lynn and Y.-J. Kim. Phase diagram of α -RuCl₃ in an in-plane magnetic field. *Phys. Rev. B* **95**, 180411 (2017).

[337] A. U. B. Wolter, L. T. Corredor, L. Janssen, K. Nenkov, S. Schönecker, S. H. Do, K. Y. Choi, R. Albrecht, J. Hunger, T. Doert, M. Vojta and B. Büchner. Field-induced quantum criticality in the Kitaev system α -RuCl₃. *Phys. Rev. B* **96**, 041405 (2017).

[338] D. Takane, K. Nakayama, S. Souma, T. Wada, Y. Okamoto, K. Takenaka, Y. Yamakawa, A. Yamakage, T. Mitsuhashi, K. Horiba, H. Kumigashira, T. Takahashi and T. Sato. Observation of Dirac-like energy band and ring-torus Fermi surface associated with the nodal line in topological insulator CaAgAs. *npj Quantum Mater.* **3**, 1 (2018).

[339] Y. Kasahara, T. Ohnishi, Y. Mizukami, O. Tanaka, S. Ma, K. Sugii, N. Kurita, H. Tanaka, J. Nasu, Y. Motome, T. Shibauchi and Y. Matsuda. Majorana quantization and half-integer thermal quantum Hall effect in a Kitaev spin liquid. *Nature* **559**, 227 (2018).

[340] T. Yokoi, S. Ma, Y. Kasahara, S. Kasahara, T. Shibauchi, N. Kurita, H. Tanaka, J. Nasu, Y. Motome, C. Hickey, S. Trebst and Y. Matsuda. Half-integer quantized anomalous thermal Hall effect in the Kitaev material candidate α -RuCl₃. *Science* **373**, 568 (2021).

[341] S. C. Morampudi, A. M. Turner, F. Pollmann and F. Wilczek. Statistics of Fractionalized Excitations through Threshold Spectroscopy. *Phys. Rev. Lett.* **118**, 227201 (2017).

[342] S. H. Baek, S. H. Do, K. Y. Choi, Y. S. Kwon, A. U. B. Wolter, S. Nishimoto, J. van den Brink and B. Büchner. Evidence for a Field-Induced Quantum Spin Liquid in α -RuCl₃. *Phys. Rev. Lett.* **119**, 037201 (2017).

[343] A. N. Ponomaryov, E. Schulze, J. Wosnitza, P. Lampen-Kelley, A. Banerjee, J. Q. Yan, C. A. Bridges, D. G. Mandrus, S. E. Nagler, A. K. Kolezhuk and S. A. Zvyagin. Unconventional spin dynamics in the honeycomb-lattice material α -RuCl₃: High-field electron spin resonance studies. *Phys. Rev. B* **96**, 241107 (2017).

[344] B. Shen, E. Insuasti Pazmino, R. Dhakal, F. Freund, P. Gegenwart, S. M. Winter and A. A. Tsirlin. Pressure-dependent magnetism of the Kitaev candidate Li₂RhO₃. *npj Quantum Mater.* **10**, 9 (2025).

[345] G. Bastien, G. Garbarino, R. Yadav, F. J. Martínez-Casado, R. Beltrán Rodríguez, Q. Stahl, M. Kusch, S. P. Limandri, R. Ray, P. Lampen-Kelley, D. G. Mandrus, S. E. Nagler, M. Roslova, A. Isaeva, T. Doert, L. Hozoi, A. U. B. Wolter, B. Büchner, J. Geck and J. van den Brink. Pressure-induced dimerization and valence bond crystal formation in the Kitaev-Heisenberg magnet α -RuCl₃. *Phys. Rev. B* **97**, 241108 (2018).

[346] Z. Wang, J. Guo, F. F. Tafti, A. Hegg, S. Sen, V. A. Sidorov, L. Wang, S. Cai, W. Yi, Y. Zhou, H. Wang, S. Zhang, K. Yang, A. Li, X. Li, Y. Li, J. Liu, Y. Shi, W. Ku, Q. Wu, R. J. Cava and L. Sun. Pressure-induced melting of magnetic order and emergence of a new quantum state in α -RuCl₃. *Phys. Rev. B* **97**, 245149 (2018).

[347] G. Li, X. Chen, Y. Gan, F. Li, M. Yan, F. Ye, S. Pei, Y. Zhang, L. Wang, H. Su, J. Dai, Y. Chen, Y. Shi, X. Wang, L. Zhang, S. Wang, D. Yu, F. Ye, J.-W. Mei and M. Huang. Raman spectroscopy evidence for dimerization and Mott collapse in γ -RuCl₃ under pressures. *Phys. Rev. Mater.* **3**, 023601 (2019).

[348] Y. Hasegawa, T. Aoyama, K. Sasaki, Y. Ikemoto, T. Moriwaki, T. Shirakura, R. Saito, Y. Imai and K. Ohgushi. Two-phonon Absorption Spectra in the Layered Honeycomb Compound α -RuCl₃. *J. Phys. Soc. Jpn.* **86**, 123709 (2017).

[349] S. Choi, H.-S. Kim, H.-H. Kim, A. Krajewska, G. Kim, M. Minola, T. Takayama, H. Takagi, K. Haule, D. Vanderbilt and B. Keimer. Lattice dynamics and structural transition of the hyperhoneycomb iridate β -Li₂IrO₃ investigated by high-pressure Raman scattering. *Phys. Rev. B* **101**, 054102 (2020).